Department of Electronic and Electrical Engineering

Grounding grid design for high voltage substations: An assessment of effectiveness for lightning currents

by

Farhan bin Hanaffi

A thesis presented in fulfilment of the requirements for the degree of

Doctor of Philosophy

2016

Declaration

This thesis is the result of the author's original research. It has been composed by the author, and has not been previously submitted for examination which has led to the award of a degree.

Signed : Date :

Acknowledgements

I would like to express my deepest appreciation and sincere gratitude to my supervisors Dr Wah Hoon Siew and Dr Igor Timoshkin, for all of their invaluable guidance and discussion, patience, time and encouragement, throughout the duration of this work. I have greatly benefited from their recognised extensive knowledge and expertise in this research field. Special thanks also go to my colleagues in the High Voltage Technology Group for sharing valuable knowledge, support and encouragement.

I would like to thank my wife Siti Suhana Sulaiman, my daughter Nur Insyirah, and my son Ilham Hazim, for their patience and support. My deep and sincere thanks also go to my parents and friends for their constant support and prayers. I am so lucky and so proud to have such a wonderful family and friends.

Last but not least, many thanks to the Ministry of Higher Education Malaysia, and Universiti Teknikal Malaysia Melaka (UTeM), which have provided financial support during my study.

Abstract

An electrical grounding system is an important element to ascertain a safe environment for both humans and equipment during fault or transient conditions. The performance of grounding systems under lightning current is quite different from the conventional frequency based power. In order to understand the grounding grid behaviour under lightning current, researchers typically carry out experiments on actual grounding systems or on laboratory scaled models. Although experiments can provide insights of the actual grounding operation, the shortcoming is that a large area of lab space is required which reflects into high costs. As an alternative, computer simulation has been introduced, and can be categorised into three different approaches, namely circuit approach, transmission line approach or electromagnetic approach.

In this work, the simulations are performed based on the electromagnetic approach under three dimensions (3D) mode due to its accurate results. For further understanding, a comparison between circuit and electromagnetic approaches is also carried out, where the resulting outcome shows that the circuit approach underestimates the impulse impedance at injection point compared with simulations by the electromagnetic approach. When the electromagnetic approach is applied, a finite element method is used to solve the partial differential electromagnetic equations in the time domain. Thereafter, the simulations results are validated with the existing published results covering the electromagnetic simulations by using the method of moment (MOM), and as well as actual field experiments. In addition, simulations are performed to understand the effect of different parameters, including lightning current, soil parameters, grounding design, and location of injection point of lightning current.

Moreover, a comparison study is carried out for potential rise between power frequency and impulse current at different grid sizes. The study shows the potential

generated at injection point for both current and saturation point when the grid size reaches a certain point. It's important to consider both types of current to get better grounding grid design. Besides that, empirical equations are used out to calculate the effective area under lightning conditions, where the effect of the down-conductor is taken into consideration as part of the grounding model. The effective area is an important parameter for the optimization of the grounding grid design when increasing grounding size does not improve the impulse impedance.

Transient ground potential rise (TGPR) above the ground is another interesting parameter to analyse. In this work, a good correlation is shown between the effective area and the impulse impedance at the injection point with rising transient ground potential. It is found that the TGPR is larger when it is closer to the injection point, but only lasts for a few microseconds. Step voltage evaluations are performed for different standing positions of the human above the grid, including the distance of the step voltage location from the injection point, and the effect of grid size to step voltage value.

List of Publications

I. F.Hanaffi, W. H. Siew and I. V. Timoshkin "Effective Size of Grounding Grid under Lightning Impulse", Universities High Voltage Network (UHVnet) Colloquium, Jan 18th – 19th, 2012, Leicester, United Kingdom.

II. F.Hanaffi, W. H. Siew and I. V. Timoshkin "Grounding transient analysis using Finite Element Method (FEM)", Universities High Voltage Network (UHVnet) Colloquium, Jan 16th – 17th, 2013, Glasgow, United Kingdom.

III. F.Hanaffi, W. H. Siew ,I. V. Timoshkin ,Bo Tan, , Xishan Wen and Lei Lan "Boundary Analysis on Transient Grounding Modelling using FEM", 8th Asia-Pacific International Conference on Lightning, Jun. 26-28, 2013, Seoul, Korea

IV. Bo Tan, , Xishan Wen and Lei Lan , F.Hanaffi, W. H. Siew ,I. V. Timoshkin "Calculation of Conductive Coupling of Substation Grounding Grid with Secondary Cable Under Lightning Stroke", 8th Asia-Pacific International Conference on Lightning, Jun. 26-28, 2013, Seoul, Korea

V. F.Hanaffi, W. H. Siew, I. V. Timoshkin "Grounding Grid Safety Evaluation under Lightning Current", Progress In Electromagnetics Research Symposium, August 12th – 15th, 2013, Stockholm,Sweden.

VI. F.Hanaffi, W. H. Siew ,I. V. Timoshkin "Transient Grounding Modelling using FEM: Infinite Boundary Condition", International Colloquium on Lightning and Power System , May 12-14, 2014, Lyon, France

VII. F.Hanaffi, W. H. Siew ,I. V. Timoshkin, Hailiang LU, Yu Wang , Xishan Wen , Lei Lan "Evaluation of Grounding Grid's Effective Area'', International Conference on Lightning Protection (ICLP), Oct 13 - 17 , 2014, Shanghai, China.

VIII. Chaoying Fang , Lei Lan, Yu Wang, Xishan Wen and F.Hanaffi, W. H. Siew ,I. V. Timoshkin, Jutian Li , Zeng Zhang "Feasibility Study on Using Jacket Structure as Natural Grounding Electrode of Offshore Wind Turbines'', International Conference on Lightning Protection (ICLP), Oct 13 - 17 , 2014 Shanghai, China.

IX. F.Hanaffi, W. H. Siew ,I. V. Timoshkin "Step Voltages in a ground-grid arising from lightning current", Asia-Pacific International Conference on Lightning (APL), Jun. 23-26, 2015, Nagoya, Japan

Table of Contents

List of Figures

List of Tables

List of Acronyms

AC	Alternating Current
BEM	Boundary Element Method
EMC	Electromagnetic Compatibility
FDTD	Finite Different Time Domain
FEM	Finite Element Method
FFT	Fast Fourier Transform
HV	High Voltage
MOM	Method of Moment
PML	Perfect Match Layer
TGPR	Transient Ground Potential Rise
2D	Two Dimensional
3D	Three Dimensional

Chapter 1
Introduction

1.1 Background

Grounding systems play an important role in protecting life or facilities from any fault or transient in power systems. The main purpose of a grounding system is to provide the lowest impedance path for unwanted current during faults or transient conditions, such as lightning and switching. Relatively, the level of safety of a protection system is influenced by the efficiency of the grounding system, where the grounding conductors can range from a horizontal rod, vertical rod, ring rod, and grounding grid depending upon the application. In a substation grounding design, the grounding grid is buried below entire installed equipment to maintain the potential rise above the ground within the safety limit during the discharging process of a fault or lightning current. Parameters that influence the potential above the ground are soil resistivity, conductor configuration and level of fault current, where soil resistivity depends on geography, water content, chemical compound and type of soil. In practice, lower soil resistivity is advantageous for grounding system. Apart from that, the grounding grid configuration also depends on the size of the grounding grid and the mesh size within the grounding grid.

For the practical scenario, it is necessary that a grounding system is designed with a low magnitude of earth resistance, so the protection device can divert the high fault current to the earth effectively. In the British Standard [1], the value of earth resistance was proposed to be below than 20Ω for the independent earth electrodes that are

associated with the local grounding of the star point of generating plant, and below 1Ω for a substation grid. In the grounding grid design, touch and step voltage are the main components that required to be guaranteed to operate below the safety limit. Step voltage is generally defined as the voltage difference between the earth surface potential experienced by an operator bridging at 1m distance and without any contact with the earthed structure. For the case of the touch voltage, it is the voltage difference between the earth potential rise at the metal and the surface potential where a person is standing at (1m) from the earthed structure. Step and touch voltage limits depend on the tolerable current flow through human body and accidental circuit. Tolerable current depends on the critical limit that human can withstand before the ventricular fibrillation happens. These values depend on the duration of shock and magnitude of the current, while the British standard defined tolerable current as dependent of current path, duration and magnitude and the American standard defined the tolerable current as the limit that depends on weight, duration and magnitude of current.

Grounding design and procedure under power frequency is well described in many standards. However, grounding will perform differently when a lightning current discharge through the system, due to the inductive and capacitive effects. A large lightning current with a fast rise time will flow to the grounding grid, which will behave like an antenna, and induces large transient potentials in the system. The resulting potential can create a huge potential rise and electromagnetic coupling, which will lead to system malfunctions and errors, or even damage the valuable and sensitive electronic equipment.

Therefore, a study of grounding systems under lightning condition is vital to improve the performance and design. The study can be performed in three categories, namely laboratory tests, site tests and analytical modelling. The analytical modelling

method can be further divided into circuit, transmission line and electromagnetic approaches. In the proposed research herein, an analytical modelling based on the electromagnetic approach is adopted to investigate the impact of lightning current towards the grounding grid design. Simulations are carried out in three-dimensional (3D) geometry modelling, while a Finite Element Method (FEM) is used to solve the partial differential equations. The electromagnetic approach is chosen due to its accuracy of results that it computes based on Maxwell's equations.

On the other hand, the performance of the grounding grid under lightning current can be improved by reducing the soil resistivity, increasing the grounding grid size and mesh density. However, the grid is limited to a finite size, which is known as the effective area, and this can be achieved when there is no significant improvement in the grounding impedance with increasing grounding grid size. Besides, it is useful to enhance more conductors near the injection point and within the effective area to improve the impulse impedances .The impulse impedance is a value used to evaluate the grounding performance under lightning current, in other word, it is a ratio between peak potential rise at injection point and peak injected current. It is very important to understand the relationship between transient ground potential rise (TGPR) and impulse impedance, which will provide insights into how lightning current is dissipated through the grid. Furthermore, the grounding grid evaluation depends on the value of ground potential rise above the ground. Since the simulations are performed in 3D, post processing can be carried out to evaluate the transient ground potential rise (TGPR).

1.2 Objective of Research

Grounding is a main element in the lightning protection system that provides low impedance path for unwanted current through the soil. In substation grounding design, it is very important to maintain low step and touch voltages, which increases the level of safety. Although the grounding response and safety limits are quite different under lightning conditions, most of the standards are still based on power frequency safety hazards without any specific guidelines that consider fast transient response within the grounding design framework. It is challenging to achieve the best protection concurrently for both humans and equipment under lightning conditions.

In order to solve these shortcomings, this research aims to achieve the following objectives:

i. Study and review the effect of lightning current in a grounding grid, and understand human safety limits under power frequency and impulse currents.

ii. Perform a 3D grounding grid system modelling by using the electromagnetic approach with FEM

iii. Analyse the effect of down-conductor through the simulation of impulse impedance and effective area

iv. Consider and assess the improvements of grounding methodologies and topologies for lightning currents by introducing effective area empirical equations as an engineering guide.

v. Investigate transient grounding potential rise throughout the conductor and above the ground

1.3 Summary of Contribution

The main contributions and achievements of this research can be summarised as follows:

I. Modelling using Maxwell's equations in Electromagnetic domain, which considers the displacement current effect. The FEM is applied to solve the equations. Open boundary problems are solved by evaluating the current density between regions of interest relative to the perfect conductor boundary. Computer simulations are performed in time domain based 3D mode. Thereafter, the validations are performed by comparing with the simulation results from MoM and actual experiments.

II. The effects of various parameters of soil, lightning and grounding grid are used for a parameter analysis. In addition, the effect of the down-conductor is investigated to obtain better results for the effective area evaluation.

III. A new empirical equation for effective area is proposed, which is developed based on electromagnetic modelling. The equation takes into consideration the effect of the down-conductor during simulation.

IV. A transient ground potential rise is analysed to understand the relationship between the grounding impedance and the effective area.

Recently, computational modelling and evaluation can be carried out in accurate methods, due to the advancement in the ability of computer simulation. The modelling of the grounding grid by using the electromagnetic approach and FEM is an effective methodology to improve the understanding of electrical systems for different conditions and designs.

1.4 Thesis Organisation

This thesis is organized into 7 chapters, as described below:

Chapter2 provides a review of grounding grid design that are adopted from different standards. The chapter also discusses the effect of lightning current on the grounding systems based on both experimental and simulation results.

Chapter3 presents a review of the analytical modelling approach that is used to model the grounding grid under lightning conditions, where circuit, transmission line and electromagnetic approaches are discussed. In addition, a comparison between circuit approach and electromagnetic approach is given in this chapter.

Chapter4 proposes a grounding grid model based on Ampere's law from Maxwell's equation. The governing equation is solved by using the FEM, where the geometry modelling is performed in 3D with a solution produced in the time domain. More specifically, the simulations are performed for different values of soil resistivity, lightning current front time, location of injection, and grounding grid design using COMSOL Multiphysics commercial simulation package. The challenges and problems related to mesh geometry and open boundary will be discussed in this chapter.

Chapter5 presents a comparison of potential at injection point between power frequency and lightning injection current for the investigation on the effective area. The effects of the down-conductor are analysed for different depths. A new empirical equation is formulated for effective area calculation under the assumption of lightning current being injected at the corner and at the centre of the grid. The proposed equation also considers the effects of the down-conductor in the simulation framework. Subsequently, the equations are compared with the published empirical equations.

Chapter6 evaluates the transient ground potential rise throughout the grid. This evaluation demonstrates the relationship between grounding impedance and effective area. Step voltages are evaluated for different locations and distances from the injection point.

Chapter7 presents a conclusion based on the results and analysis drawn from this study, and recommendations are formed for future work within this chapter.

Chapter 2

A Review of Electrical Grounding under the Condition of Lightning Current

2.1 Introduction

The demand on electrical supplies is continuously increasing, hence making it more challenging to provide a high-efficiency system that ensures a constant power delivery to customers. Consequently, there is a steep rise in the development of new substation technologies and designs, which requires an improved safe grounding design. The following objectives need to be achieved to successfully design a safe grounding for a substation:

I. A low-impedance path to earth under normal conditions should be provided for circuit or signal reference, under fault conditions, and even at high frequencies (lightning currents).

II. A safe condition for human and equipment from ground potential rise (GPR) should be facilitated under any condition, and the radiation and conduction of electromagnetic emission either between or within the systems should be reduced.

Therefore, this chapter will present a review on the grounding grid design according to the standards and human electrocution limit that are proposed for impulse current. Thereafter, a review of the experimental and simulation results will be

presented to aid the understanding of grounding behaviour under lightning current. Apart from that, the TGPR are also discussed to gain a better understanding of step voltage and electromagnetic coupling under lightning current.

2.2 Tolerable Voltage for grounding grid design

The main objective of designing the grounding system is to provide a safe potential rise above the ground for both human and equipment. In order to design a safe substation, the values for limit of transfer, step and touch voltages are adopted from different standards. The limit is influenced by the definition of the step and touch voltages, allowable permissible current flow through human body and accidental circuit.

2.2.1 Tolerable voltage definition

The limits of step, touch and transfer voltages are a reference for grounding grid design. However, the definitions of each type of the voltages are different among the international standards. Touch, step and transfer potentials' definition can vary in various standards, as discussed in the followings:

According to **IEEE80[2]:**

- Touch voltage is the potential difference between the GPR and the surface potential in a situation where a person is standing and concurrently in contact with a grounded structure.
- Step voltage is the difference in surface potential experienced by a person that is bridging a distance of 1m with the feet, but without contacting any other grounded object.

- Transferred Voltage is a special case of the touch voltage, where the voltage is transferred into or out of the substation from or to a remote point that is external to the substation site.

According to **BS EN 50522[3]:**

- Touch voltage is the voltage between conductive parts that are simultaneously in contact

  NOTE: The value of the effective touch voltage may be appreciably influenced by the impedance of the person that is in electric contact with the conductive parts.
- Prospective touch voltage is the voltage between simultaneously accessible conductive parts with no contacts between the parts.
- step voltage is the voltage between two points and both will be attached to the earth's surface with a 1 m separation from each other, where the distance is considered as the stride length of a person

According to **BS 7354[4]**:

- Touch voltage is the sum of the voltage across a 1m surface along a diagonal line outside the corner of the grid, with the voltage difference of the grid with ground surface above
- Step voltage is the voltage over a 1m surface that is diagonally outward from the corner of the grid

2.2.2 Tolerable body current

Electrical current flow through the human body is a critical element that need to be considered to enable the evaluation of the safety system of an electrical system. The body current limit is the maximum current that can flow through the human body before it becomes fatal. Current flow through human body may induce the followings [5, 6]:

I. Asphyxia: Muscles in the respiratory system are required for inhaling and exhaling air through the lungs. Electric shock affects these muscles by inducing contraction, which consequently leads to death as a result of suffocation.

II. Cardiac arrest cause by ventricular fibrillation: The human heart is a pump that coordinates a rhythmical contraction and expansion of its muscular fibres to ensure circulation of blood throughout the body. When an electric current flows through these fibres, the heart rate becomes irregular, this factor causes uneven pumping of the heart, and eventually that leads to total cardiac arrest which the heart stop operating. Fibrillations are usually fatal because all of the heart muscle cells move independently.

III. Muscular contraction: This phenomenon can occur as a result of sufficient current flowing through a person when they are in contact with a live part of a transmission line. Muscular contraction occurs when the part of the body is in contact to the live part and the affected person does not have enough strength to escape from the grasp.

IV. Burns: Part of the electrocution process that heats up the tissues.

Each standard adopts different assumptions and values, which leads to different allowable step and touch voltages in the grid. One of the main parameters is the safe limit of current to conduct through the human body. The limits are defined based on the fibrillation threshold, which influences the current magnitude, current path, current time duration and frequency. The body current limit proposed in IEEE80 [2] is shown in Equation (2-1) for both 50kg and 70kg body weights at 50-60Hz .

In the case of British standards, curve C_1 and C_2 were used for left hand to feet as proposed in IEC 60479-1[7], which is depicted in Figure 2.1. The boundary between curve C_1 and C_2 represents a probability of ventricular fibrillation of up to 5%, while for the boundary between C_2 and C_3, the probability of ventricular fibrillation is also up to 50%. In order to find an alternative path for current flow, the current from the curve is divided with the hearth current factor, as shown in Table 2.1. These limit are applied for frequencies between 15-100Hz. However, no standard actually provides a detailed guideline for lightning current and high frequency current [8] .

$$I_B = \begin{cases} \frac{0.116}{\sqrt{t_s}} \text{for 50kg body weight} \\ \frac{0.157}{\sqrt{t_s}} \text{for 70kg body weight} \end{cases} \quad (2\text{-}1)$$

where t_s is duration of shock

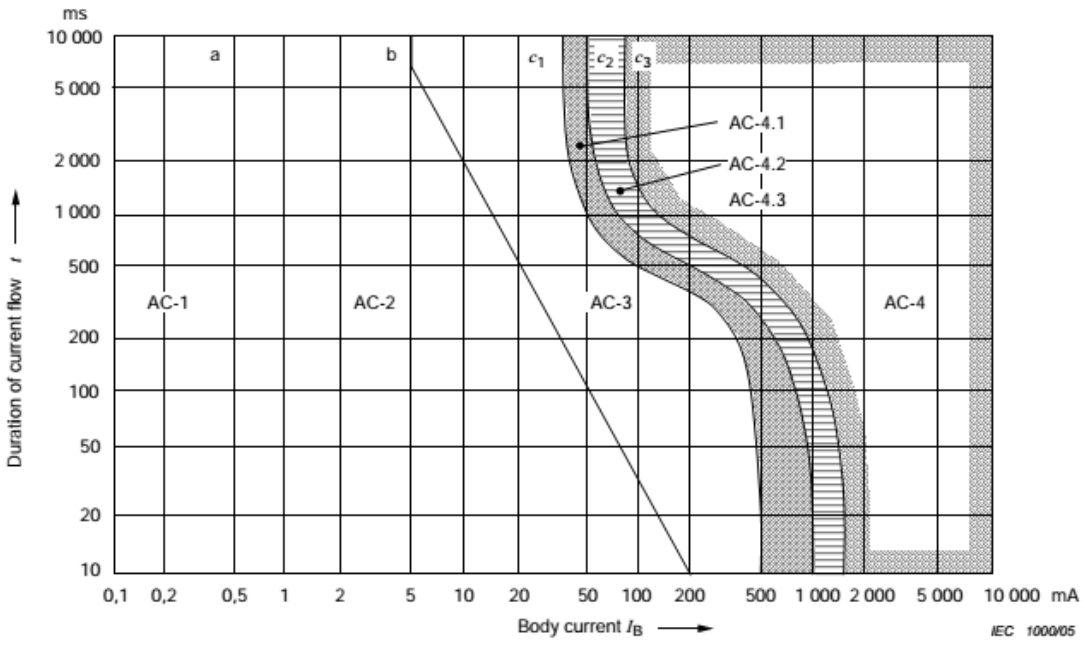

Figure 2.1: Effect of AC (15Hz to 100Hz) towards human body, from left hand to feet as defined in IEC 60479-1[7]

Table 2.1 Heart-current factor F for different current paths [7]

Current path	Heart-current factor F
Left hand to left feet, and right feet or both foot	1
Both hands to both foot	1
Left hand to right hand	0.4
Right hand to left feet, right feet or to both foot	0.8
Back to right hand	0.3
Back to left hand	0.7
Chest to right hand	1.3
Chest to left hand	1.5
Seat to left hand, right hand or to both hands	0.7
Left feett to right feett	0.04

2.2.3 Safety limit

The important parameters that need to be considered for a substation grounding design are the potential rise above the ground should be as low as possible to guarantee a safe current flow through the human body. ENA SR S36 [9] classified the substation as hot or cold depended on the transfer potential. A substation is classified as hot when the transfer potential exceed 430V and 650V depending on the reliability and speed of the protection circuit, as shown in Table 2.2.

Table 2.2 Maximum EPR for cold substation and the permitted transfer voltage [9]

Substation Voltage	Transfer Voltage	Comment
400kV, 275kV and 132kV	650V	
66kV and 33kV	650V	High reliability with main protection that normally operates between 0.15seconds and 0.5seconds, and has a backup protection
	430V	Normal reliability lines or clearance time in excess of 0.2 seconds
20kV, 11kV, 6.6kV	430V	

The definition of the touch and step voltages from different standards were presented in the previous subtopic. Generally, the limits of step and touch voltages are taken from the open-circuit voltage across the human body, which derives from the Thevenin theory. Figure 2.2 illustrates the equivalent circuit that is used to determine step and touch voltages according to the suggestion of American standard IEEE80-2000 [2].

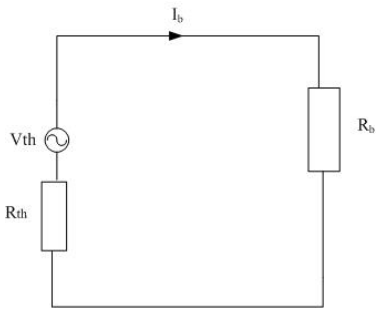

Figure 2.2 Equivalent circuit for touch and step voltages that adheres the IEEE 80 standard [2]

In Figure 2.2, *V*th is the Thevenin voltage (step or touch voltage), *R*th is the ground resistance of one foot which assumed as circular metallic disc with a radius of 0.08m, where the touch voltage is 1.5ρ and the step voltage is 6.0ρ. In this circuit, the footwear resistance is ignored and body resistance is assumed as 1000Ω. I_b is the body current calculated based on Equation (2-1). High resistivity layer normally spread at surface of soil above the grounding grid to increase the contact resistance between the soil and the foot of a person in a substation. In order to consider the high resistivity layer effect, a corrective factor C_s is introduced to compute the foot resistance as shown in Equation (2-2), where ρ_r is the resistivity of the surface material and h_r is the thickness of the layer.

$$C_s = 1 - \frac{0.09\left(1-\frac{\rho}{\rho_r}\right)}{2h_r+0.09} \tag{2-2}$$

Step and touch voltage limits can be calculated by applying Equation (2-3). The value of C_s is equal to one when there is no protective layer in the design.

$$V_{touch} = I_b(R_b + 1.5C_s\rho)$$
$$V_{step} = I_b(R_b + 6C_s\rho) \tag{2-3}$$

According to BS7354 standard [4], the touch voltage has a parallel formation, while the step voltage has a series formation, as depicted in Figure 2.3.

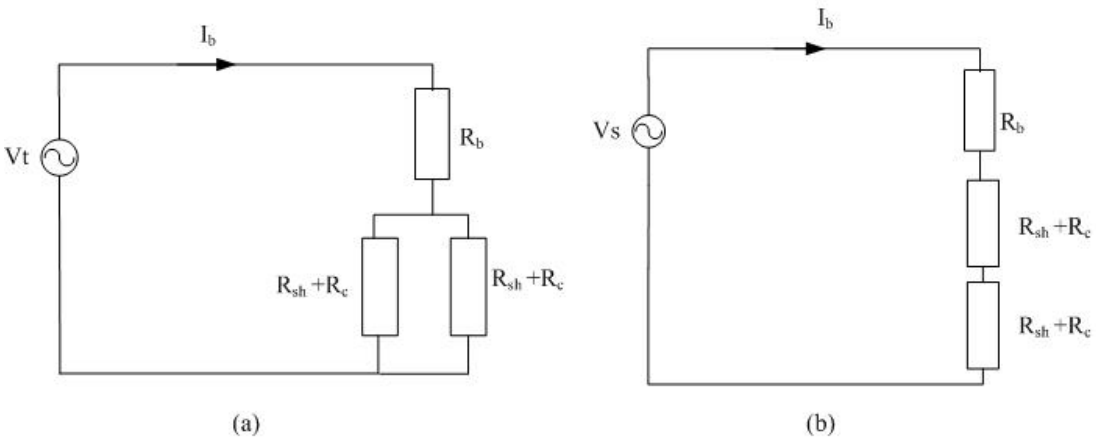

Figure 2.3 Accident circuit topologies for (a) touch voltage and (b) step voltage designed according to BS 7354 [4]

In Figure 2.3, *V*t is the touch voltage, *V*s is the step voltage, footwear resistance (R_{sh}) is fixed at 4kΩ, contact resistance (R_c) is 3ρ and body resistance is similar to IEEE80-2000 standard, assumed as 1000Ω. Current flow through the body is taken from curve *c*2, which corresponds to a 5% probability of ventricular fibrillation. Therefore the permissible voltage can be calculated by applying Equation (2-4). High resistivity layer can be considered as an effective resistivity to replace soil resistivity, ρ_{eff} as shown in Equation (2-5).

$$V_{touch} = I_b\left(3000 + \frac{(3\rho)}{2}\right)$$
$$V_{step} = I_b(9000 + 6\rho) \quad (2\text{-}4)$$

$$\rho_{eff} = \rho_{rock}\left(1 + \frac{h_r(\rho_{soil} - \rho_{rock})}{20(\rho_{soil} + \rho_{rock})}\right) \quad (2\text{-}5)$$

According to BS 50522 standard [3], if a grounding is satisfied as permissible touch voltage, step voltage will not contribute any hazardous factor. The maximum

permissible voltage is calculated based on the circuit shown in Figure 2.4 and Equation 2-6

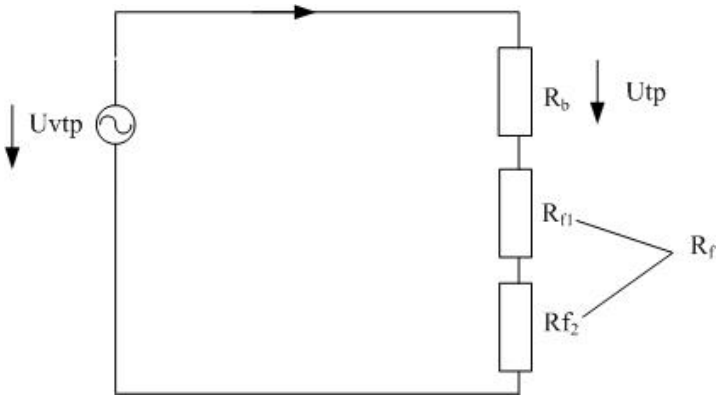

Figure 2.4 Accident circuit according to BS 50522 standard [3]

Where:

U_{vtp} Voltage difference acting as a source voltage in the touch voltage circuit with a limited value that guarantees the safety of a person when additional known resistances are applied (for example footwear, standing surface insulating material).

R_b Total body impedance depends on the touch voltage and current path. Body impedance for hand to hand or hand to foot are adapted from IEC 479 standard. A correction factor needs to be applied for different paths of current. For example, 0.75 for hand to both foot and 0.5 for both hand to foot.

I_b Current flowing through the human body. Curve *C*2 from curve in figure with probability of ventricular fibrillation is being less than 5% for left hand to feet.

U_{tp} Permissible touch voltage, the voltage across the human body is based on graph show in Figure 2.5.

R_f additional resistance (RF = RF1 + RF2)

R_{f1} Resistance of the footwear is 1000Ω

R_{f2} Resistance to earth of the standing point is assumed as 1.5ρ

$$U_{vTP} = U_{tp}(t_f) + (R_{f1} + R_{f2})I_b \quad (2\text{-}6)$$

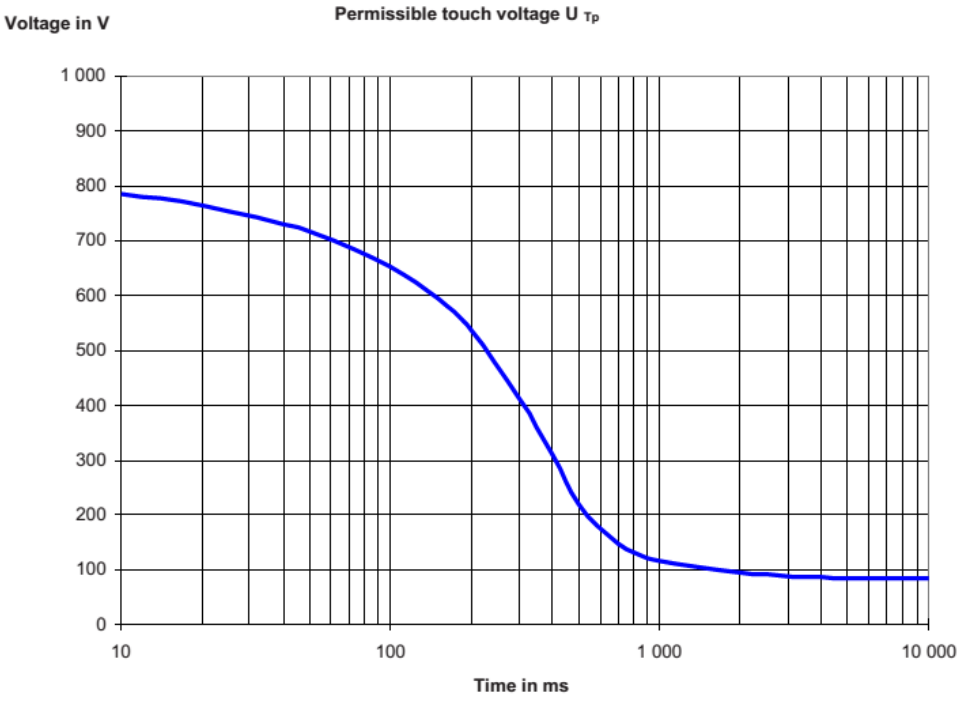

Figure 2.5 Permissible touch voltage based on fault duration [3]

Different standard required different accident circuit and body current limit, hence providing different safety limit in the grounding grid design. Table 2.3 presents the parameters that are considered as the limits for touch and step voltages by IEEE80, BS 7354 and BS EN 50522 standards.

Table 2.3: Parameters from different standards to calculate step and touch voltages limit [10, 11]

	IEEE80-2000	BS7354	BS EN50522:2010
Body resistance (R_b)	1000Ω	1000Ω	Related to the current path and touch voltage, 50% probability of body impedance
Thevenin resistance (R_{th})/ contact resistance R_c	1.5ρ for V_t 6ρ for V_s	1.5ρ for V_t 6ρ for V_s	1.5ρ for V_t
	Where V_t= Touch Voltage , Vs= Step Voltage and ρ= soil resistivity (Ω.m)		
Surface layer resistivity (ρ_r)	Considered in $C_s\rho_r$ (C_s: correction factor)	Considered in ρ_{eff}	Mentioned, but no value provided
Footwear resistance (R_{sh})	Ignored	4kΩ	1kΩ
Tolerable body Current (I_b)	Equation 2-1	Curve C2 IEC60479-1	Curve C2 IEC60479-1

2.3 Electrical safety under lightning current

Lightning is a natural phenomenon, which occurs during the electrostatic discharge in cloud that attempts to strike the ground. Lightning contains a huge amount of energy that contribute damage to any path that it chooses to reach the ground. Table 2.4 presents the fatality rate per million people categorised by country due to lightning [12]. It can be observed that for a nation, the state of economic development and geographical location actually determines the number of lightning accidents [13], which is directly related to ground flash density at global level. It is well known that the ground flash density around the equator is the highest compared to other locations [14, 15].

Table 2.4 Annual lightning fatality rate per million people categorised according to different countries[12]

Region Country	**Period**	**Annual fatality rate per million**
Africa		
S. Africa	1997-2000	6.3
Malawi	2007-2010	84
Swaziland	200-2007	15.5
Uganda	2007-2011	0.9
Zimbabwe	2004-2013	14-21
Asia		
China	1997-2009	0.3
India	1967-2012	2
Japan	1990-1997	>0
Malaysia	2008-2011	0.8
Singapore	1970-1979	1.5
Australia		

Australia	1980-1989	0.1
Europe		
Austria	2001-2010	>0
France	1990-1995	0.2
Greece	2000-2010	0.1
Lithuania	1994-2003	0.1
Poland	2001-2006	0.3
Turkey	2012	0.3
United Kingdom	1993-1999	0.1
North America		
United state	2003-2012	0.3
Canada	1190-2004	0.2
South America		
Brazil	2009-2009	0.8
Colombia	2000-2009	1.8

Electric shock experiments were carried out before the era of 1950s on different types of animal, where the experiments included sheep, calf, pig and dog hearts to analyse the effect of the current on ventricular fibrillation [16]. In the 1930s, electrical shocks were tested on rats, with injection terminal placed on different locations [17, 18]. Later, tests for different frequencies of the injection current were carried out [19]. In the mid-1950s, Kouwenhoven et. al [20] tested capacitor discharge through a dog's heart. Based on the experimental data published from 1930 up until late 1950s, Dalziel [21-24] extrapolated the animal data to humans, simply because such test cannot be performed on humans. Using a statistical analysis with a minimum possibility of 0.5%, Dalziel [25]proposed the formulation that engineers will apply during the safety evaluation of an electrical system and design, as shown in Equation 2-1. However, the

behaviour and effect of current flow in human body is different in high frequency or impulse current [26-28].

Currently, there is a very limited knowledge about the safety limit of impulse currents that can pass through the human body. Based on the animal electrocution experiments by using power frequency current, a comparison was made with impulse electric shock accidents, as depicted in Figure 2.6. As a result, Dalziel [29] found that the impulse current rating is 50 watt-seconds.

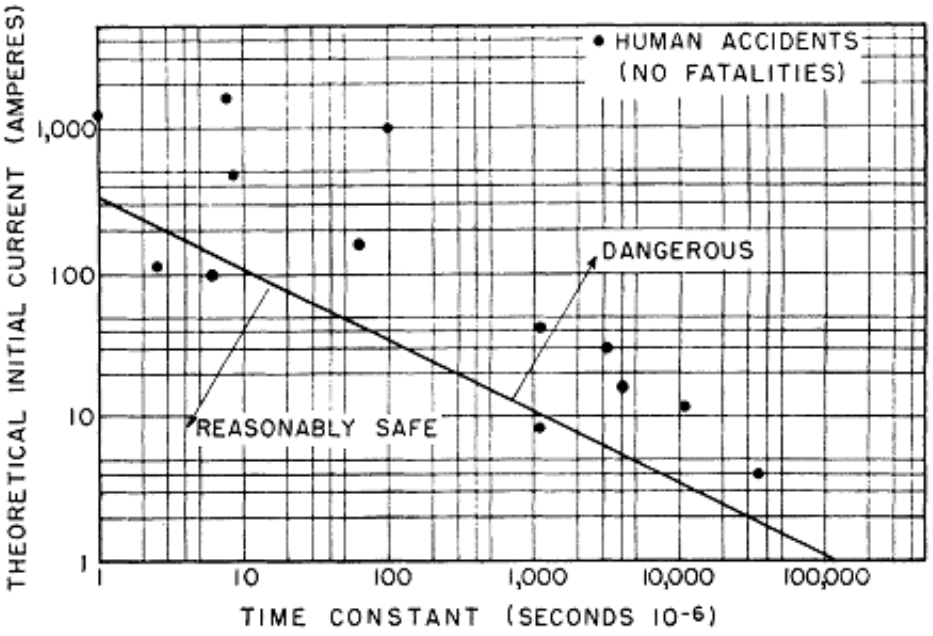

Figure 2.6: Relationship between theoretical initial current to time constant and computed points from human surge discharge accidents [29]

In the 1970s to 1980s, experiments were performed by T.Ishikawa on warm-blooded animals, including rabbits, rats and mice [30, 31]. The effect of an artificial respiratory system, multiple lightning strokes, and the location of injection current were also studied in various experiments by T.Ishikawa. Such experiments were carried out to establish the lethal energy that is proportional to the weight of the animal. A value per unit weight of 62.6±11.9J/kg was suggested as lethal for life, while, Portela

[32] introduced a perception limit and pain limit, based on charge as shown in Equations (2-7) and (2-8).

$$S_{perception=} \int |i_c|\, dt \leq 0.36\mu C \text{ to } 0.9\mu C \tag{2-7}$$

$$S_{pain} = \int |i_c|\, dt \leq 7.6\mu C \tag{2-8}$$

The International Electrotechnical Commission (IEC) provided the parameters for the limit of tolerable body current as a function of impulse current [7, 33]. Figure 2.7 shows the probability of fibrillation when the rms current flows between the human left hand to the foot for a duration between 0.1ms and 10ms. This result basically exhibits the amount of current that can pass through a human body. I_{rms} for impulse can be calculated by converting either a sinusoidal or a capacitor impulse to a rectangular impulse, as shown in Figure 2.8.

T.Bernstein [34] suggested that 10 to 50 Joules will be absorbed by the human body, which will lead to ventricular fibrillation. The suggestions were formed on the value proposed by Dalziel on impulse current, and the relative energy absorbed in the power frequency minimum energy limit [34]. In a radiated field study, radiation field is not established as a factor that can cause ventricular fibrillation or cardiac problems. However, the exposure to radiated electromagnetic fields was primarily related to heat that can damage human tissue [35]. The guide in Appendix A [35] provides the safety limits for human exposure to electric and magnetic fields. Table 2.5 presents a summary of the published electrical safety limits for humans. It is important to note that the values of safe energy for impulse current are still lacking of factual information, due to lack of research and limitations of experiments.

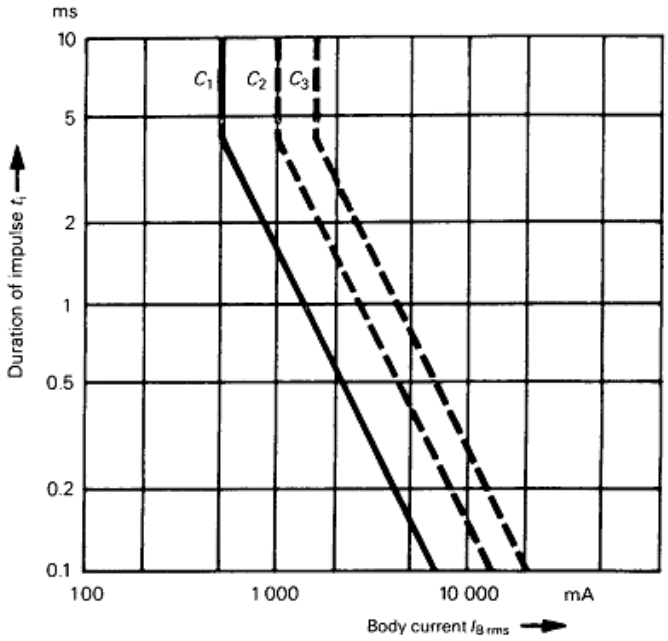

The curves indicate the probability of fibrillation risks for current flowing in the path left hand to feet.

below C_1: no fibrillation,
above C_1 up to C_2: low risk of fibrillation (up to 5 % probability),
above C_2 up to C_3: average risk of fibrillation (up to 50 % probability),
above C_3: high risk of fibrillation (more than 50 % probability).

Figure 2.7: Lightning hazard impulse current flowing through human [7]

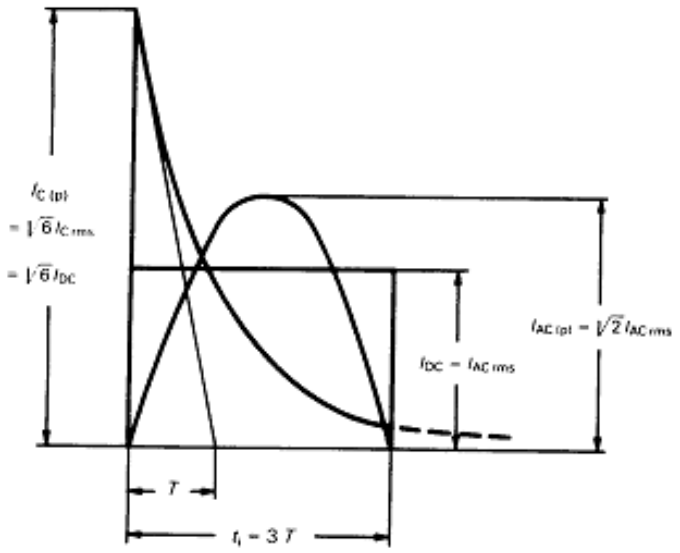

Figure 2.8 Rectangular, sinusoidal and capacitor discharge impulse demonstrates similar energy level for a fixed shock duration [7]

Table 2.5: Summary of published electrical safety limits for humans

Reference Document	Publish Level
IEEE [2] (Power frequency)	$I_B = \begin{cases} \frac{0.116}{\sqrt{t_s}} \text{ for 50kg body weight} \\ \frac{0.157}{\sqrt{t_s}} \text{ for 50kg body weigh} \end{cases}$ Assumes 1000Ω body resistance energy limit is 13.46J for 50kg and 24.65J for 70kg weight.
IEC 60479-1 (10Hz to 100Hz) [7]	Figure 2.1
Dalziel [29]	50J with 1000Ω body resistance
T.Ishikawa et al. [30,31]	62.6±11.9J/kg
Portela [32]	$S_{perception=} \int \lvert i_c \rvert \, dt \leq 0.36\mu C \; to \; 0.9\mu C$ $S_{pain} = \int \lvert i_c \rvert \, dt \leq 7.6\mu$
IEC 60479-2 [33]	Refer to Figure 2.7, limitation from 0.1ms to 10ms duration of square impulse
T.Bernstein [34]	10J-50J
ICNIRP [35] (Radiated field)	Electric and magnetic field limit (Appendix A)

2.4 Effect of impulse current on grounding system

In a lightning protection system, there are two methods that divert the lightning current into the grounding system. Firstly, when the lightning directly strikes the ground structure, as illustrated in Figure 2.9(a). Secondly, when lightning strikes a nearby transmission line, where a surge arrester diverts the lightning surge to ground before it reaches the system, as depicted in Figure 2.9(b)

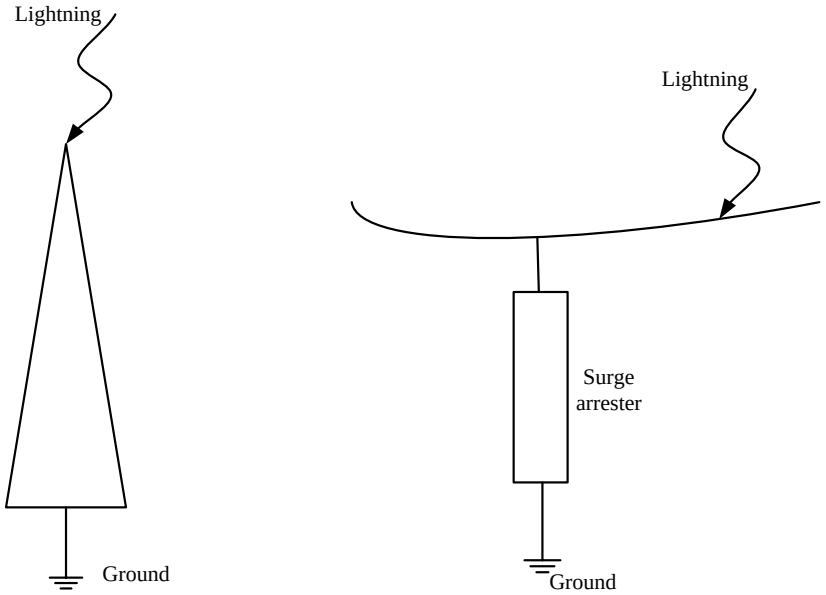

(a) Direct strike (b) Indirect strike

Figure 2.9: Lightning current path diverted to the ground by lightning protection system

Since the early 19th century, the performance of grounding systems for lightning current had been studied to gain better understanding and to introduce new improvement to the protection system [36-39]. Basically, any ground termination point presents resistive, capacitive and inductive effects. Furthermore, at lower frequencies, the resistive effect is significant, but at higher frequencies, the inductance and capacitance influence the behaviour of the grounding system.

During the transient investigation, impulse impedance is commonly used to represent the performance of the grounding under impulse current. Generally, the impedance value can be determined by the ratio of peak voltage to current at the feeding point of electrode at specific time instants. However, usually the impedance value is calculated as a ratio of maximum voltage to maximum current [40]. Since the current and voltage peak does not occur at the same time , some of the researcher calculate the impulse impedance as a ratio of voltage to current at the instance of maximum measured current [37, 41]. Although transient impedance is a dynamic change to the grounding electrode under impulse condition, it can still be calculated as the ratio of instantaneous voltage, V(t) rising to the excitation of current, I(t)[42, 43]. In this research framework, impulse impedance is defined as the ratio of peak voltage to peak current at the injection point, as formulated in Equation (2-9) .

$$Z = \frac{V_{peak}}{I_{peak}} \tag{2-9}$$

In order to relate the grounding performance under impulse current to grounding resistance at power frequency, the impulse coefficient can be calculated as:

$$A = \frac{Z}{R} \tag{2-10}$$

where Z is the impulse impedance and R is resistance at power frequency. Values of A can be larger or smaller than 1, which depends on the soil parameters and grounding design. A number of field tests, lab experiments and computer simulations have been performed to improve the understanding of grounding system behaviour under impulse current.

There are two main characteristics that influence the dynamic behaviour of grounding impedance under lightning current:

I. Soil behaviour as a semi-conducting medium will absorb high energy current, which is influenced by the soil parameters.

II. Electromagnetic coupling between all grounding components, including wave propagation effects that are influenced by grounding conductor arrangement and design.

The first characteristic improves the grounding performance by effectively increasing the size of the grounding conductor during soil ionisation, while the latter may result in increased grounding impedance at higher frequencies, compared to the low-frequency grounding resistance.

2.4.1 Single electrode configuration

Early field tests and experiments demonstrated that the impulse coefficient to be less than unity for vertical and horizontal grounding rod configurations [44-46]. In addition, the reduction of impulse impedance was proportional to the magnitude of the current for the grounding electrode test [37, 47]. In some lab experiments and tests on soil samples, it was found that soil ionisation behaviour led to dynamic behaviour of the grounding impedance [41, 47-49]. Soil ionisation takes place when the current density is concentrated to the surrounding of the conductor surface, and subsequently current flows through the soil. As a result, the electric field in this region exceeds the critical field value, which causes ionisation and electrical discharge in the soil. In the era of 1970s, Liew et al. [41] assumed that the soil breakdown increases the effective diameter of the conductor uniformly along its length, as depicted in Figure 2.8. This behaviour will increase the electrode dissipation area due to the enlargement of the size of the grounding conductor, see Figure 2.10. The dynamic model proposed by Liew can be further divided into three stages, see Figure 2.11, where stage (a)

represented a constant resistivity for the increasing current density; stage (c) demonstrated when the current density reached the critical current density, which led to soil breakdown and decreasing soil resistivity value; and for stage (b) as the current decreased, the resistivity recovered to the original value.

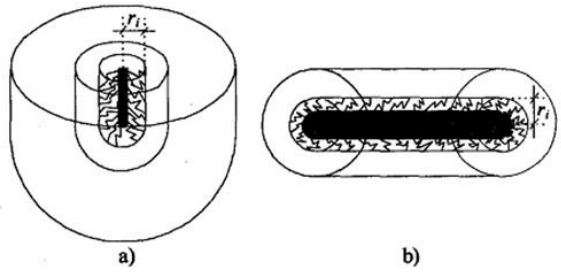

Figure 2.10: Soil breakdown model proposed by Liew[41]

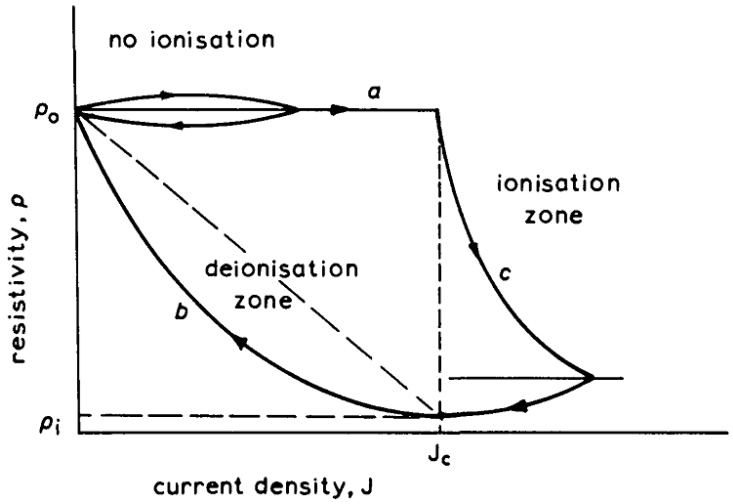

Figure 2.11: Dynamic model for soil ionisation process [41]

As current discharges to the ground electrode, electric field will be generated according to the following expression, $E=\rho*J$. Therefore, the current density is proportional to the electric field surrounding the electrode. The electrical critical value, E_c had been determined by many researchers through a series of experiments on different types of soil. Various values of E_c were suggested by previous researchers, where A.M. Mousa [49] suggested a value of 300 kV/m, while Cigre [50] suggested

a value of 400 kV/m as the critical field strength before the ionisation occurred in the soil. The effect of the soil resistivity, impulse polarity and electrode dimensions were investigated though various lab experiments [51]. In the case of electric field critical value, the range of 550kV/m to 900kV/m were suggested. The threshold of electric field depended on the grounding configurations, soil profile, and impulse impedance of the grounding [48, 52, 53].

The recent field test revealed that the behaviour of grounding the rod was different when the length increased [45]. Figure 2.12 illustrates the impulse and DC resistance for different electrode lengths, where it is clear that the impulse resistance will reach a saturation point quicker compared to the DC resistance. In the test, impulse resistance is measured as the ratio of peak value voltage V_p rise to peak excitation current I_p. The saturation point is defined as the effective length, which shows no improvement in electrode resistance with further increase in length. It can be observed from the graph that the grounding impulse resistance will be higher than the DC resistance when it reaches certain length.

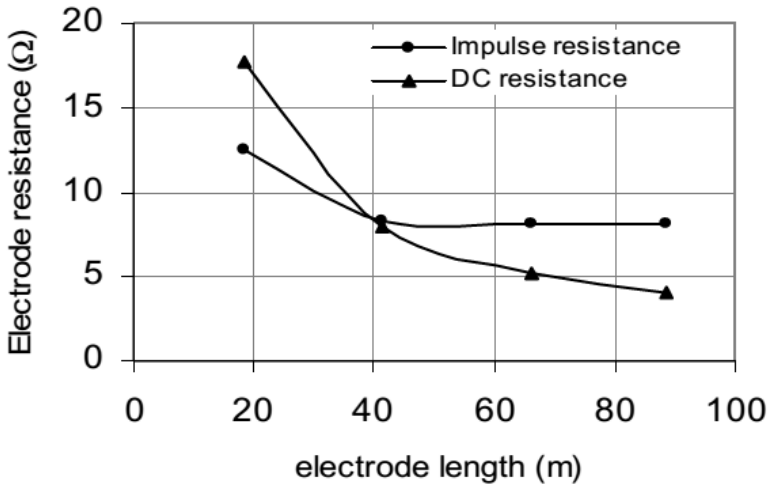

Figure 2.12: Electrode resistance for different lengths of grounding electrode [45]

Visacro et al.[44] tested different lengths of grounding rod with various impulse front times, including for both low and high-resistivity soils. The results revealed that the impulse coefficient is greater than unity when the grounding rod achieved its effective length (L_{EF}), as depicted in Figure 2.13 [54]. Most importantly, the relationship exhibited that the effective length is achieved when the grounding impedance equals to the grounding resistance.

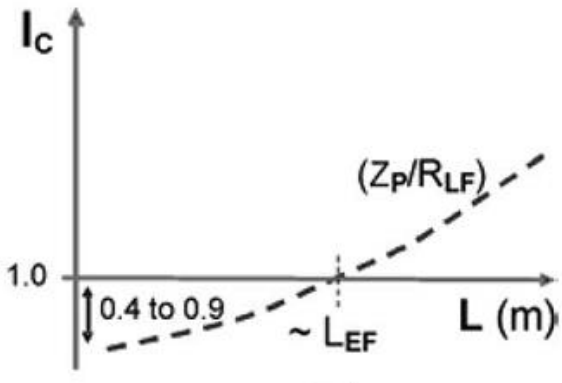

Figure 2.13: Impulse coefficient for different lengths of electrode [54]

The effective length value can be calculated based on the equations suggested from mathematical modelling and simulation for different soil resistivity and front times [55, 56] . Lightning current test on practical grounding configuration with multiple rods were done to improve the knowledge on grounding rod behaviour under lightning current [57-60] .

2.4.2 Grounding grid configuration

The grounding grid configuration is a more complex design, which involves more grounding conductors that covers a bigger area. Grounding grid configuration is normally used for substation grounding design to avoid hazardous step and touch voltages from humans or equipment located above the ground. There are very costly

to conduct experiments or tests to study grounding grid behaviour under lightning or impulse conditions.

Gupta and Thapar [40] prepared a 6m diameter hemispherical electrolytic tank to perform laboratory tests on grounding grids. Two resistivity values based electrolytes were used, namely 19Ω.m and 7.2Ω.m. Grid sizes were 1m x 1m and 2m x 2m, with a 16 mesh grid, and impulse current was injected at either the corner or the centre of the grounding grid. From this experiment, it was shown that the impulse impedance was greater than the power frequency impedance for all cases, and the effect of location of injection demonstrated that the corner injection impulse impedance was slightly higher compared to the centre injection. The experiment related to injection location was also performed by Rammamorty.*et.al* [61], who showed that the corner injection generated a greater potential rise compared to centre injection.

Stojkovic et al. [62] completed an experiment on two layers of soil, where the first layer is with 20Ω.m and 50Ω.m on the second layer. The thickness of first layer is 0.6m. An impulse generator was used to produce a 3.5μs to 16μs front time with 4.7 to 12.1A impulse current. Three configurations of grounding grid and location of injection are shown in Figure 2.14 are buried 0.5m below the surface. The voltage at the injection point was measured to calculate the impulse impedance. The results for all the cases demonstrated that the impulse impedance was greater than the power frequency resistance. In addition, it was also found that a short front time generated more potential at the injected point.

Visacro et al. [63-65] developed an experiment for 16m x 20m grid size with a 4m x 4m mesh size, buried 0.5m deep in a 250Ω.m resistivity soil. Low frequency resistance was measured at 6.5Ω. Different front times at 150ns, 0.7μs, 2μs, and 4μs were injected at the corner, side and centre of the grid, as shown in Figure 2.15. Table

2.3 presents the impulse impedance for different front times and locations of injection. It can be observed that the short front time and injection at the corner of the grid generated more potential in all scenarios. In addition, impulse impedances were larger compared to low-frequency resistance for most of the scenarios, except for the cases of centre and side injection for a 4μs front time, and centre injection for a 2μs front time impulse. The author believed that this differences were due to the effect of the slow front time, which increased the effective length of the grid.

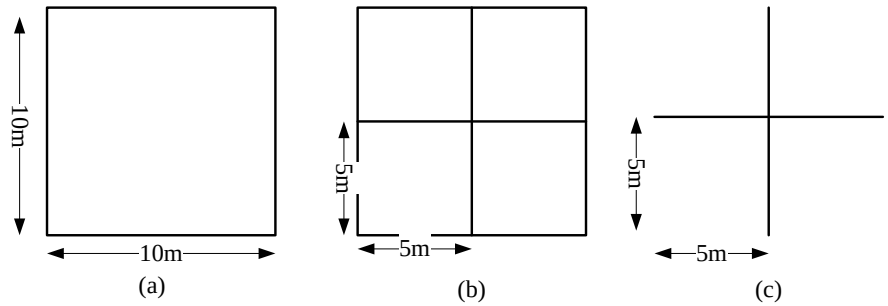

Figure 2.14: Stojkovic grid configuration [62]

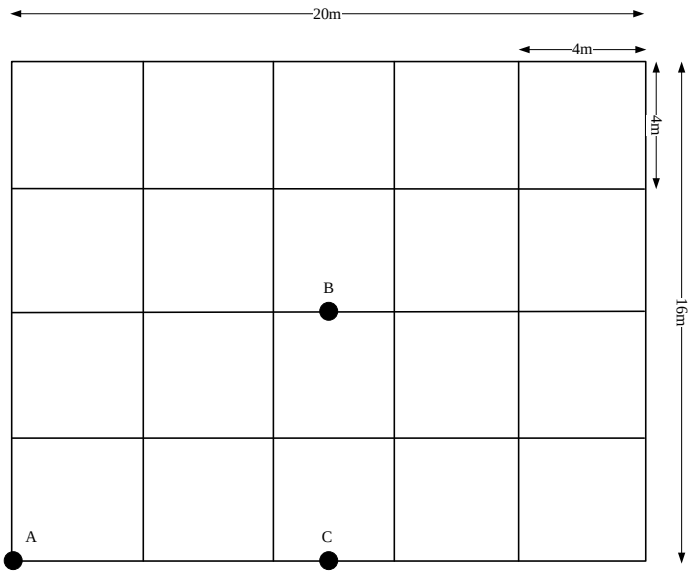

Figure 2.15: Grid configuration and injection point location

Table 2.6: Grounding impedance for different locations of injection point and front time [63-65]

	Grounding impedance ($Z=V_p/I_p$) Ω			
Front time	150ns	0.7μs	2μs	4μs
A(Corner)	49	21	9.5	6.9
B (centre)	32	10	5.8	5.3
C (Side)	36	12	6.7	5.6

In a different scenario, D.Guo et al. [66-68] developed an experiment on a reservoir to provide more data to understand the grounding grid behaviour under impulses. A 5m x 5m grid was used, with 25 equal meshes positioned at 0.2m below the water surface. In this experiment, a low voltage impulse current with 12/40μs waveform was injected at the corner of the grid, to calculate the ground resistance of the grid. As a result, the ground resistance value demonstrated a good agreement with measured values by applying both DC and 50Hz sinusoidal current. In addition, experiments were performed to analyse the potential distribution at the surface of the water with 52Hz of AC current and 12/40μs impulses injected directly to the grid.

It can be concluded from the experiments that a short front time can lead to a high potential, and centre injection provides better performance compared to a corner injection point. From these experiments and field tests, it is clear that the resulting outcome are very useful to verify any analytical or numerical simulation modelling.

2.5 Simulation of grounding grid under impulse current

Experimental and field testing of grounding grids is very limited, due to the requirement of large space and the associated high cost. In order to improve the knowledge in this area, many researchers carry out investigation of transient grounding either in analytical or numerical models. Simulation can be used to study other parameters that influence the behaviour of grounding grids under transients, and the resulting information can be used by engineers to design better grounding grids. Apart from that, simulation and modelling can also be applied to evaluate the grounding grid configurations, soil properties and impulse waveforms.

2.5.1 Influence of soil parameter and grid configuration

Soil resistivity is the main parameter that influences the grounding impedance, where the resistivity depends on several factors, namely chemical composition, geology, water and salt contents of the soil. Most of the factors have a dependency on the geographical characteristic and seasonal factor [1]. Therefore, engineers need to know the soil profile and characteristics before selecting a grounding location. Ground potential rise was reported as proportional to the soil resistivity value by previous researches [69]. Al Maghribi and Zedan [70, 71] simulated 100m x 100m grounding grid by using CDEG software to analyse the effect of different parameters. The results shown a similar trend on the potential rise at injection point, which reflects on the proportionality with soil resistivity. However, soil permittivity contributes a significant effect when the soil resistivity is above 1kΩ.

As shown in Section 2.4.2, the front time of the lightning current and location of the current injection influences the potential at the injection point. A short front time generates higher potential compared to the long front times, as proven both

experimentally and via simulation in [72-74]. The work in [73] showed maximums of the transient GPRs are occurred on the highest steepness of the current impulses for different front time. It can be concluded that the steepness is the high frequency element that increases the inductive effect of the grounding grid.

Grounding configuration and design is essential to provide optimum protection from any potential rise above the grid. Figure 2.16 exhibits the size and the span that can be used to achieve better grounding performance. Grid size is total size of the conductors while being covered, and mesh is the distance between conductors inside the grid. As reported in [40, 56, 74], increasing the size of grid reduced the grounding impedance, but the reduction was limited to certain sizes known as effective area, and will be discussed further in the next section. Applying the dense mesh size near the injection point can reduce the grounding impedance at injection point [56]. This hypothesis agrees with the results revealed by Al Maghribi and Zedan [70, 71], which increased the mesh density from 4 meshes to 16 meshes and finally to 100meshes, with 100mx100m grid size that improved the potential rise at injection point.

In addition, the location of the current injection can influence the potential rise value. L.Grcev and Gupta [40, 56] showed that the corner injection will have double potential compared to centre injection. While Zeng et al. [74] reported that corner injection produced a ground potential rise of 60% higher compared to centre injection. This is because the centre injection point generates less potential compared to corner injection point

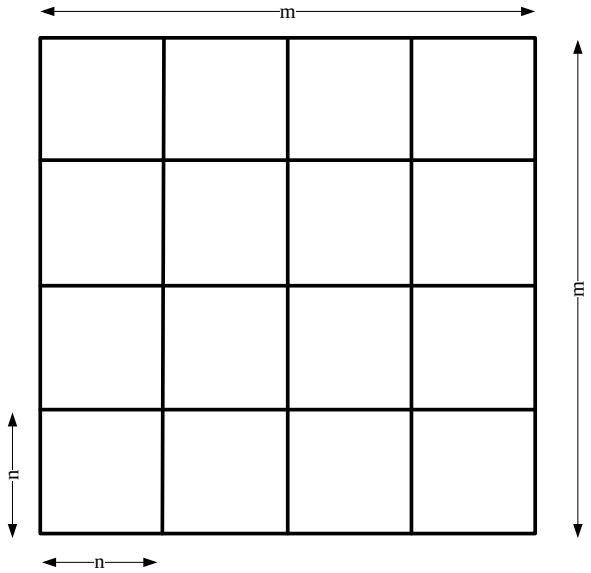

Figure 2.16: Grounding grid size and mesh size

2.5.2 Effective area of grounding grid

The effective area is an important criterion to improve the grounding grid design under the circumstance that require the handling of lightning current. There are several definitions leading to different numerical equations to calculate the effective area for a transient current flow. Gupta-Thapar [40] defined the effective grounding area that is shown in Figure 2.17, where this result is achieved when the grounding impedance at the injected point was maintained within 3% of the final value of the grounding impedance [40]. The final value is achieved when the grounding impedance remained constant with the increments of grounding grid size.

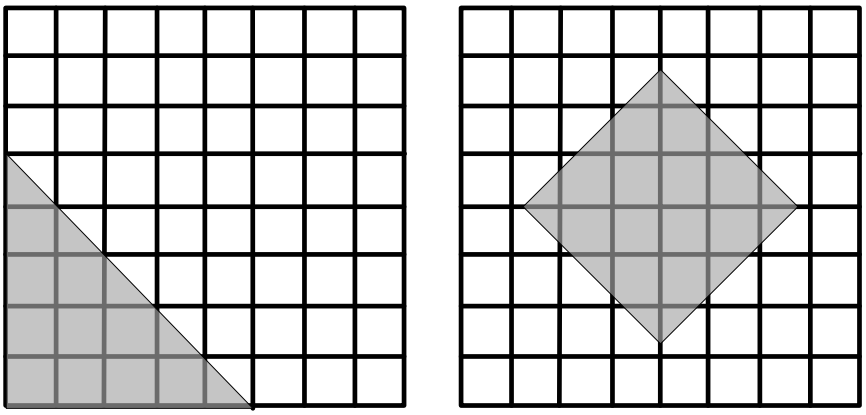

Corner Injection point Centre Injection point

Figure 2.17: Illustration of effective area as proposed by Guptar and Thapar [40]

The effective area is represented by an equivalent circle, with a radius calculated by using Equation (2-11)

$$\begin{aligned} r_{effective} &= K(\rho T)^{0.5} \\ K &= (1.45 - 0.05S) \text{ for center fed grid} \\ K &= (0.6 - 0.025S) \text{ for corner fed grid} \end{aligned} \tag{2-11}$$

where ρ is the soil resistivity in Ω.m, S is the spacing between conductors of the grid in m, and T is the wave front time in μs. On the other hand, Equation (2-12) is an alternative formula that was introduced by Zeng et al.[74]. This is similar to Gupta's definition, but the analysis is based on a circuit model that considers the soil ionisation. In the equation, limit of grid size is not mentioned but it is based on simulation that used 5mx5m mesh size[74].

$$\begin{aligned} r_{effective} &= 0.21\rho^{0.42}T^{0.32} \text{ for corner fed grid} \\ r_{effective} &= 0.34\rho^{0.42}T^{0.32} \text{ for center fed grid} \end{aligned} \tag{2-12}$$

Grcev [69] defined the effective area as the platform of the grid that can reduce the impulse impedance by applying increasingly dense meshes within the area, where the illustration is shown in Figure 2.18.

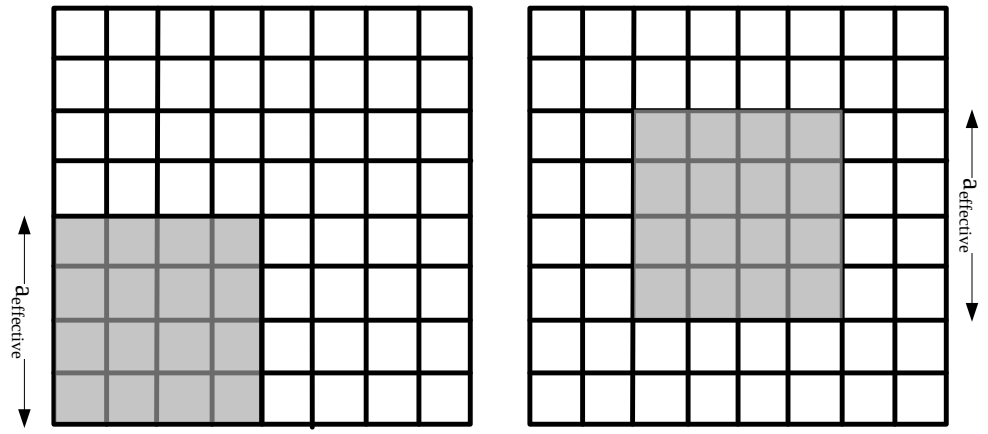

Figure 2.18: Illustration of the effective area as proposed by L.Grcev [57]

By determining the impulse coefficient, the effective area is achieved when the grounding impedance value is equal to the low frequency resistance. The side position of a square effective area can be calculated by using Equation (2-13). The equation has a limitation of 5m to 10m mesh size.

$$a_{effective} = K.\exp\left[0.84(\rho T)^{0.22}\right] \quad (2\text{-}13)$$

$K = 1$ for center fed grid

$K = 0.5$ for corner fed grid

All of the above formulations are based on impulse impedance (at the injected point), which reduces with the increasing size of the grounding grid. Table 2.7 presents a comparison of simulation parameters that are used for the proposal of empirical equations for the effective area. It can be observed that all of the previous simulations do not consider the depth impact of the buried grid, and as well as ignore the effect of the down-conductor to the grid. In addition, the Grcev formulation is based on a fast rise time and different soil resistivity, which did not take into consideration the long rise time.

Table 2.7: Comparison of simulation data from literatures to determine the effective area

Effective area equation	Injection point	Data used to determine the equation	
		Front time (μs)	Soil resistivity (Ω.m)
Gupta et al.[40]	Direct to the grid (Middle injection), buried depth was not reported	5	50,100,500,1000
		1,3,4,5,9	100
Grcev [56]	Direct to the grid (Middle injection), with 0.5m buried depth	0.8	10,30,50,100,300,500, 1000
Zeng et al. [74]	Direct to the grid (corner injection), with 0.8m buried depth	1	100,500,1000
		2.6	
		5	
		9	

2.5.3 Ground Potential Rise

The ground potential rise above the ground is a major contributing factor to lightning accidents. The gradient of the voltage over distance can create a harmful potential difference for humans, animals and equipment. Table 2.8 presents the

distribution of lightning accidents categorised according to various mechanisms. The table exhibits that the step voltage is the main mechanism of lightning incident that affected humans. Therefore, it is very important to keep the ground potential rise below a safety value.

Table 2.8: Distribution of lightning accidents categorised according to mechanisms [75, 76]

Mechanism	**Distribution**
Direct strike	3-5%
Side flash	30-35%
Contact potential	15-20%
Step voltage	50-55%
Upward streamer	10-15%

Dawalibi et al. [77, 78] simulated the potential rise throughout the grid with injection current frequencies of 60Hz and 500 kHz. Current was injected directly into the grid or at a structure above the ground. Figure 2.19 illustrates the scalar potential rise for both frequencies over the grid. It is clear that the scalar potential rise for high frequency current possesses a very high peak value near the injection point, and decreases along the distance. It can create high potential differences between two points that are near to the high frequency injection point. As reported in [79], high peak potential rises near the injection point within the first few microseconds. During the transient period, the potential between the points are required to be considered in the grounding evaluation. The transient potential rise is proportionally larger for high currents and poor resistivity soil [80]. Transient potential rise induces the step and touch voltages to rise near the injection point, and then to gradually fall [81]. Step

voltage evaluations on different grounding terminations in the case of lightning current were reported in [82-84]. Step voltage limits are derived from the limits suggested by IE60479-2 standard, as shown in Figure 2.7, which considered the heart current path factor [7, 33].

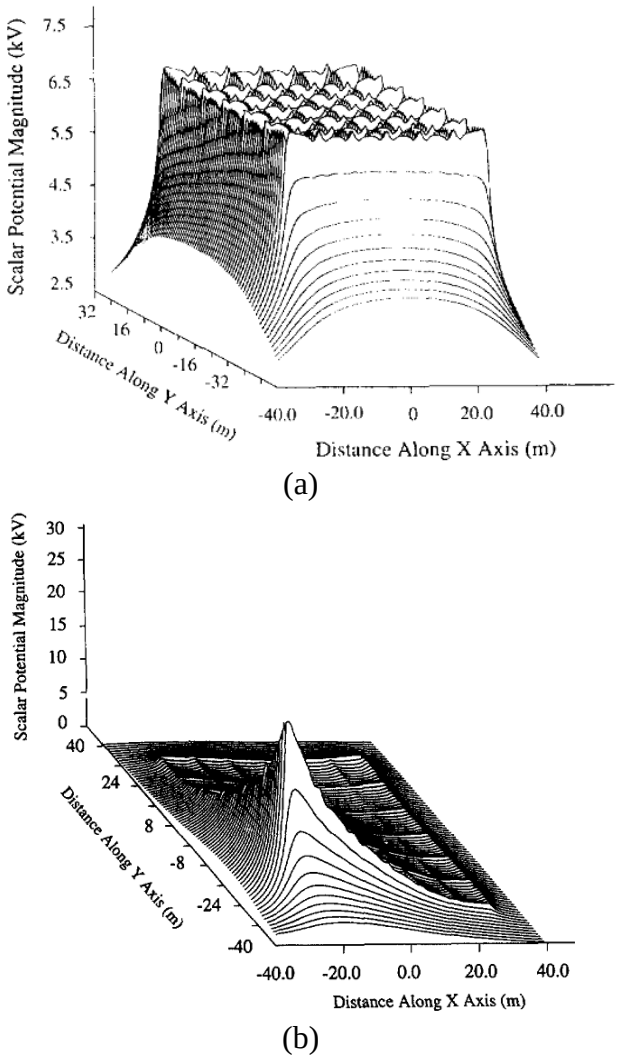

Figure 2.19: Scalar potential at grounding grid with current injection ratings of (a) 60Hz and (b) 500 kHz [77, 78]

Lightning is one of the main sources of electromagnetic interference, and grounding systems can be a coupling path to the sensitive electronics equipment in the substation room or enclosure. Lightning surge can propagate to sensitive electronic equipment through ground potential rise or radiation [85].

2.5.4 Improvement of grounding design under impulse current

Improvement of the grounding performance under lightning current is influenced by the resistivity of soil, impulse or fault current, and grounding grid design as discussed in section 2.4.2. Some influential parameters that reduce the ground potential rise is beyond control, including lightning current waveform and magnitude. Although low soil resistivity can improve the grounding performance, but it is influenced by the types of soil. This shortcoming can be improved by introducing low resistivity compound, such as bentonite, however rigorous maintenance as a function of time is required. Location of the injection can also improve the performance, one example is by injecting near to the centre of the grid.

IEEE 80-2000 standard considers human body to be able to tolerate high current arising from lightning surge. Therefore IEEE guideline on designing the grounding system due to lightning current is similar for power frequency. However, British standard and researchers recommended to concentrate on local grounding system enhancement to produce better protection against lightning current. There are several recommendations on improving the grounding performance under lightning current, namely:

i. BS EN62305 [86] standard recommended that the grounding design for lightning protection should have grounding resistance of less than 10Ω
ii. BS EN 50522 [3] standard suggested for a sufficient mesh density at the injection point to attenuate the impulse current. In addition, high voltage grounding should be part of the lightning protection system. Apart from that, interconnection between buildings grounding system is also required to for consideration when more than one building surrounds the area.

iii. Zedan [71] introduced an identical insulated grounding grid of 6cm (which can buried under the chipping) above the ground and connected it to the grid through a down conductor. In the simulation study, 100mx100m grounding grid was used with injection current of 1A and 8/20μs at the centre of the grid. Simulation was performed by using the CDEGS software. It was found that the enhancement can improve the potential rise by 20%, as depicted in Figure 2.20.

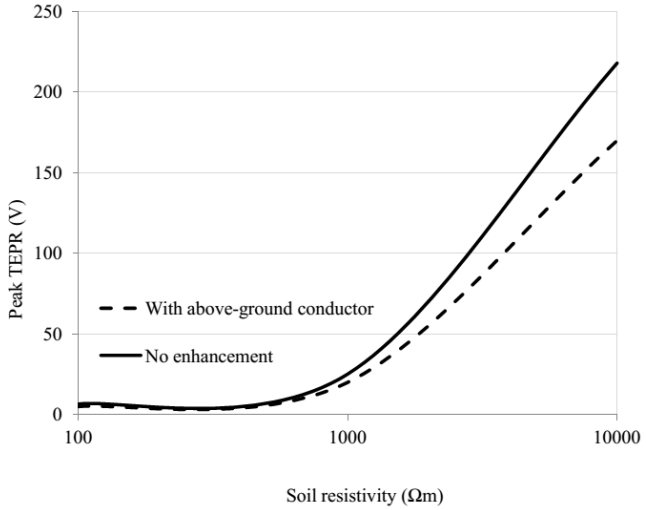

Figure 2.20: Improvement to the grounding grid by introducing parallel insulated conductor of 6cm above the grounding grid [71]

iv. Increasing the grid size and mesh density can improve the grounding grid performance. Therefore, Cigre[85] and Grcev[87] proposed two approaches to improve the transient potential rise, firstly by placing the injection point away from the edge, and secondly by increasing the mesh density closer to the injection point and within the effective area of the grid.

The corner of grid is considered as worst case scenario. Generally the location of injection by system faults 50Hz will be known as grounding connection for substation equipment . However, during lightning the lighning current can inject through any point but the risk to people being electrocuted will be low as operation unlikely during lightning incidence. However, it may be issues with coupling and emc effects to equipments.

2.6 Conclusion

The grounding behaviour of 50Hz/60Hz applications was widely discussed and elaborated in this chapter. Grounding systems were designed based on the power frequency electrocution limit, which followed the guideline of many standards. However, grounding systems behaved differently under lightning current. The performance of grounding with lightning current injection had been studied both in the perspective of experiment and numerical modelling. The outcome of experiments revealed that the grounding rod impedance was actually lower than the grounding resistance up until certain length was achieved. On the other hand, researchers suggested that soil electric field surrounding the conductor can cause ionization between soil particles. The Soil ionization may improve the grounding impedance at the injection point, but it was ignored in long conductors owing to the relatively low current density in the surrounding conductors. Experiment and laboratory, especially in the case of complex grounding grid configurations, require bigger space and higher cost to conduct. Therefore, analytical evaluations are developed to understand the working principle of different parameters and grid configurations. It is shown that a faster rise time and higher soil resistivity proportionally increases the potential rise and grounding impedance. Better performance can be observed when the current is injected

at the middle of the grid, compared to edge or corner injection. Grid size and mesh size can reduce the impulse impedance, but the functionalities are limited to the effective area. Gupta et al. [40] observed that the effective area had not significantly improved the impulse impedance by further increasing the grid size. On the other hand, Grcev [57] evaluated the effective area when the impulse impedance value was equal-to or less-than the grounding resistance. Based on the numerical simulation, three different empirical equations were suggested by a previous researcher [40, 69, 74] . Analytical and numerical modelling method will be discussed in next chapter.

Chapter 3

Review of Numerical Modelling and Simulation Method

3.1 Introduction

Computer modelling and simulation became important methods to enhance the understanding of transients in the grounding system. The popularity of simulation is due to the requirement of high cost and large space to perform field or laboratory tests. Generally, grounding simulation and modelling can be classified based on the theoretical background, namely circuit approach, transmission line approach, and electromagnetic approach.

In the early stages of simulation related to grounding systems, a number of assumptions were made to simplify the equations, which resulted in lower accuracy models compared to the recent methods. A grounding analysis model based on both circuit and transmission line theory approaches can be defined as the followings:

I. The grounding is considered as lumped or distributed finite segments.

II. Thereafter, the equivalent lumped circuit components or distributed circuit components are calculated for each segment. Circuit components such as inductance, capacitance, conductance and resistance are included in the calculation.

III. The representative circuit is solved by using basic circuit theory or telegrapher's equations

Recently, numerical solution based development is gaining momentum due to the dramatic increase in the computer processing speed and memory. Consequently, complex equations can be solved quicker and with better accuracy in the modelling. The electromagnetic modelling approach is performed by solving Maxwell's equations directly or indirectly. In the indirect electromagnetic approach, circuit theory is engaged by considering mutual electromagnetic coupling as a circuit element. On the other hand, the direct approach solves Maxwell's equations either in differential or integral form. The partial differential equations are solved by using numerical methods, such as the finite element method (FEM), the method of moment (MOM), the finite different time domain (FDTD), the transmission line matrix (TLM) and the partial element equivalent circuit (PEEC).

3.2 Circuit Theory Approach

Grounding system model functions based on the effect of two components, namely the leakage current that spreads into the soil and the current that is transferred to the remaining electrode length. Internal loss and magnetic field inside the electrode and its surrounding act as the components of resistance and inductance. In the case of the leakage current created by electric field in the soil, the components of conductance and capacitance can be observed. In order to consider the whole grounding system, the electromagnetic coupling between all the elements need to be looked into. The circuit approach applied in this study to a modelling machine is based on either circuit theory or nodal analysis to solve the approximation circuits. The circuit method is less complex and computationally quicker. In addition, circuit-based software has much easier approach to integrate transient studies of full electrical systems.

The circuit approach for solving the transient electromagnetic fields in the grounding electrode conductors was introduced by Meliopoulos et al.[88] in 1983, with passive circuit element parameters (ΔL, ΔC, Δr, ΔG) to model grounding system. The computations parameter are derived based on the Maxwell equation, and the equivalent circuit is converted to a resistive network followed by applying Nodal analysis method to solve the circuit. In later publications, Meliopoulos et al. [89] extended the proposed model with frequency dependence of each segment of the components based on a quasi-static Maxwell equation. The models are compatible with the Electromagnetic transient analysis program (EMTP) to effectively simulate the transient performance of an electrical system. An improvement of the model was performed by Geri in 1999, who considered the soil ionisation effect for grounding rod modelling [90]. Geri replaced the resistance-inductance and capacitance-conductance branch with equivalent conductance that is linked in parallel to an ideal current generator to create a new resistive based equivalent circuit. In the final equivalent resistive circuit, the nodal equation can be applied to solve the circuit. Otero et al. [91] proposed a method that solves the electric circuit both in the frequency and time domains, which was possible by applying a Fourier transform technique. In this model, the mutual coupling between elements is described by a basic electromagnetic equation. Thereafter, Otero et al. [92] further improved the model by considering the soil ionization effect, which increased the radius of the conductor when an electric field exceeded a critical value at the conductor surface .

In the grounding grid analysis, a simplified circuit approach had been introduced by Rammamorty [61], by representing the grounding grid in small segments of lumped circuits with self and mutual inductance, and self-leakage conductance to earth. Circuit theory was used in [61] to calculate voltages and currents at every nodal between the

segments. In another work, Zeng et al. [36] considered mutual coupling among the conductors by improving the Sundae equivalent circuit by added mutual inductance between the divided elements. The soil ionization effect was considered as 3kV/cm in this model and Kirchhoff's law was used to solve the equivalent circuit.

As the performance of the simulation tools and computers increased, many modelling methods are developed to consider mutual coupling between divided segments. One of these methods is known as the *hybrid* method, which uses the electromagnetic equation to produce a more accurate result.

The hybrid approach was first introduced by Dawalibi [93, 94] in 1987, and later, Y. Liu [34] used the FEM to calculate the per-unit length parameter of each component based on a differential Maxwell equation, except for resistance. Boundaries for the FEM are chosen based on the distance used to measure the ground resistance, as proposed by the IEEE standard [95] . The boundaries are about 10 times the buried depth, or two to three times the spacing between the conductors in the grid. Transient analyses of the grounding systems are simulated by using ATP-EMTP software that operates based on a nodal equation. The model developed by Visacro [96, 97] operated in the frequency domain. It was developed based on the fundamental idea that current carrying conductors operated as a source of transversal and longitudinal currents. The model divided the current path into small elements, and the electromagnetic coupling was calculated for each pair. Nodal analysis was then used to calculate the potential and current at every node.

Marcos [98] used lumped components by taking a node as the reference and the connections between the nodes as transmission lines, where each node was presented by an equivalent circuit consisting of resistance, inductance, capacitance, conductance and mutual coupling between the segments. Every component and mutual

coupling was calculated based on the transmission line modelling method (TLM) [99]. Circuits were solved by replacing each line with Thevenin equivalent circuit, and each grid node solved for every step time.

B. Zhang et al. [100] proposed an improvement to the circuit method that can consider non-linear soil ionization, the shielding effect among conductors, and the frequency-dependence of soil parameters. Circuits in the frequency domain for a grounding grid were modelled by using MoM. The frequency-dependence and self-impedance of the electrode, and the shielding effect among electrodes were also considered. Then, each frequency-dependent element in the circuit was substituted with frequency-independent parameters by using a Vector fitting method. Finally, a circuit consisted of frequency-independent parameters was solved by using EMTP. Considering the time-varying soil ionization, corresponding parameters were varied at each time step.

P.Yutthagowith et al. [101] used a partial element equivalent circuit (PEEC) to model the grounding system under transient current. PEEC solved an integral Maxwell equation by transforming it into an equivalent circuit, where circuit theory was used to solve the model [102].

3.3 Transmission line Approach

In the early stage of modelling, transmission line theory was used to represent the flow of transient current through the grounding grid. Simplifications and assumptions were applied to the analytical analysis due to the absence of powerful numerical methods and computers [36, 41]. The transmission line approach is quite similar to the circuit approach, but applied a lossy transmission line equivalent circuit, as shown in Figure 3.1 to represent the current flow through the grounding system.

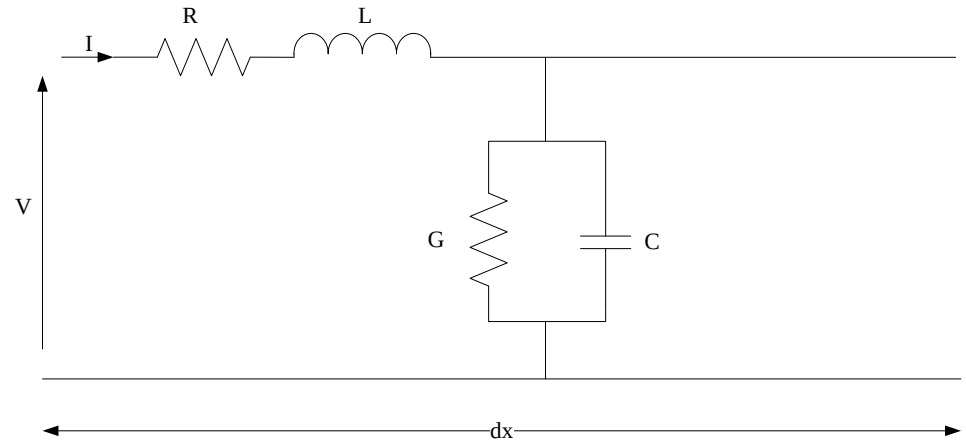

Figure 3.1: Transmission Line equivalent circuit

An alternative solution to the transmission line approach is by solving the telegrapher's equations, as presented in Equation (3-1) to calculate the voltage and current along the grounding wire, where *R* is the per-unit-length series resistance, *L* is the per-unit-length inductance, and *C* and *G* are capacitance and conductance of the conductors.

$$\frac{\partial V}{\partial x} + L\frac{\partial I}{\partial t} + RI = 0$$
$$\frac{\partial I}{\partial x} + C\frac{\partial V}{\partial t} + GV = 0 \qquad (3\text{-}1)$$

The solution to the above equations for voltage and current along a grounding conductor was performed in the s-domain and converted back to the time domain [42, 103, 104]. Thereafter, solutions were formed in the time domain by considering the soil breakdown effect [105, 106]. Transmission line analysis is useful for fast transient analysis.

Y.Liu et al. [30] introduced a non-uniform segmentation model to predict the effective length of a grounding conductor. All mutual coupling between different segments and parts of the grounding conductor was considered by using effective per

unit length parameters, which is both space and time dependent. The FDTD method was used to solve the telegrapher's equations.

3.4 Electromagnetic Approach

The electromagnetic approach carries out the modelling of the transient problem by solving the complete Maxwell's equation, where the equation can be presented in both differential and integral forms [107]. Solving the Maxwell's equation is not a straightforward task compared to the circuit approach. Therefore, numerical electromagnetic analysis was developed to solve the Maxwell's equation, where normally the methods applied in the grounding problems were FDTD, MOM and FEM.

The FDTD method for electromagnetic waves was introduced by Kane Yee in 1966 [99]. It is based on discretisation of the Maxwell's equation directly in both time and space to rectangular cells. Each electric field component was located at a half-cell width from the origin in the direction of its orientation, while each magnetic field component was offset from the centre of three faces of the cell. Hence, solution was achieved in the time domain and solving linear equations were unnecessary, because FDTD seemed to need less computational time than other numerical methods. The disadvantages of this method was cubical meshing, where there were problems when the requirements of curve geometry and small time steps arise. K. Tanabe [108, 109] implemented the FDTD method to simulate transient response of grounding electrodes and grounding grids. Later, FDTD was used to study the responses of a horizontal grounding electrode in three different arrangements that involved a current lead wire and a voltage reference wire [110]. Then, the simulation result is used to verify EMTP simulation based on s modified Sundae equivalent circuit proposed by [111].

The MOM technique operates in frequency domain, which computes based on the residual weight that solves an integral equation. The transient analysis of the grounding system based on the MOM technique was developed by Gcev and Dawalibi [112, 113]. The simulation of the technique need to be carried out in the frequency domain via Fourier transform with discretised time domain data according to sampling time. The solution of the MOM models the problem by using the Sommerfeld integral form. Most importantly, current distributions for every segment of grounding conductors were solved using the MOM technique, followed by the calculation of leakage current and electric fields surrounding the conductor. Potentials at different reference points can be calculated by integrating the electric field from the surface of the conductor to the remote earth. For a reversal step, inverse Fourier transform can be applied to convert back to the time domain. Appendix B presents a flow diagram of the MOM method on simulating the transient grounding behaviour. In [114], the author integrated the solution of MOM with EMTP, where the self and mutual impedance from potential were calculated using MOM. Although this method can generate accurate data, it takes significant amount of computer memory for computation and, concurrently, the nonlinear behaviour of the soil in frequency domain will be complicated to compute.

M.Trlep et al. [115] solved Poisson's equation by applying Galerkin's formulation of FEM and grounding conductors' model in 1D and, subsequently, coupled it with 3D soil models to improve the simulation time [116]. The new model and its boundary at both infinity and surface of the soil is shown in Appendix C (Equation (C-1) and (C-2)). Thereafter, L.Qei [117] applied the same equation for complex conductivity ($\sigma+j\omega\varepsilon$) to study the frequency effect on soil parameters. Following the modification, M. Trlep et al. [118] improved the basic equation by considering the displacement

current. The governing equations of conducting medium and non-conducting material are presented in Equation (C-3), (C-4), and (C-5) within Appendix C. It is found that the displacement current effect is significant for low conductivity soil and high slope of lightning current.

Nekhoul et al. [119] found a new formula by using magnetic vector potential (A) and scalar potential (V). The A-V formulation was based on the application of magnetic vector potential during the interaction with eddy current [120, 121]. Three domains, namely low conducting media (soil), conducting media (conductors) and non-conducting media (air), were modelled with different governing equations, and subsequently the weak forms were derived based on the Galerkin's weight function. Governing equations for conducting material (conductor and soil) and for non-conducting domain (air) are presented in equation (C-6), (C-7) and (C-8) in Appendix C. Thin wire structure approximation was used in the simulation to reduce the computational time. The equations used and solution method used in this thesis will be discussed in section 4.2.

In some of the methods that were developed, quasi static assumption was applied to simplify the equation to accelerate the finding of the solution . However, it had been reported in [102, 103], the quasi static assumption resulted in error compared to the actual solution at high frequency.

3.5 Comparison Circuit and field Approach

Circuit approach is simpler with fast computation time compared to the electromagnetic approach. The vertical grounding rod modelling by using RLC lumped circuit, distributed parameter and electromagnetic approach were compared in [122]. It was found that the application of a lumped circuit was restricted to a rod with

a length of less than one tenth of the wavelength in soil. Although distributed parameters demonstrate better result compared to lumped circuit, but circuit approach overestimates the potential rise at high frequency.

In this work, circuit and electromagnetic approaches for the model grounding grid under impulse current are compared. The grounding grid is modelled by using the circuit approach that was proposed by Ramamorthy et al.[61], while the electromagnetic approach is solved by using FEM. Rammamorthy's [61] equivalent circuit is shown in Figure 3.2, which consists of lumped parameters for conductor and mesh equivalent circuit. In this circuit model, the capacitance and internal resistance are neglected. Conductance of soil and inductance of grounding grid are calculated based on Equations (3-2) and (3-3). Mutual inductance for parallel conductor is calculated based on Equation (3-4), as depicted in Figure 3.3.

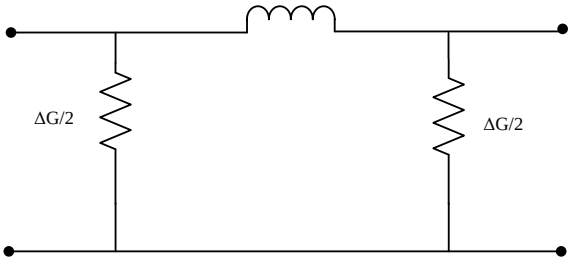

a) Lumped element of the conductor

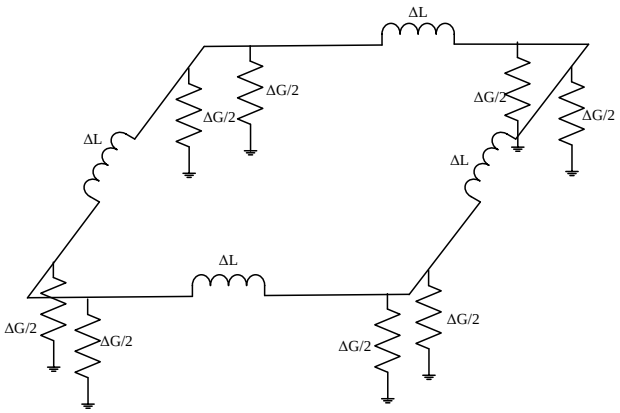

b) Square mesh equivalent circuit

Figure 3.2: Equivalent circuit by Ramamoorty et al. [61]

$$G = \frac{\pi l}{\rho}\left(\ln\left(\frac{2l}{2ad}\right)^{0.5} - 1\right)^{-1} mho \quad (3\text{-}2)$$

$$L = 0.002l\left(ln\left(\frac{2l}{a}\right) - 1\right)\mu H \quad (3\text{-}3)$$

Where *a* is radius of conductor, *d* is depth of buried grid, l is length of conductor and ρ is soil resistivity value.

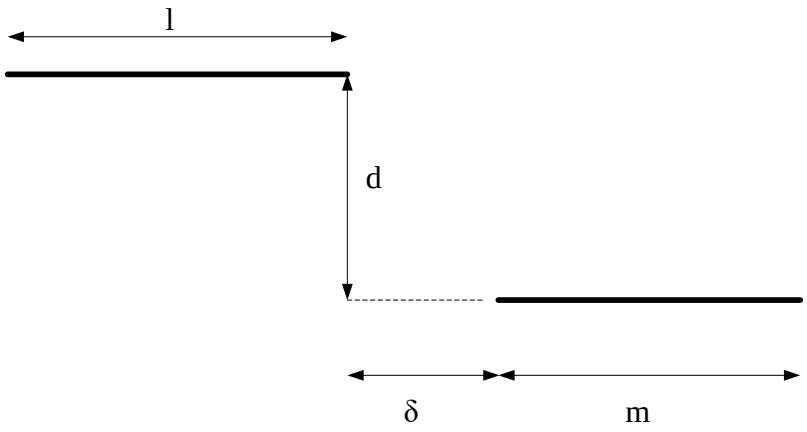

Figure 3.3: Mutual Inductance between parallel conductors

The mutual inductance between two parallel segments can be calculated by using the following equation:

$$M = \frac{\mu_0}{4\pi}\left(\alpha sinh^{-1}\frac{\alpha}{d} - \beta sinh^{-1}\frac{\beta}{d} - \gamma sinh^{-1}\frac{\gamma}{d} + \delta sinh^{-1}\frac{\delta}{d} - \sqrt{\alpha^2 + d^2} + \sqrt{\beta^2 + d^2} + \sqrt{\gamma^2 + d^2} - \sqrt{\delta^2 + d^2}\right) H \quad (3\text{-}4)$$

where

$\alpha = l + m + \delta$

$\beta = 1 + \delta$

$\gamma = m + \delta$

if the conductors overlap, the term δ is to be used with a negative sign

In order to show the circuit modelling element calculation example, grounding grid which is constructed from four 5m conductors are considered as shown in Figure 3.4. Each conductor has radius of 8mm and buried 0.5m below the soil. The soil resistivity is 1000Ω.m. Figure 3.5 show the circuit that simulate using Pspice which each conductor represent by lumped element . The elements value are shown in Table 3.1 Circuit components value. Figure 3.6 shows the voltage at injection point when the 1.2/50μs impulse current inject at corner of the grid for 5mx5m and 40mx40m grid size. It can be observed the voltage rise time faster for 40mx40m grid compared to 5mx5m grid. It due the inductive effect of the grounding conductor. The results pattern agree with simulation using FEM as shown in Figure 5.3 but the circuit modelling underestimate the peak voltage value. Meanwhile the Fem modelling is verified with simulation done using MOM and experiment as shown in section 4.4. For comparison between FEM and circuit modelling, impulse impedance are used which calculated by divide peak voltage value with peak injected current.

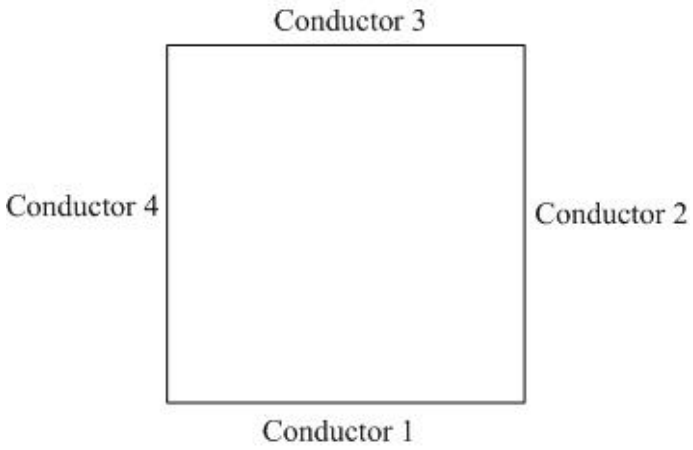

Figure 3.4 Grounding grid (5mx5m)

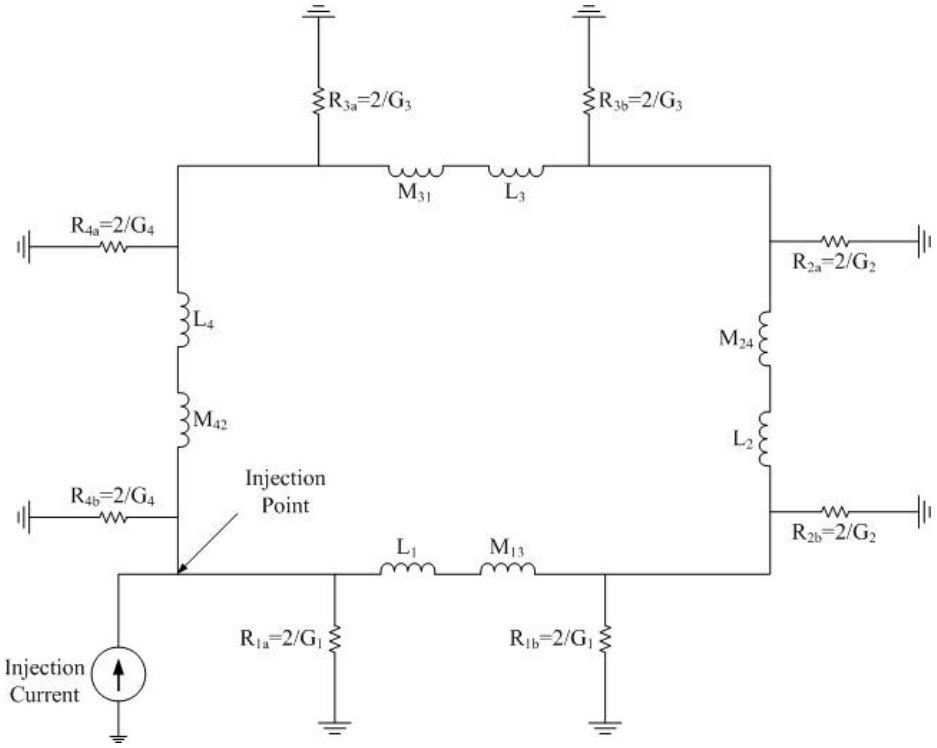

Figure 3.5 Circuit model base on Ramamoorty et al. [61] simulated using Pspice

Table 3.1 Circuit components value

Component	Value	Formulation	Parameter value
Conductance (G_1,G_2,G_3,G_4)	0.0042 mho	Equation (3-2)	a = 8mm l =5m ρ =1000Ω.m depth, d=0.5m
Self-Inductance (L_1,L_2,L_3,L_4)	0.0613μH	Equation (3-3)	
Mutual inductance (M_{13},M_{24},M_{31},M_{42})	0.4672 μH	Equation (3-4)	l = 5m m = 5m d = 5m δ = -5m

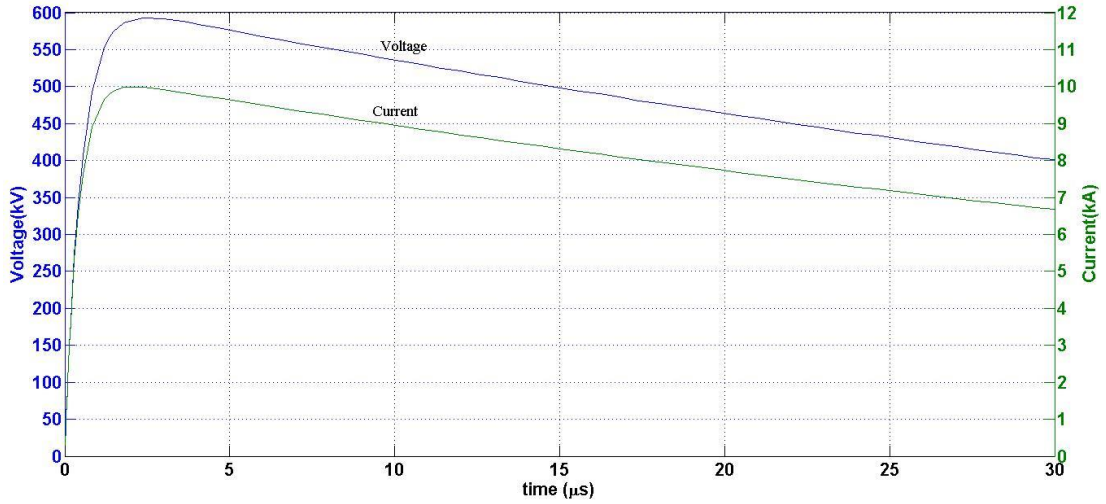

(a) Grid size =5mx5m

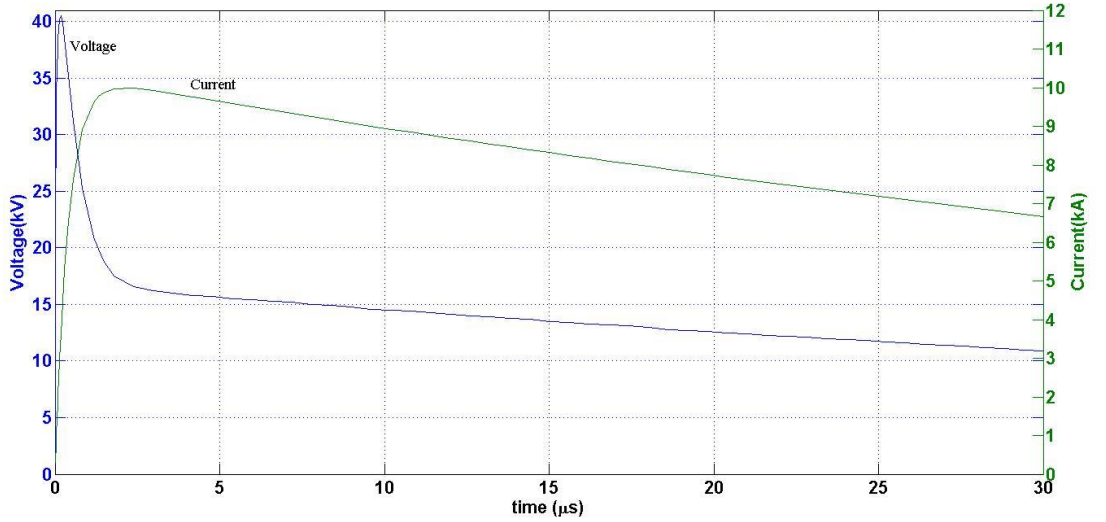

(b) Grid size = 40mx40m

Figure 3.6 Voltage at injection point when 1.2/50μs impulse current injected at corner of grid, grid size= (a) 5mx5m and (b) 40mx40m

The circuits are simulated by using Orcad Pspice software, where comparisons are made for different soil resistivity and sizes of grounding grid at impulse currents of 1.2/50μs and 10/350μs.Figure 3.7 demonstrates an impulse impedance at injection point for different sizes of grid, ranging from 5mx5m to 40mx40m. Impulse current at 1.2/50μs and 10/350μs are injected at corner of the grid, while the grids are buried in

the soil with 1000Ω.m resistivity. In Figure 3.7, it can be observed that the simulation by circuit approach underestimates the potential rise compared to electromagnetic approach for both current waveforms. Both approaches exhibited that the potential rise improvement is insignificant after crossing certain size, which is due to the effective area of the grid. In Figure 3.8, the simulation of different soil resistivity at 1.2/50μs impulse current is demonstrated while being injected at the corner of 20mx20m grid. The difference in the simulated impulse impedance between electromagnetic and circuit approaches increased proportionally with soil resistivity. For instance, the difference is around 5% when the soil resistivity is 50Ω.m, while it proportionally increased to nearly 60% when the soil resistivity increased to 1000Ω.m. Therefore, it can be proven that the circuit approach is inaccurate in modelling the grounding grid under lightning current. The error might be due to the circuit approach assumption that does not consider the wave propagation effect, because the wave propagation effect becomes dominant when high frequency and complex conductor configuration are involved. The wave in the impulse contained high frequency component, which reflects and transmit when the impedance changes, especially at the cross over between conductors.

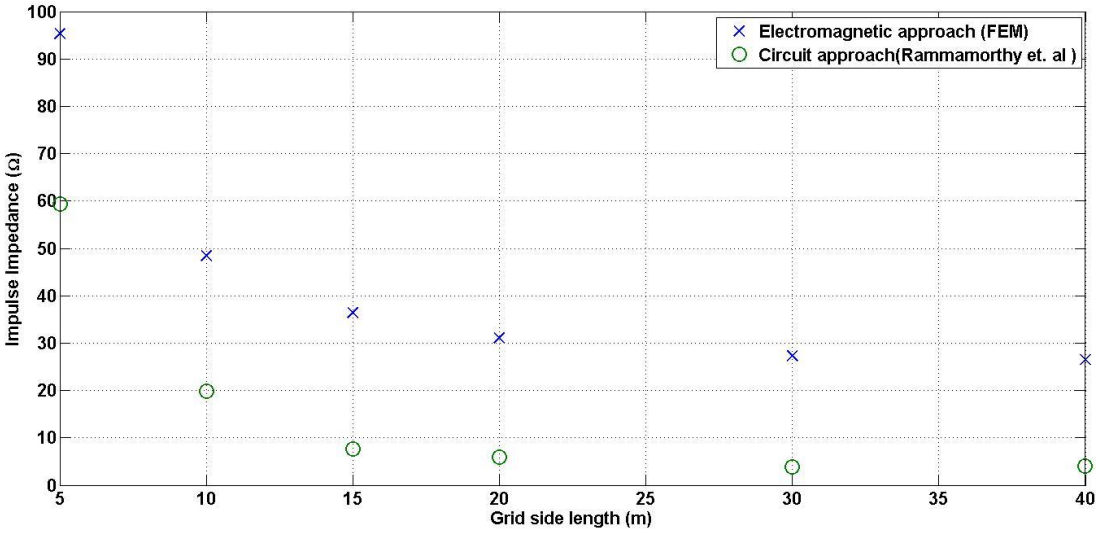

(c) Injection current front time at 1.2/50μs and soil resistivity at 1000Ω.m

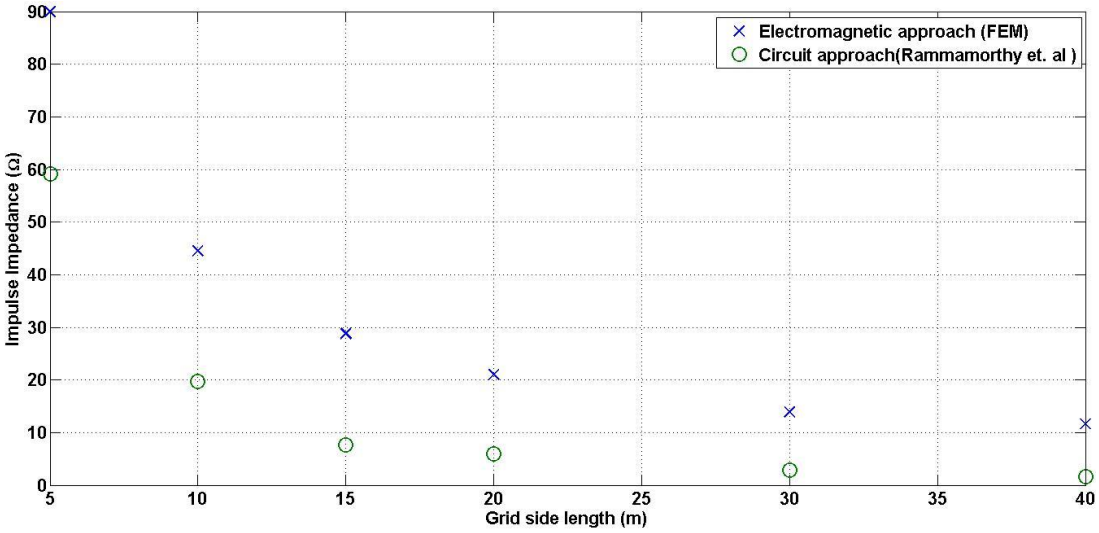

(b) Injection current front time at 10/350μs and soil resistivity at 1000Ω.m

Figure 3.7: Impulse impedance simulation for different sizes of grid by using both circuit and electromagnetic approaches

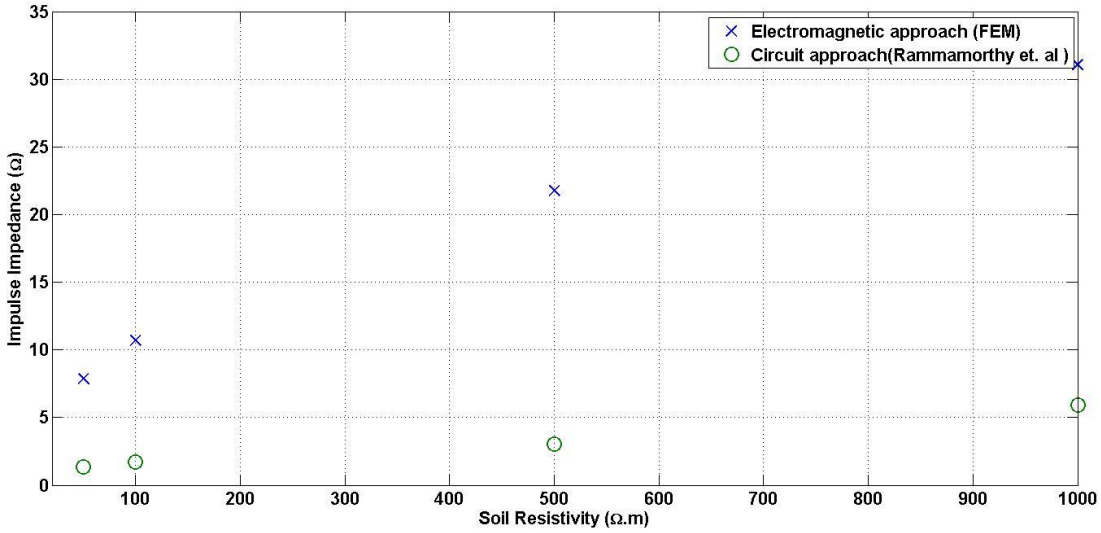

Figure 3.8: Impulse impedance simulation for different soil resistivity by using circuit and electromagnetic approaches, where the front time is 1.2μs and grid size is 20mx20m

3.6 Conclusion

Analytical formulation and computer simulation can provide a variety of analysis and knowledge of different parameters in a grounding system. Various approaches were proposed by previous researchers to produce accurate result, quick simulation time and straightforward modelling method. Table 3.2 presents a comparison between all the approaches. Through the comparative analysis given in this chapter on various approaches, the electromagnetic approach is handpicked for the simulation, due to its accuracy and fewer assumptions. The Maxwell's equation is solved by using the FEM technique, where the FEM in 3D mode will be further discussed in the next chapter. FEM is chosen due to its flexibility in considering the complex geometry of the grounding grid.

Table 3.2: Comparison between circuit, transmission line and electromagnetic approaches

Approaches	Circuit Approach	Transmission Line	Electromagnetic
Formulations	Circuit theory	Circuit theory +telegrapher's equations	Maxwell's equation (integral or differential form)
Solution domains	Time domain	Time domain	Time domain or frequency domain
Advantages	- Easy to use - Quick simulation time	- Easy to use - Quick simulation time - Robust	- Full wave solution - Most accurate result - Robust
Disadvantages	- No full wave solution ability - Wave propagation delay cannot be analysed	No full wave solution ability	- Complicated modelling technique - Requires high computer memory and long simulation time

Chapter 4

Proposal for grounding grid modelling by using Finite Element Method (FEM)

4.1Introduction

The Electromagnetic modelling method will provide accurate results with the shortcomings of additional computational time and memory, as discussed in the previous chapter. Figure 4.1 presents the outline of the study that will be discussed in this chapter. The simulations framework carried out in this chapter are in 3D geometry mode, whereby FEM technique is adopted that solves the Maxwell's equation and a radio frequency (RF) module in the COMSOL simulation package is used as well. The advantage of the method is that an electromagnetic field can be calculated at any point within the boundary of the model. Therefore, the simulation has additional ability of calculating the grounding impedance at the injection point. Apart from that, geometry drawing, post-processing, meshing, and governing equations will be jointly discussed in this chapter. The major challenge in defining the 3D geometry of a grounding grid is the meshing procedure, simply because the geometry contains very small and long grid conductors coupled with large boundaries. In addition, the reflections from the boundary is required to be avoided in order to be able to simulate the open boundary problem. Analysis and simulation are carried out to determine the boundary limit of the simulation that is being performed. The models that are used in the simulations are

validated with previously-published results by using the MOM technique and as well as from experiments. Thereafter, parameter analyses are performed for different front times of lightning currents, soil resistivity, mesh size, grid size and location of injection. The purpose of the parameter analyses is to understand how the simulation parameters affect the grounding impedance.

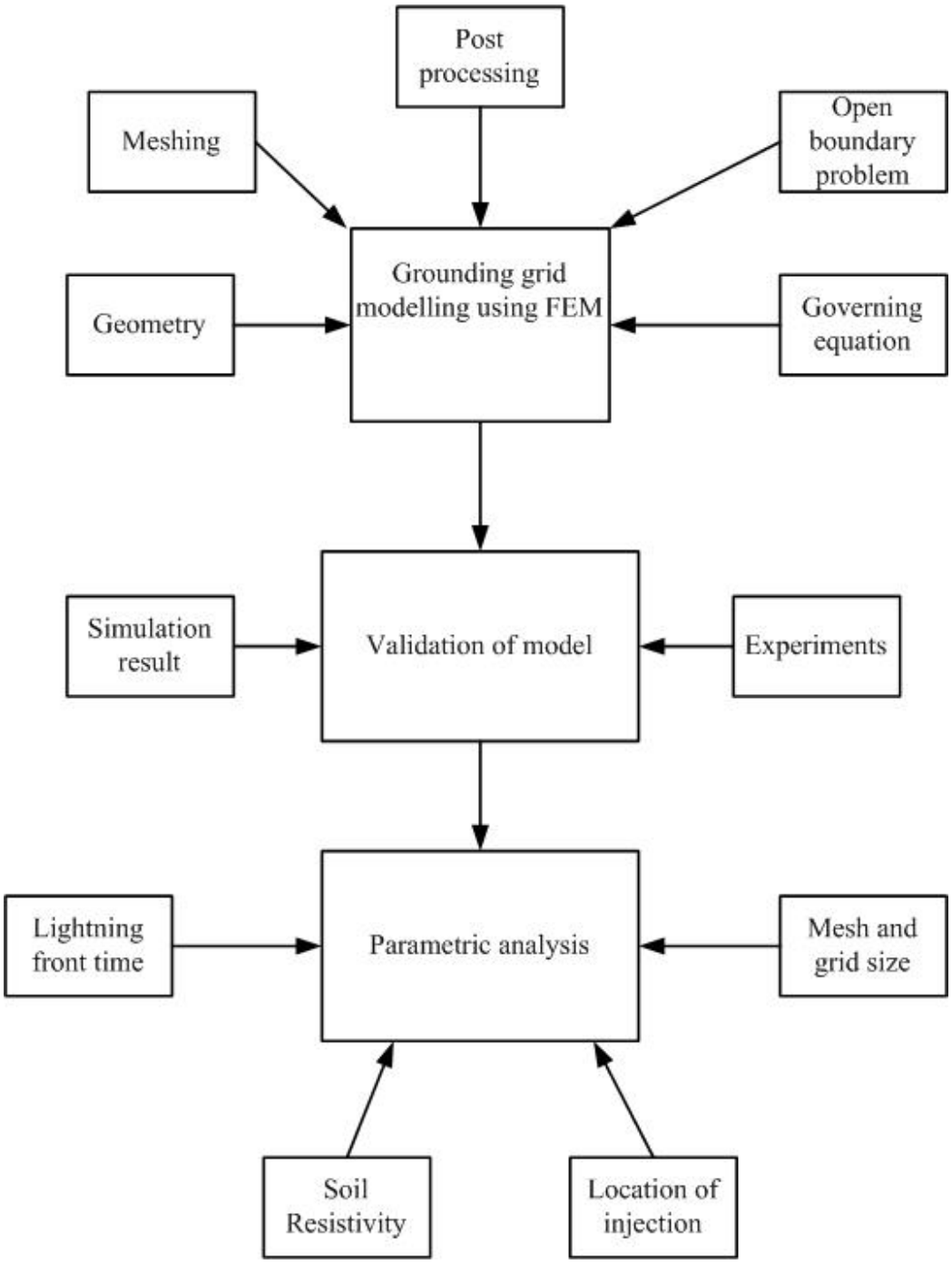

Figure 4.1: The structure of the chapter 4

4.2 Finite Element Method (FEM) Modelling

The FEM technique is a numerical method that is primarily applied to solve partial differential equations (PDE) or integral equations by converting the equations to matrix format. It was introduced back in the 1940s to solve problems in the structural analysis field of aircraft design [123]. In the late 1960s, the FEM technique was applied to solve electromagnetic problems on waveguide[124]. Since then, the method had advanced rapidly in the areas of waveguide problems, micro strips, semiconductor devices, and electromagnetic radiation[124]. The analysis conducted by using FEM technique generally involves the following four steps [125, 126]:

i. Discretisation of the geometry to a sub-region or an element (meshing) that is typically in the shape of triangular or tetrahedron. The technique produces flexible features to describe the geometry of the model due to its ability in applying unstructured sub-domain elements in the meshing stage. Figure 4.2 illustrates the finite elements that are used in the FEM technique for 1D, 2D (triangular or rectangular) and 3D (tetrahedral and hexahedral) shapes. The associated problems will be formulated in terms of unknown function at the node relative to the element.

ii. Selection of interpolation function that provides an approximation of an unknown solution within the element. Interpolations are selected from linear, quadratic or higher order, where higher order interpolation can provide more accurate results with increased complex solutions.

iii. Formulation of the system is a major step in the FEM technique. The governing equations are formulated by either using the Ritz method or Galerkin method, followed by the assembly of all the equations into a solution region to form a group of system equations.

iv. Solve the system equations that are obtained.

The FEM technique requires the meshing of all elements within a considered boundary. The limitations of FEM technique in modelling is the open boundary problems, such as scattering and radiation. A larger boundary is required to avoid reflection that does not occur in real-time environments. Therefore, the method of absorbing boundary was proposed to overcome the aforementioned problem [123, 127].

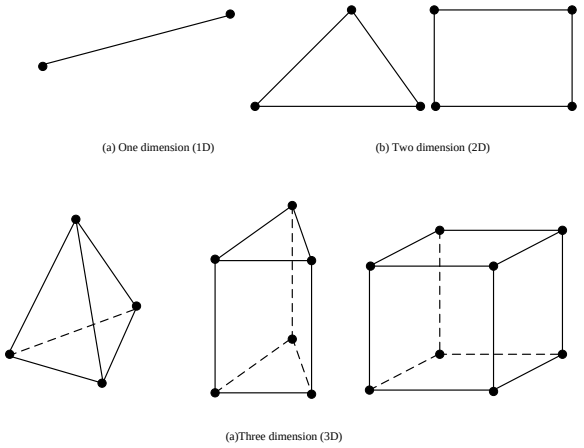

Figure 4.2: The basics of finite element

In this thesis, COMSOL Multiphysics software is applied to solve the PDE problem by primarily using the FEM technique. Figure 4.3 depicts a flow diagram of FEM simulation. The software inputs are based on the geometry of the user's model, where it can be in 1D, 2D or 3D geometry [128]. In the case of 3D models, fewer assumptions will be made compared to the actual geometry, however it requires additional computational time and provides a complex solution. Materials for every domain are assigned according to the physical parameters for analysis that is based on the governing equation. In COMSOL package, the governing equation is different for different modules, since this research is based on the radio frequency (RF) module, hence the transient electromagnetic waves are applied to simulate the problem in time

domain [129]. Thereafter, the post-processing can be performed to calculate the relative physical parameters. The tool has a feature to allow the input of the user's own equation, irrespective of integral, differential and basic mathematical operations, and a graph plotting tool is provided to plot in any dimension.

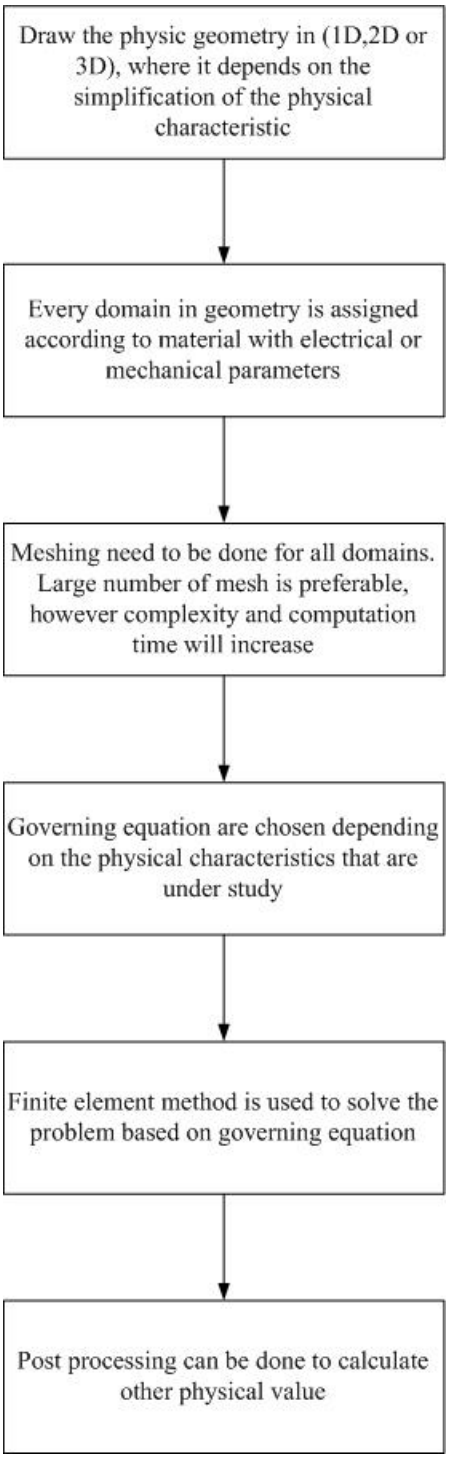

Figure 4.3: Modelling steps in COMSOL package

4.2.1 Geometry and Material

The COMSOL package uses the geometrical modelling as an input. Therefore, the user is required to design the geometry to closely depict the real-life physical object. Therefore, in this research, a grid of conductors is drawn from a 2D shape, followed by extruding it into a 3D object, as shown in Figure 4.4. The conductor size that is used is in the size of 2cm x 1cm, with copper acting as the conductor. In the case of the grid, the size is between 5m x 5m and 60m x 60m, with a 5m span between the conductors.

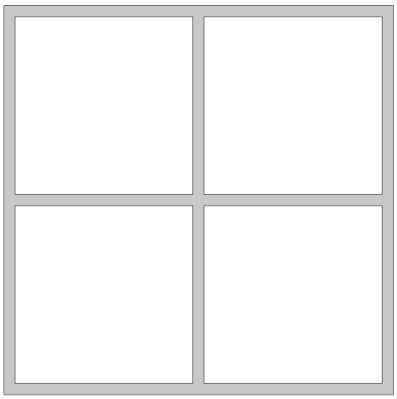

(a)

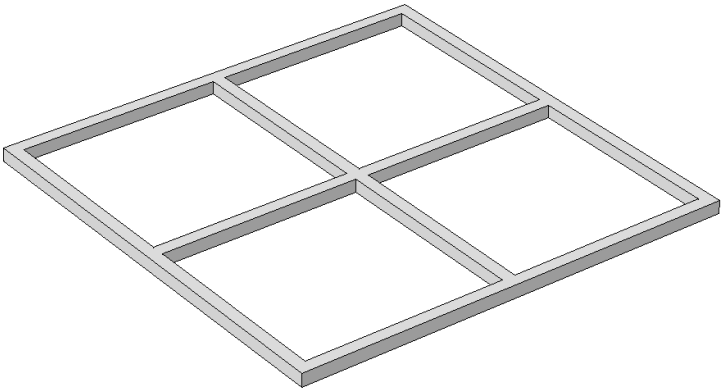

(b)

Figure 4.4: Geometry of conductor in (a) 2D drawing and (b) depiction of the extrudition to 3D

Figure 4.5 shows the complete geometrical model, where air and soil are modelled as a box. The size of the box depends on the boundary size, which will be discussed in detail later. The soil resistivity values that are used ranges from 10Ω.m to 1000Ω.m, while the lightning current is injected from a line to the grid conductor.

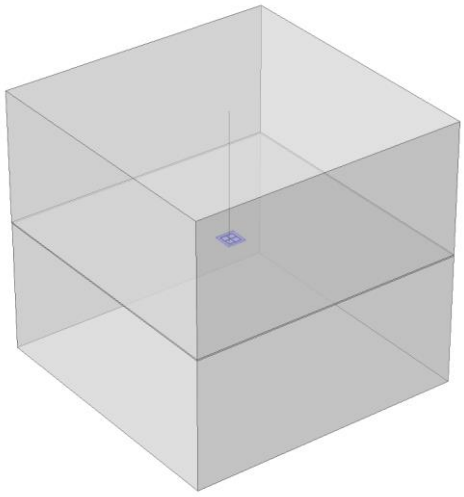

Figure 4.5: Complete depiction of the geometry of FEM model

4.2.2 Meshing

It is the requirement of FEM technique to mesh the entire domain. Therefore, the COMSOL package has pre-defined mesh sizes with a range of very fine to coarser selections. However, it is very challenging to use the pre-defined features if the model has a large ratio between the smallest and the largest domain. As a result, manual mesh settings can be used to avoid this problem. meshed.

Table 4.1 presents five different parameters that can be used to mesh the geometry manually. A finer mesh will provide a more accurate data, however it requires higher

computational memory and longer time period. It is very important to control the mesh density by using different mesh settings according to different areas, which depends on the focus area.

The focus area actually depends on the gradient of the electric field in the model, where the gradient increases as when it moves closer the conductor and injection point. Therefore, finer mesh size is used when the gradient is closer to the injection point and the grounding grid conductor. Apart from there, the gradient of the electric field is very small inside the copper conductor due its high conductivity material. Therefore, small numbers of mesh are used inside the conductor. Mesh size is adjusted to coarser mode within the boundaries of the surface of conductor. Boundaries are important condition because the gradient of the electric field is smaller towards the boundaries, which will result in quicker simulation time and reduced memory usage.

In order to achieve the finest mesh on the surface that is close to the conductor, the meshing process starts with the smallest and the most-complex domain, namely the grounding grid conductor. The surface on the top of the conductor is meshed with triangles, the swept to the entire conductor domain without any layer to reduce number of mesh inside conductor. As a result, a rectangular mesh will be created at the side of the grid conductor. The ‘convert’ function is used for converting the rectangular element to triangular element, thus paving the way to combine with a tetrahedral mesh for rest of the domain

Small boxes are drawn surrounding the grid, as shown in Figure 4.6 to control the mesh density that is formed towards the boundary. Furthermore, the small boxes will reduce the ratio between the smallest and largest geometry in one meshing step, and concurrently enable an easier tuning of the parameters for meshing. In this research framework, the single box that is surrounding the grid solves the mesh problem up to

a grid size of 20mx20m with 5mx5m mesh. However, in the case of a bigger grid size, multiple sized boxes will be introduced to mesh the grounding model. It is easier to control the mesh when the model is divided into various sized boxes. Figure 4.7 illustrates the mesh that is completed for all domains, where the following process is to implement the finite element solution with the entire domain being meshed.

Table 4.1: Defining meshing parameters

Parameter	**Setting**
Minimum element size	Less than the minimum size/length in geometry
Maximum element size	Depending on the model
Element growth rate	Minimum 1
Resolution of curvature	Range from 0-1
Resolution of narrow region	Range from 0-1, higher resolution will create more mesh and degree of freedom in solution

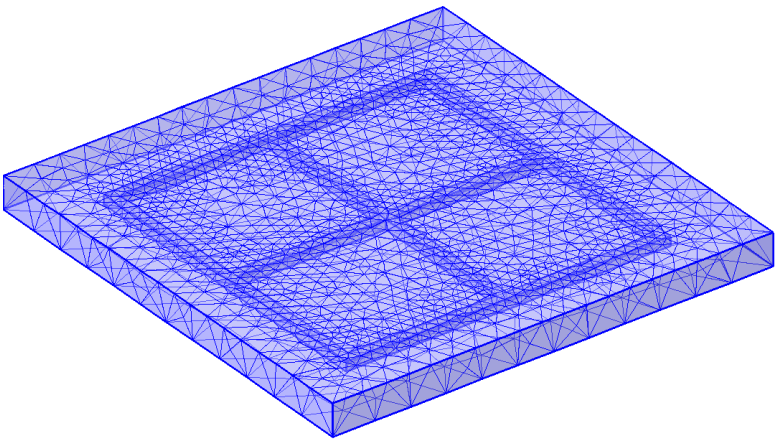

Figure 4.6: Meshing process for small grid configuration

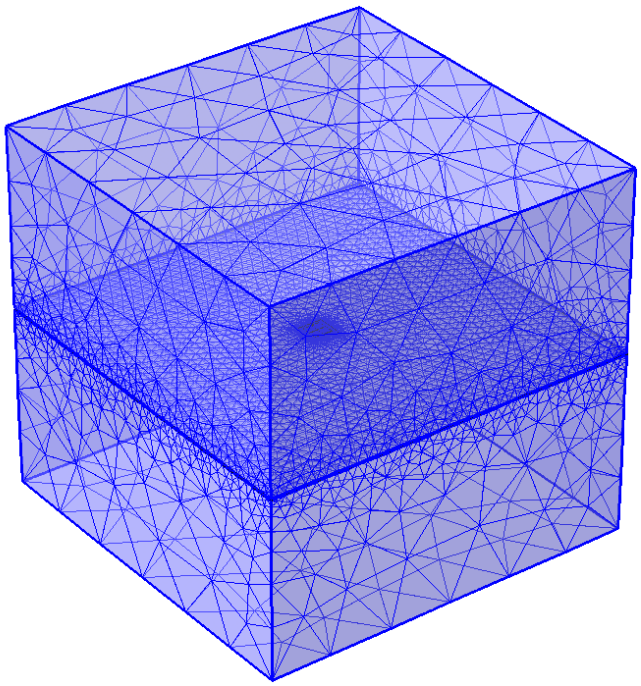

Figure 4.7: Meshing process for all domains

4.2.3 Governing equation

The electromagnetic modelling approach is used to simulate the performance of the grounding grid under transient conditions. The PDEs are solved by using a Finite Element Method. The governing equation for the model is derived from the Maxwell's equation that is presented in equation (4-1)

$$\nabla \times H = J + \frac{\partial D}{\partial t} \tag{4-1}$$

where the vector magnetic potential A is introduced as:

$$B = \nabla \times A \tag{4-2}$$

followed by introducing the scalar potential V as:

$$E = -\nabla V - \frac{\partial A}{\partial t} \quad \textbf{(}4\text{-}3\text{)}$$

The governing equation for the model can be re-written to the following A-V formulation:

$$\nabla \times \mu_r^{-1}(\nabla \times A) + \sigma\mu_0 \frac{\partial A}{\partial t} + \mu_0 \frac{\partial}{\partial t}(\varepsilon_0 \varepsilon_r \frac{\partial A}{\partial t}) = 0 \quad (4\text{-}4)$$

The magnetic vector potentials are solved for every node within the mesh element through the Comsol Multiphysics software package. The electric fields are then calculated from the expression of magnetic vector potential.

4.2.4 Post-processing

COMSOL package will compute the values of the electric field at any instant within the boundary of given geometry. The potential can then be calculated between two points in the boundary by applying the following equations:

$$V = \int_a^b E.dl \quad (4\text{-}5)$$

where

$$E = \hat{x}Ex + \hat{y}Ey + \hat{z}Ez$$

$$dl = \hat{x}dx + \hat{y}dy + \hat{z}dz$$

The post-processing in the COMSOL package requires to determine the line or surface parameters before carrying out any mathematical operations. Thereafter, the electric fields are generated in x, y, and z planes for every points. Therefore, users need to use

a formulation to get the correct answer for a line integral, as shown in the example below. All the graphs in this thesis are plotted by using Matlab™.

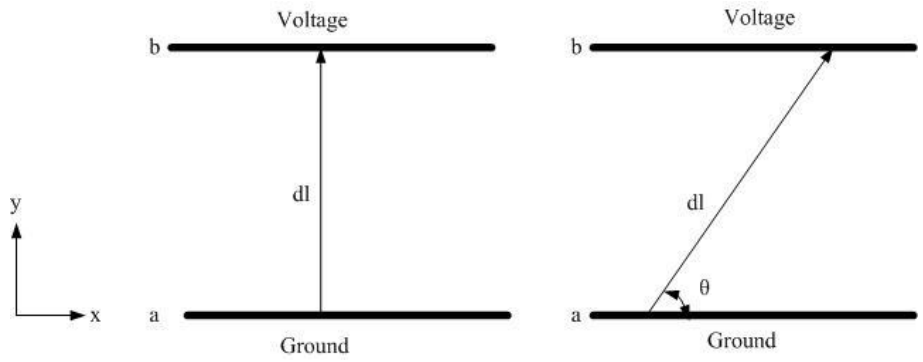

Case I Case II

Figure 4.8: Example of line integral path in COMSOL

Case I

$$V = \int_a^b E_y dy \tag{4-6}$$

Case II

$$V = \int_a^b (E_x \cos\theta + E_y \sin\theta) dl \tag{4-7}$$

4.3 Boundary Condition analysis

Open boundary problem is shown in Figure 4.9, which requires infinite boundary for simulation. However, simulating an infinite boundary condition is highly complex and requires significant computational time. Since the grounding system modelling is an open-space problem, which has no reflection of electric field towards the source, it is a challenge in FEM simulation to determine the boundary of the simulation space for an un-bounded problem.

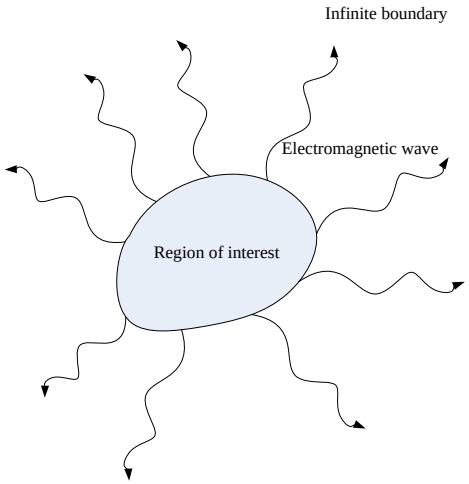

Figure 4.9: Open boundary problem

Most software packages suggested the use of absorption layer known as the perfect match layer (PML) to avoid the reflection from the boundary [124]. The demonstration of PML that is used to absorb all the electromagnetic waves is shown in Figure 4.10. In the transient study within COMSOL package, PML cannot be implemented due to the complexity related to the procedure of the required solution. Alternatively, to avoid the boundary problem, is to increase the boundary size to achieve a current density close to zero at the boundary. Although that can be implemented in simulation, the computational time will be increased as the size increases.

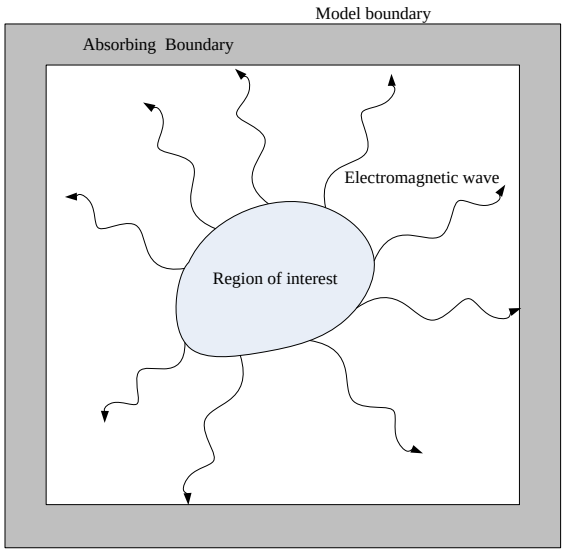

Figure 4.10: Absorption layer implementation

In this study, a perfectly-reflecting boundary must be used. Therefore, it is important to choose the right boundary size for FEM simulation to achieve insignificant reflection. Boundary size was determined by evaluating the current density at various points between the grounding structure and boundary. A grounding grid of 20m x 20m and 60m x 60m is used to compare different grid sizes. The mesh size of the grid is 10m x 10m. Figure 4.11 illustrates the evaluation distance between grounding grid conductor and boundaries, which is denoted as b.

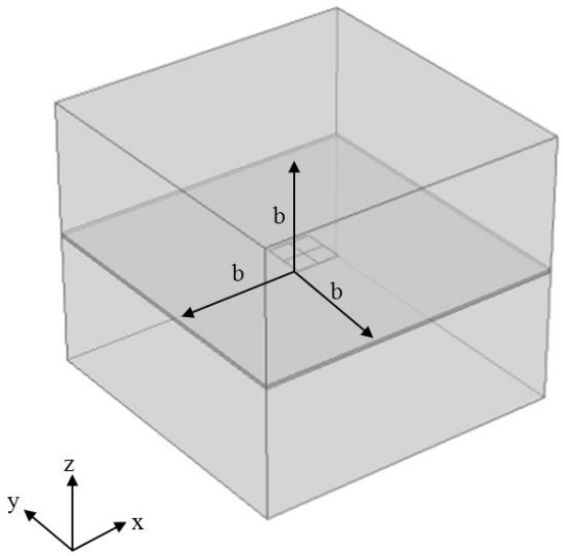

Figure 4.11: Illustration of the boundary size

In order to analyse the boundary size that is required for FEM simulation, five different distances between the grounding structure and boundary are considered, while distances, b, are 30m to 150m. The simulation used high-resistivity soil of 1000Ω.m and a short rise time (0.3μs) to compute the worst-case scenario. Figure 4.12 shows the peak current density from the location of the injection point to the boundary for each distances. It is clear that the reflection from the boundary will occur, and if the distance is not far apart, then potential errors may occur in the simulation result.

Figure 4.13 exhibits results for 60mx60m grid with 100m and 120m boundaries, where based on observation, the grid structure does not influence the current density flow through to the boundary as long as the distance is more than 100m. Furthermore, the simulation results revealed that a 100m distance is sufficient, because no significant improvement is found by increasing the distance further. Therefore, this will be the suggested distance for the simulation framework herein.

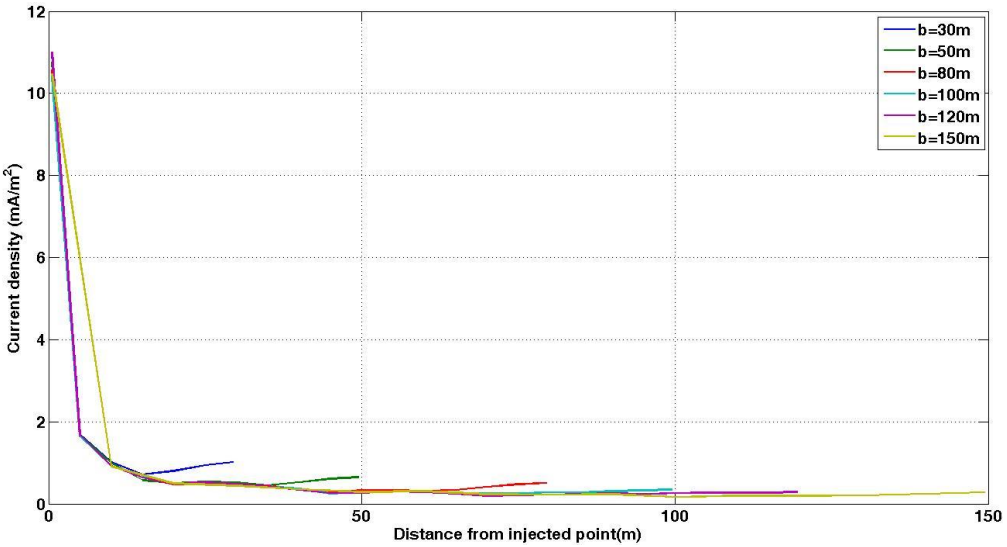

Figure 4.12: Current density from injected point to boundary (20mx20m)

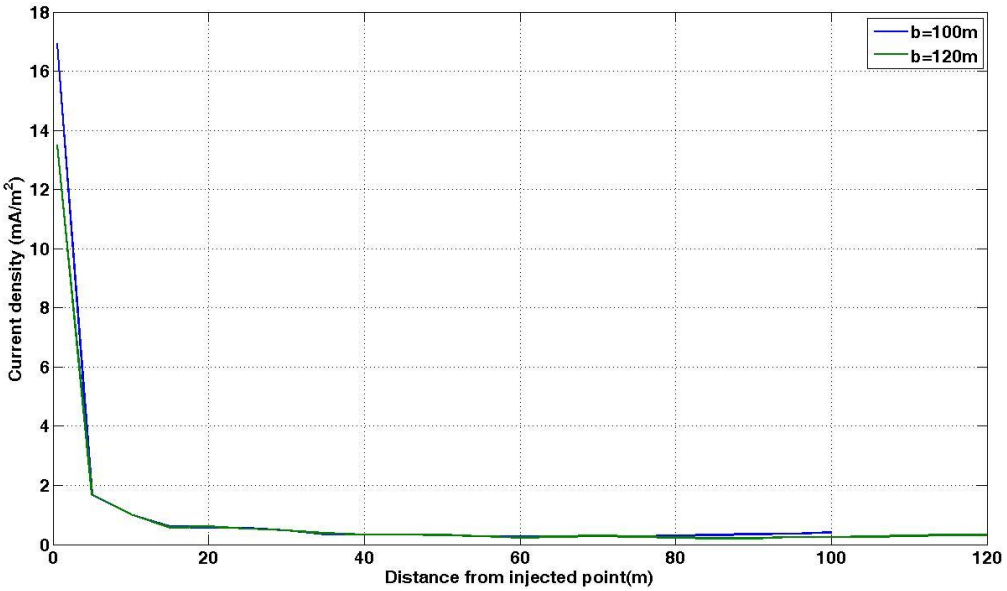

Figure 4.13: Current density from injected point to boundary (60mx60m)

4.4 Validation of the model

In order to validate the simulation approach, the result of the potential rise is compared with the published experimental data and numerical modelling. The comparison is carried out for various sizes of the grid that were simulated by Grcev by using the MoM [73], and concurrently compared with the experimental data that was generated by Stojkovic [62].

4.4.1 Validation with simulation using method of moment (MOM)

The grounding grid is constructed from 7mm radius copper conductors, and buried 0.5m below the ground. A homogenous soil structure is used, with a resistivity of 1000Ω.m. An illustration of the configuration is shown in Figure 4.14.

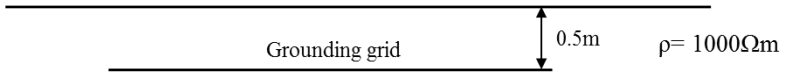

Figure 4.14: Grounding grid buried in homogeneous soil

A fast wave shape current was injected at one corner of the grid, the rise time of the impulse current applied for each simulation is between 0.3μs and 0.4μs, the tail time is fixed at 27μs and the arbitrary current peak is 1A. Figure 4.15(b) shows the injected current that is used in this simulation, which is an attempt to replicate the reference waveform, as shown in Figure 4.15(a). Rest of the parameters of the simulation data are similar to the data published in [73]. The author validated the simulation by using MOM technique with experiments that were reported in [56, 79]. Figure 4.16 depicts the grounding grid configuration with four different grid sizes, namely 10m x 10m, 20m x 20m, 30m x 30m and 60m x 60m. All of the grids consisted of a 10m x 10m mesh.

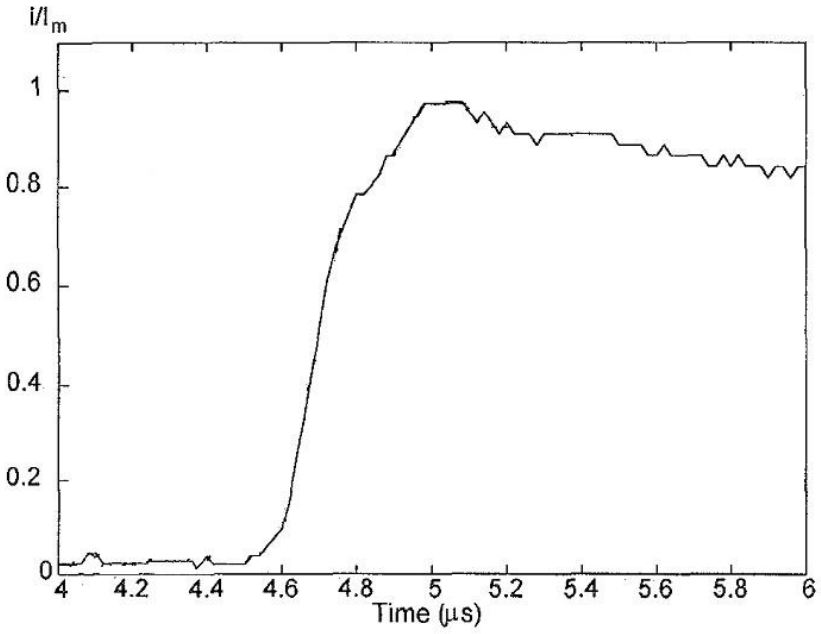

(a)

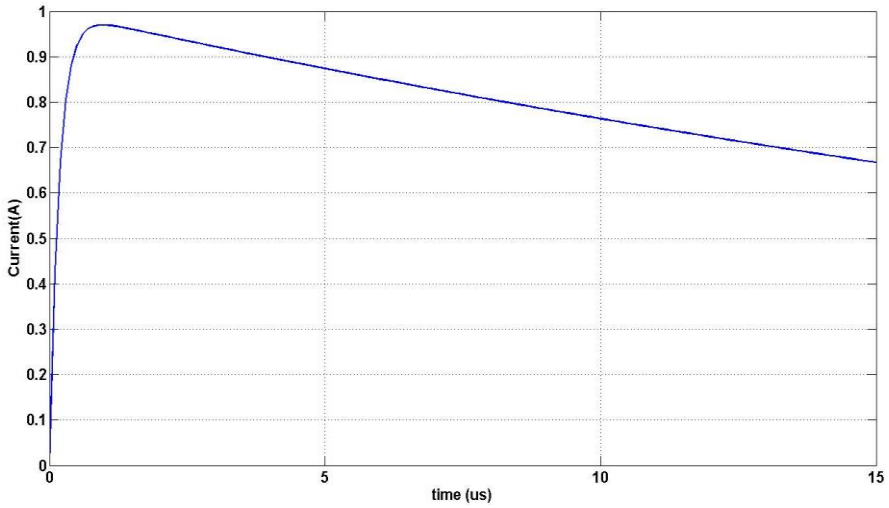

(b)

Figure 4.15: (a) Injection current from [73] and (b)Injection current from simulation

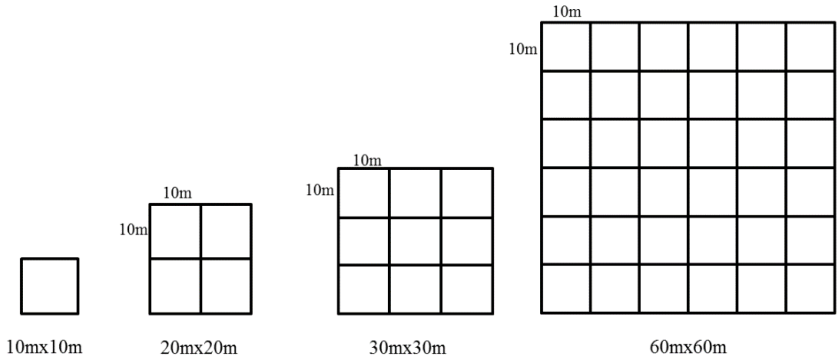

Figure 4.16: Grounding grid configuration

The potential at the injection point of each configuration grid is simulated according to the depiction shown in Figure 4.17 (a). A comparison of the simulated result by using the maximum potential rise at injection point is shown in Table 4.2. It is found that the simulation using FEM is in good agreement with the published result, where only 10% difference is observed on the peak potential rise at the injection point. However, the oscillation is larger in the FEM simulation, especially for a smaller grid size. The differences observed could be due to the injection current not being exactly the same as it was in [73] due to the solutions variation between FEM and MOM.

Table 4.2: Maximum potential rise at injection point (kV)

	Maximum potential rise at injection point (kV)		
Grid size	Simulation by Grcev	Simulation using Comsol	Difference (%)
10mx10m	51	55.86	9.53
20mx20m	38	36.71	-3.39
30mx30m	38	41.77	9.92
60mx60m	38	38.38	1.00

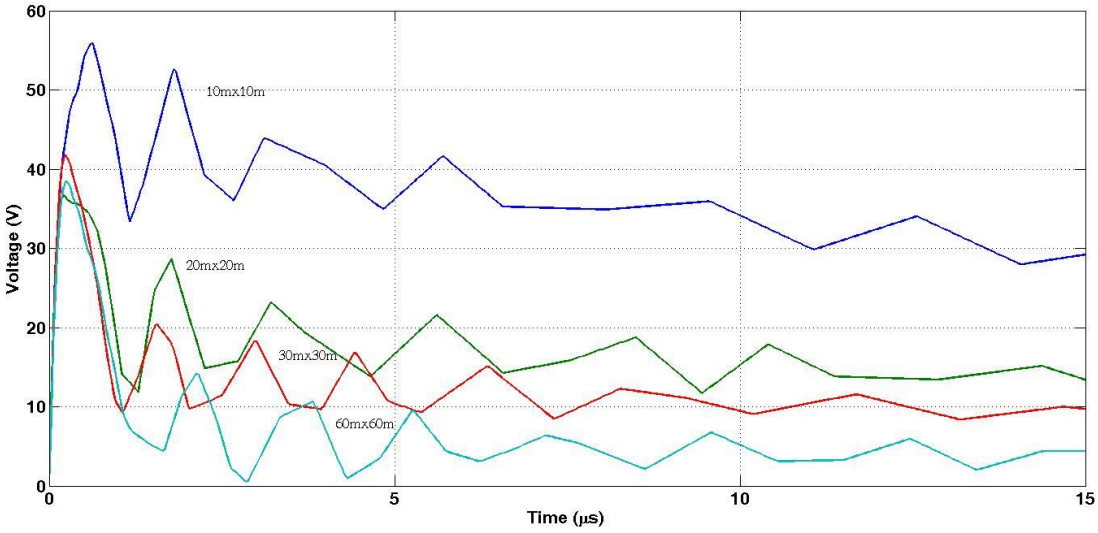

(a)

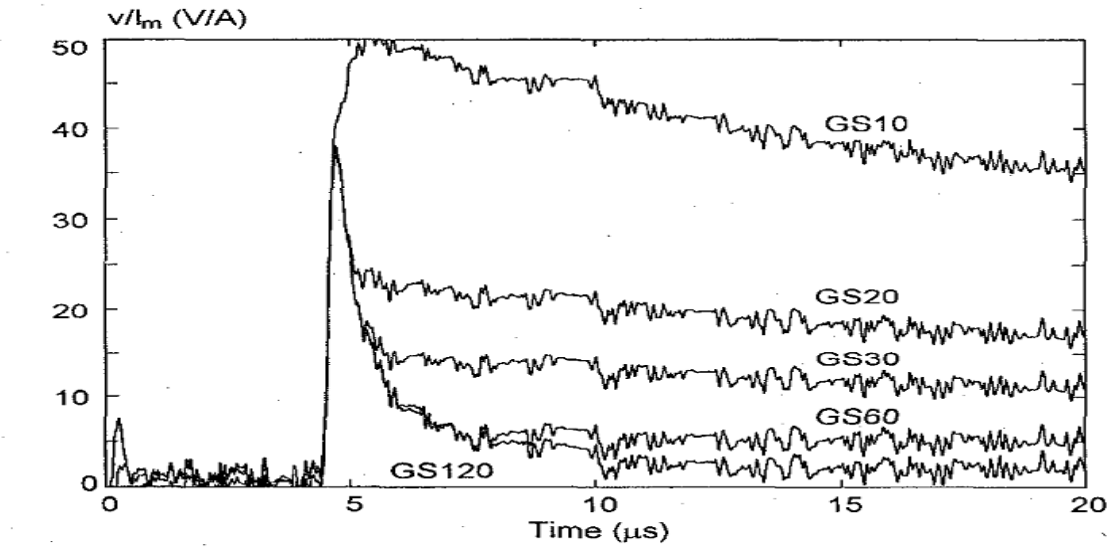

(b)

Figure 4.17: Potential rise at injection point, where (a) simulation using FEM and (b) simulation using MOM [67]

4.4.2 Validation with Experimental Results

Experiments were conducted by Stojkovic [62] on the grounding grids. The grounding grid was constructed from a 4mm radius copper conductor, and buried at 0.5m below the ground. A two-layer soil structure was used, with a resistivity

ρ1=50Ωm for the upper soil, and ρ2=20Ωm for the lower soil, while the thickness of the upper soil was 0.6m. An illustration of the configuration is depicted in Figure 4.18.

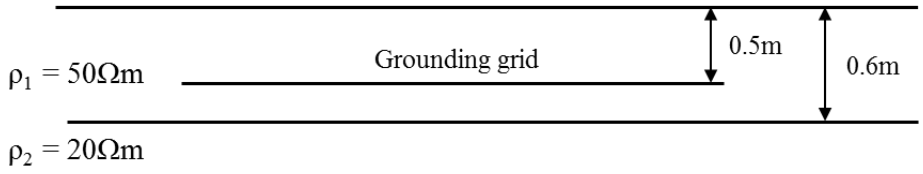

Figure 4.18: Grounding system with two-layer of soil

Figure 4.19 illustrates the experimental setup for a 20m x 20m grid. A slow 15/91 μs transient current with a peak value of 8.5 A was injected at one corner of the grid, and the potential at the injected point was calculated to compare with the measured value.

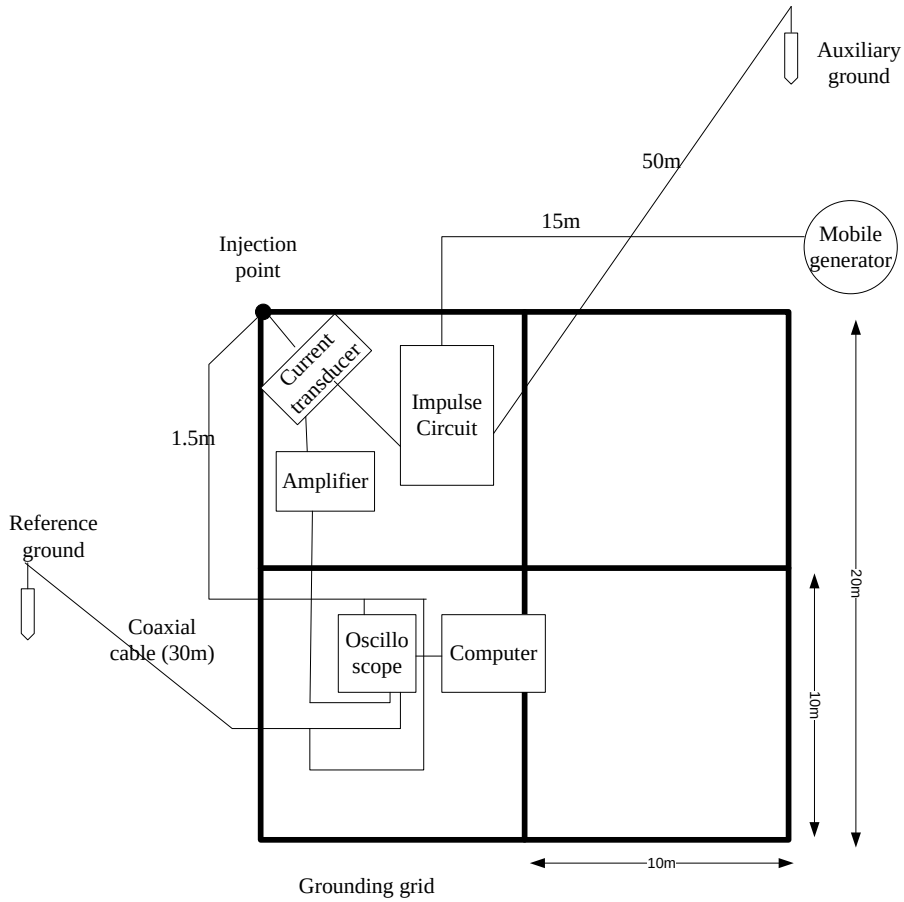

Figure 4.19: Grounding grid experiment layout

In Figure 4.20, the simulated and measured values of the experiment are shown, where 10% underestimation on the potential magnitude is observable from the result. Besides, the rise time of the simulation result is slightly quick by 1μs compared to the measurement. In order to understand the difference, sensitivity analysis were carried out on the impulse front time, depth of double layered soil, and soil resistivity. Figure 4.21 shows different front times investigated in the simulation. The magnitude of the potential rise increased when the front time decreased. For example, decreasing the front time from 15μs to 11μs resulted in increased peak potential from 11.8V to 12.5V. Apart from that, the values of soil resistivity for upper and lower layers of soil were investigated. Figure 4.22 depicts the potential rise at the injection point for different soil resistivity, for both upper and lower layer. It can be observed that the potential increased proportionally with the soil resistivity. The lower layer of soil resistivity was highly impacted due to the conductor being buried in that same layer. In other word, increasing 5Ω.m soil resistivity in lower layer from 20Ω.m to 25 Ω.m will result in the increase of the potential from 11.8V to 13V. In the case of upper layer soil resistivity, varying the value from 40Ω.m to 50Ω.m resulted in the peak potential rise increasing from 10.9V to 11.2V.

The difference between calculated and measured values is a consequence of the integration time, input data accuracy (soil parameter), and accuracy of the measured potential and current. In addition, it should be noted that the calculated results of the computations were only voltages relative to the neutral ground at the surface of the buried grid conductor. It is important to note that connecting conductors and the measurement circuit with a 30m long coaxial cable were not included in the simulation.

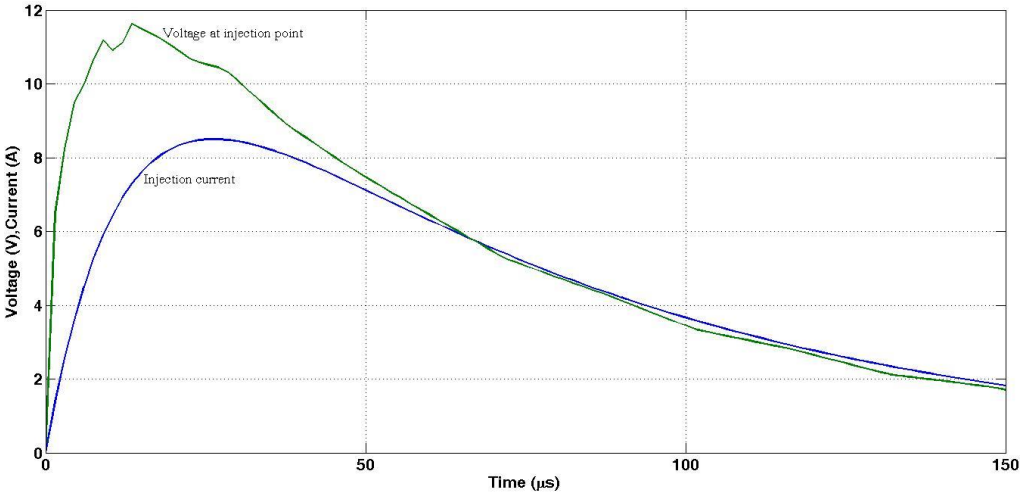

(a)

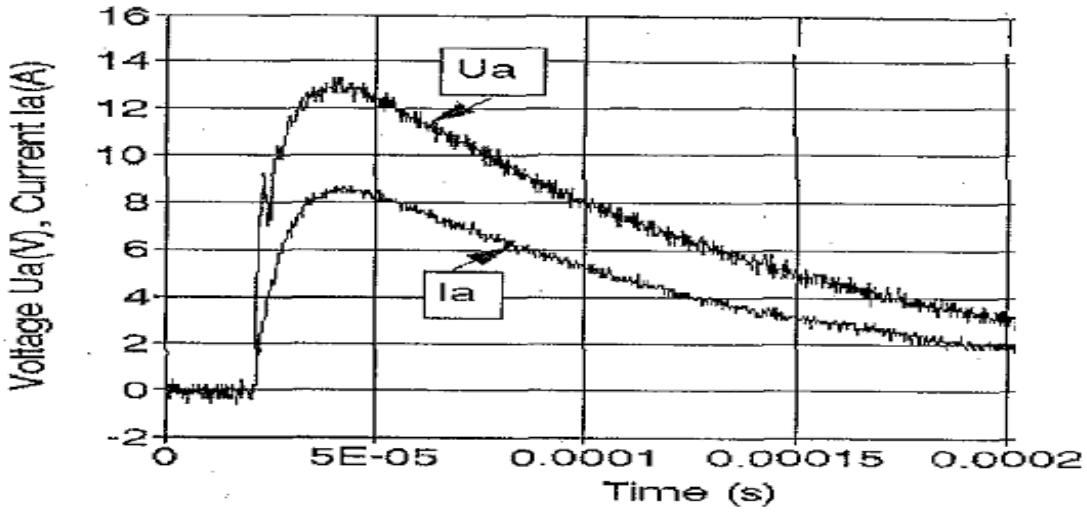

(b)

Figure 4.20: Voltage and current at the injection point for (a) simulation using FEM and (b) experimental setup by Stojkovic's

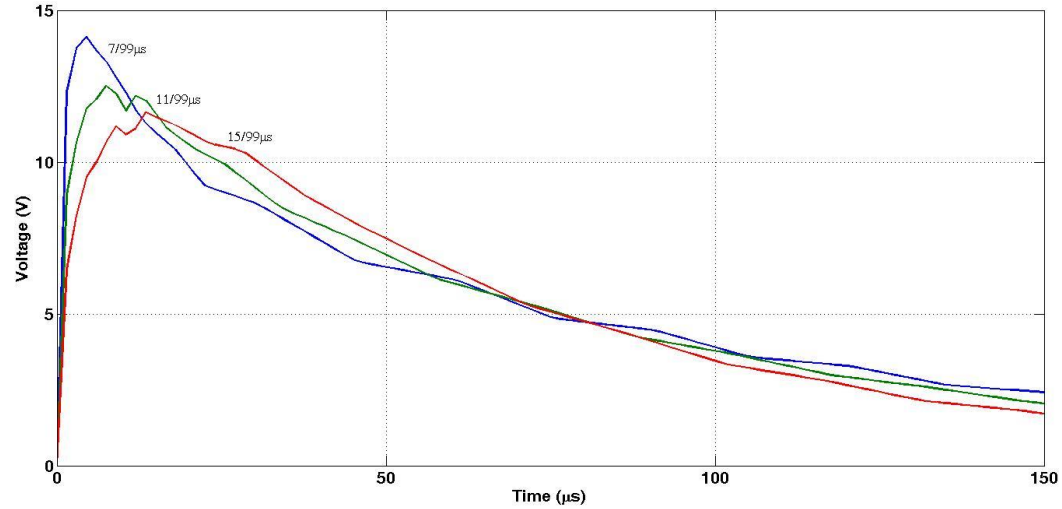

Figure 4.21: Effect of the front time of the injected current

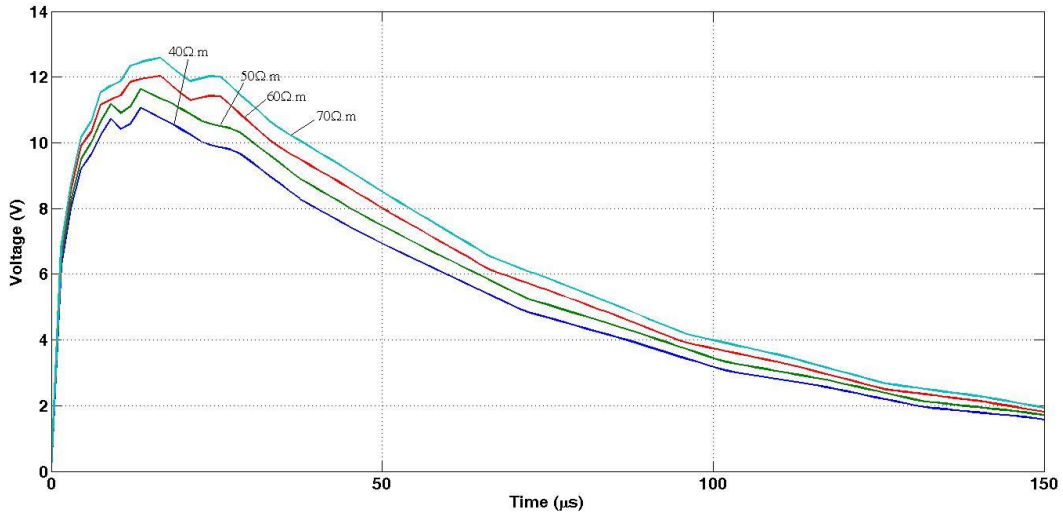

(a)

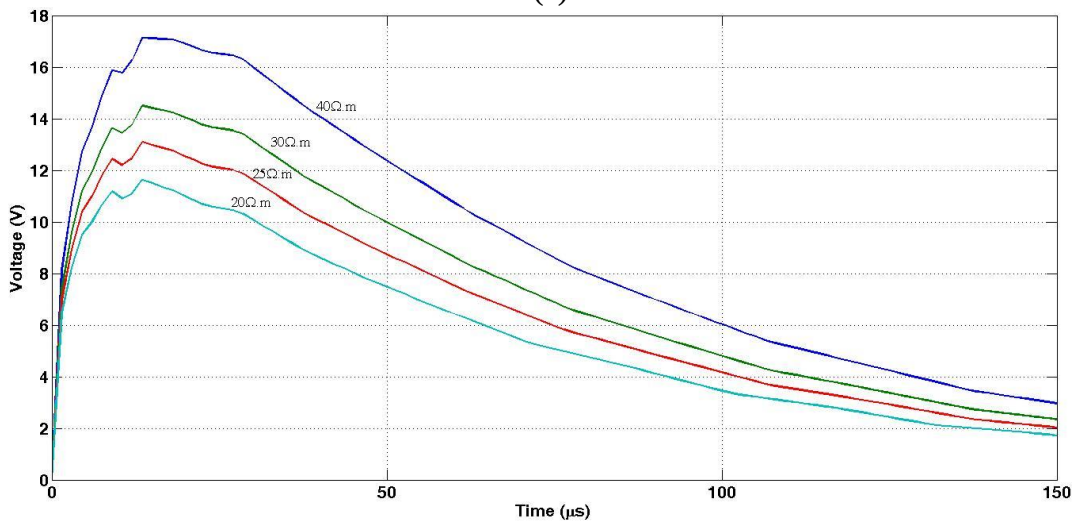

(b)

Figure 4.22: Effects of different soil resistivity for (a) different upper layer with lower layer =20Ω.m and (b) lower layer with upper layer =50Ω.m

4.5 Performance of grounding grid under lightning current

Simulation is performed to evaluate the effect of different parameters towards the grounding grid under lightning current. The analyses are done for different soil resistivity values, front times, grid sizes, span between conductors (mesh sizes), and locations of the injection.

4.5.1 Effect of soil resistivity

Soil resistivity is the main parameter that describes the type of soil, which depends on the geography and the water content of the soil. In order to investigate the effect of soil resistivity, six values are used ranging from 10Ω.m to 1000Ω.m. A lightning current of 10kA with a 1.2/50μs waveform is injected through the down conductor to the corner of the grid, which is buried 0.5m below the soil surface. The grid size is 20m x 20m and the mesh size is 5m x 5m.

The ground potential rise at the injection point for different soil resistivities is shown in Figure 4.23, where it is clear that the increase of potential proportionally increases with the soil resistivities. Figure 4.24 shows the peak ground potential rise for different soil resistivity. The peak magnitude of the potential in soil resistivities of 10 Ω.m is more or less 35kV with gradual increase with higher soil resistivity. For example, the ground potential rise is about 310kV when the soil resistivity is 1000 Ω.m. Therefore, it is important to have low soil resistivity for better grounding design.

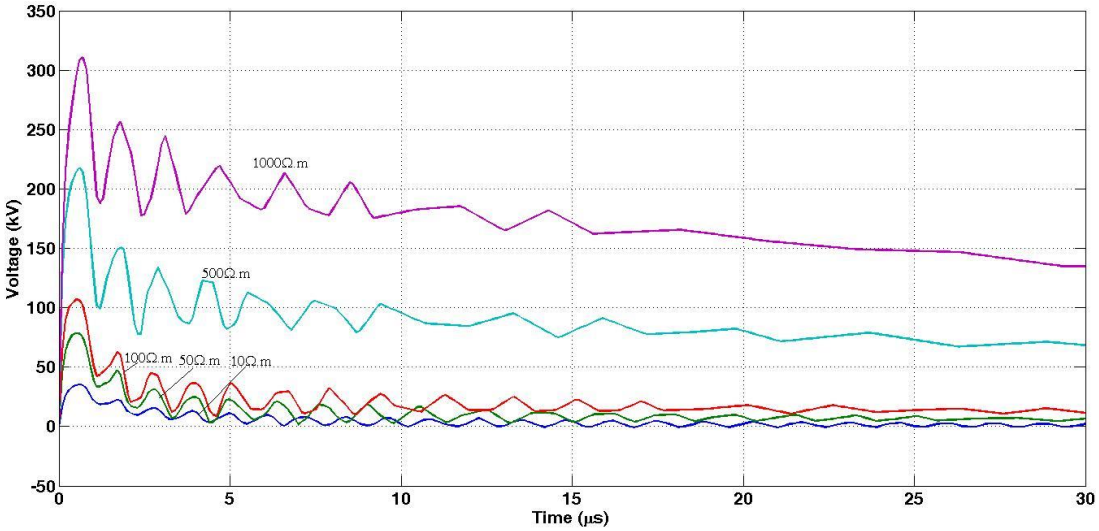

Figure 4.23: Potential rise at the injection point for different soil resistivities with injected current of 10kA 1.2/50µs at the corner of a 20mx20m grounding grid

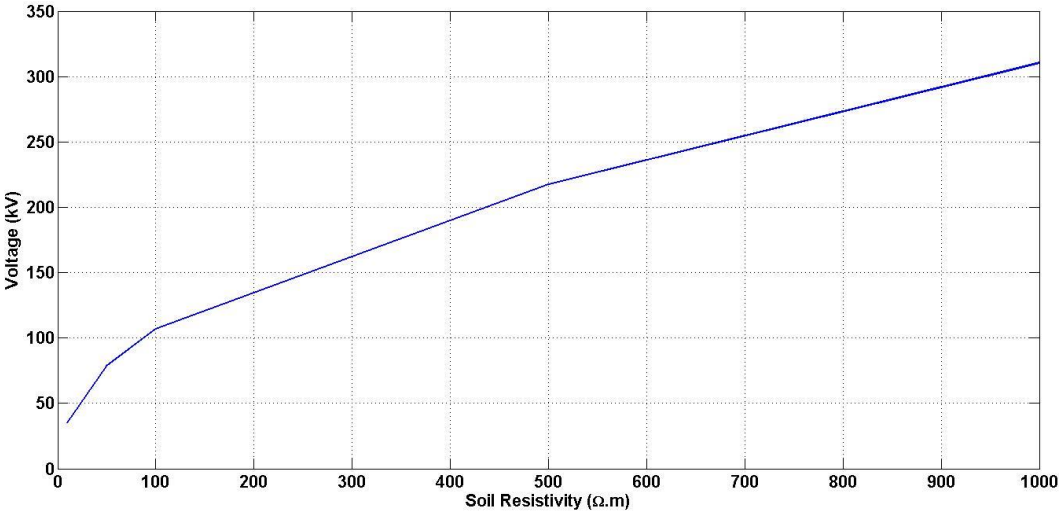

Figure 4.24: Peak Voltage for different soil resistivities with injected current of 10kA 1.2/50µs at the corner of 20mx20m grounding grid

4.5.2 Effect of current waveform

The front time of lightning current defines the frequency content of the current. Therefore, it is a critical component to consider in simulation. In order to investigate the effect of the lightning current waveform, three different lightning currents are used in the simulation, namely 1.2/50μs, 2.6/50μs and 10/350μs. The magnitude of the current is fixed at 10kA. Thereafter, the currents are injected at the corner of a 20m x 20m grid with 5m x 5m mesh size. The grids are buried 0.5m below the surface of the soil with 1000Ω.m resistivity.

Figure 4.25 exhibits the potential rise at the injection points for varying impulse waveforms. From the figure, it can be observed that a 1.2/50μs front time generates almost double the potential compared to the 2.6/50μs front time. A quicker front time with a steeply-changing current can create a higher potential rise, because quicker front time consists of high- frequency elements, hence the impulse impedance of the grounding system will increase. The ripple is obvious and larger for shorter front time, which is might due to the reflection of the wave when the impedance change at the junction of the grid conductor or numerical instability of the software. The reflection can be estimate by calculate velocity of the electromagnetic wave. The velocity of the electromagnetic wave can be estimate as 100m/μs when permittivity of soil, $\varepsilon_r = 9$. From the figure is shown the first ripple happen approximately at 1μs, if the reflection happen it will be 50m from injection point. However, at 50m from the injection point, the characteristic impedance is not changing as the soil is uniform. Therefore, the ripple can be improved by refine the mesh size especially for shortest rise time in order to improve the numerical calculation. However, the finer mesh need more computational time and memory. Besides that, the potential rise value is expected lower than shows in Figure 4.25 when the soil ionisation effect is considered.

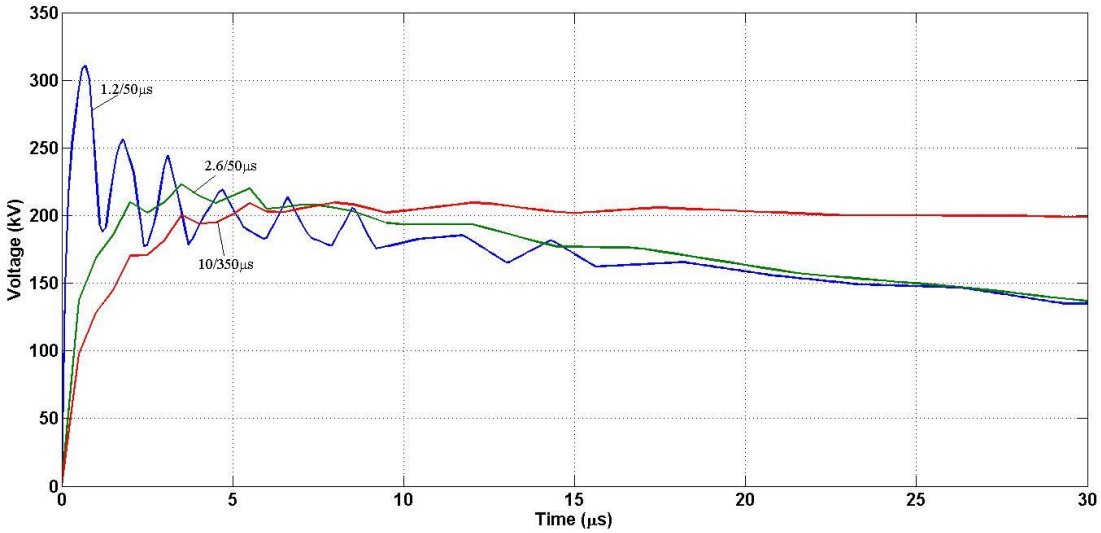

Figure 4.25: Potential rise at the injection point for varying front times injected at the corner of 20m x 20m grounding grid with ρ = 1000Ω.m

4.5.3 Effect of grid Size

Increasing the grounding grid size can provide additional paths to dissipate the unwanted current, which also means that more conductors are required resulting in increased cost. In order to investigate the effect of the grid size, six different grid sizes are used, ranging from 5m x 5m to 40m x 40m, are used in this simulation as shown in Figure 4.26. Mesh size is fixed at 5mx5m for all grid sizes, while the current with a 1.2/50μs shape is injected at the corner of the grid, and the soil resistivity is 1000Ω.m. Specific grids are chosen to investigate the effect of impulse current when the size of the square grid is increased, where practically the grounding grid can achieve more than 100m of side length.

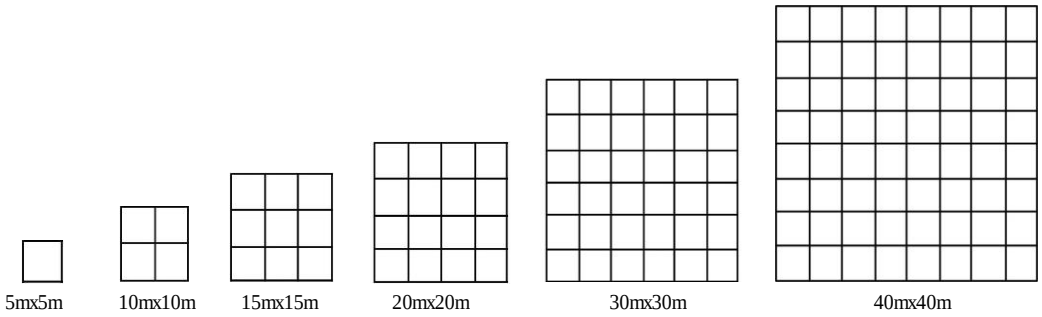

Figure 4.26: Different sizes of grounding grid

Figure 4.27 illustrates the ground potential rise at the injection point. It can be observed that the potential reduces with the increasing grid size of 5m x 5m to 40m x 40m. However the reduction rate reduces when the grid size increases. For example, the potential reduces by almost 50% when the grid size increases from 5m x 5m to 10m x 10m, while increasing the grid size from 15m x 15m to 20m x 20m allows the potential to induce a reduction 15% to the ground potential. Figure 4.28 exhibits the peak potential at the injection point when the area of the grid increased. Significant reduction in the ground potential rise can be observed for below 600m^2, while no improvement for areas beyond 600m^2. As a result, it can be understood now that for the effective area of the grid, whereby increasing the grid size beyond a certain degree will not contribute significant improvement to potential rise at injection point. While, Figure 4.29 illustrated normalise value of potential rise and injected current to its maximum value. It can be observed that the rise time of the potential at injection point is faster with increase in grid size. It shows the inductive component is greater for larger size of grid.

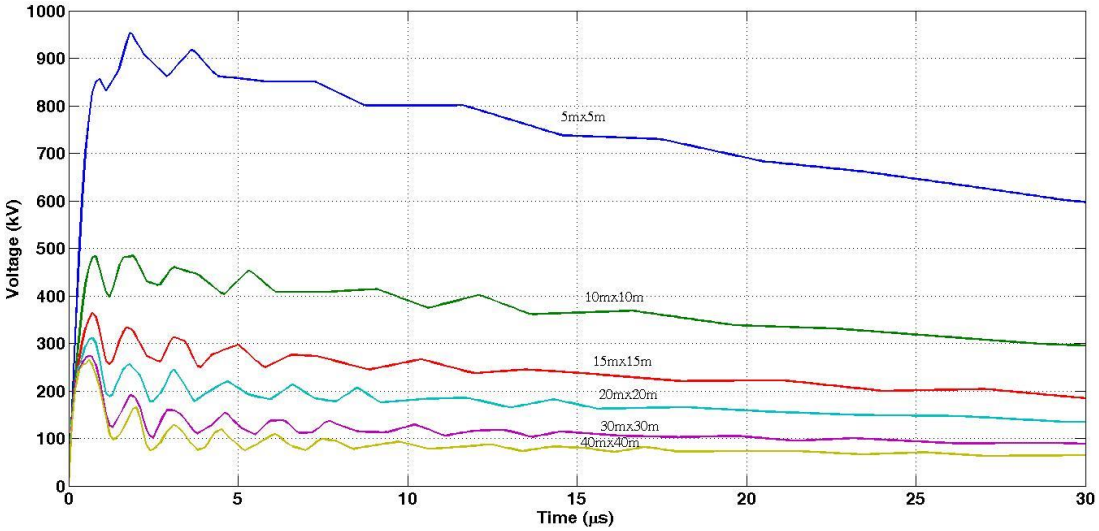

Figure 4.27: Ground potential rise at the injection point for different sizes of grid with injected corner current of 10kA 1.2/50µs and ρ=1000Ω.m

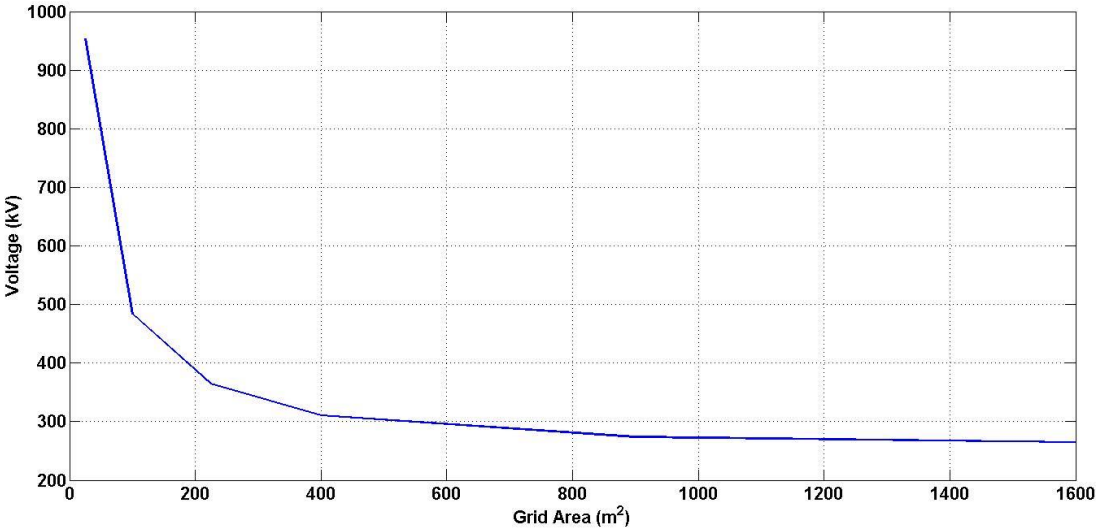

Figure 4.28: Peak voltages according to varying grid sizes

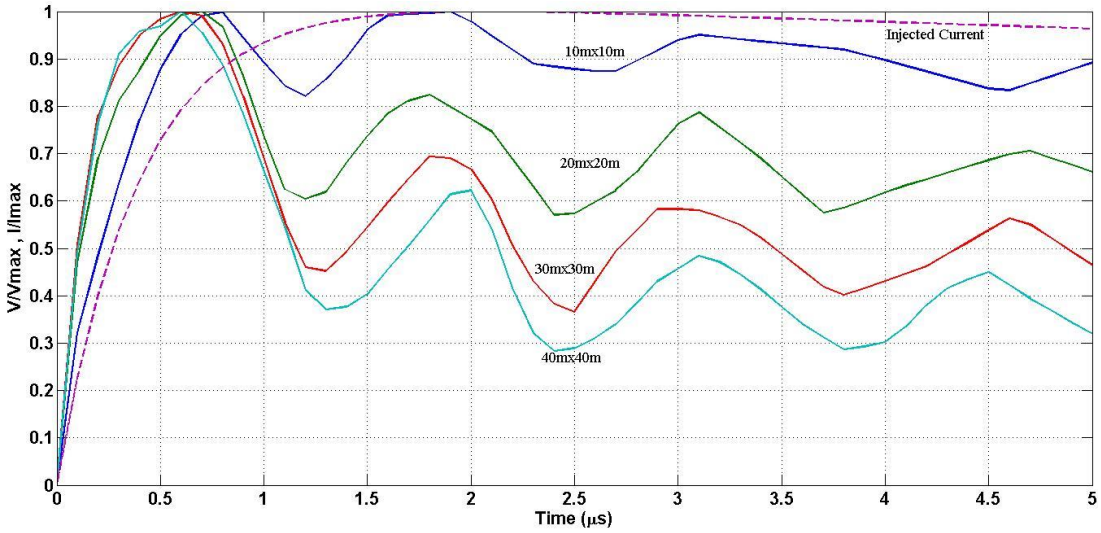

Figure 4.29 Normalise potential rise at injection point and injected current to its maximum value

4.5.4 Effect of grid mesh size

In the grounding grid, mesh is referred as the separation between conductors. The mesh designed to minimise the possibly arising step and touch voltages. In this section, different mesh sizes are used as shown in Figure 4.30. A single grid size of 40m x 40m is applied for a number of mesh sizes, namely S40 (grounding grid without mesh), S20 (20m x 20m), S10 (10m x 10m), S5 (5m x 5m), and S205 (5mx5m for 20m x 20m near the injection point). Soil resistivity is 1000Ω.m with a 1.2/50µs impulse current injected at the corner of the grid. Figure 4.31 shows the potential rise at the injection point for all mesh sizes. It can be observed that the potential rise is improved when additional mesh is placed inside the grid. In addition, when the mesh that is closer to the injection point increases, the peak potential improves, which can be observed from the peak potential of S205 configuration that achieved better peak compared to the S10 configuration.

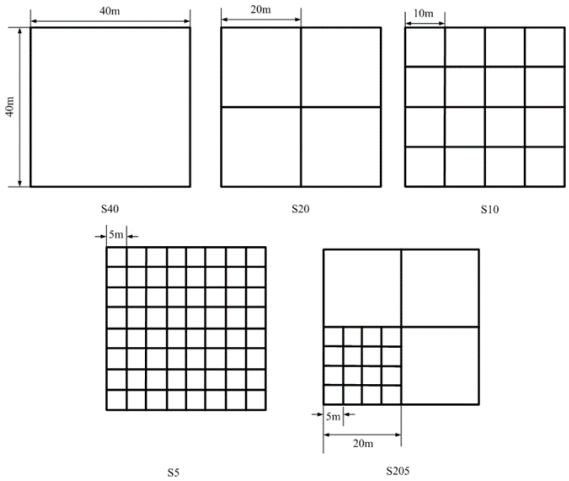

Figure 4.30: Illustration of meshes with various sizes

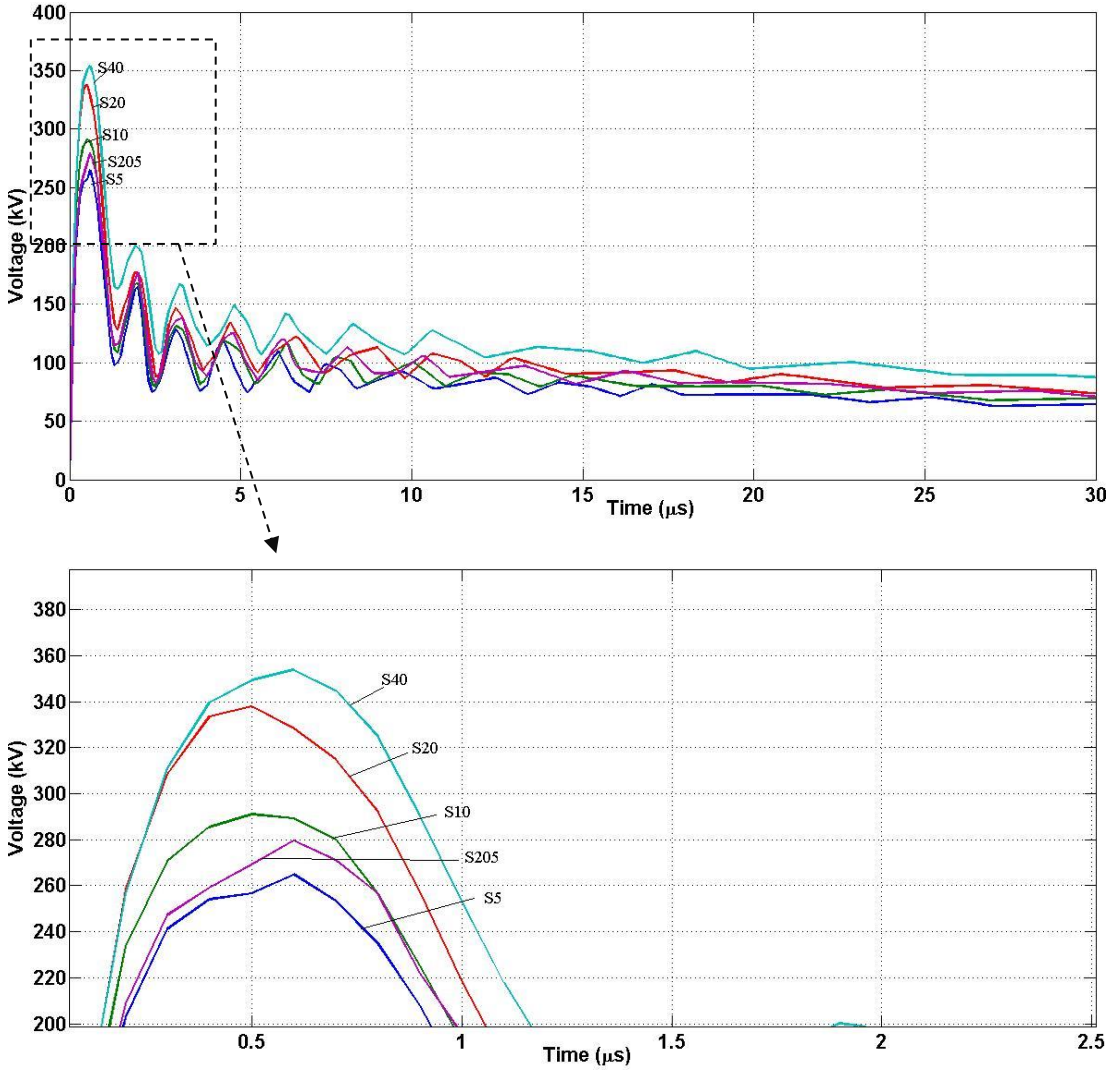

Figure 4.31: Ground potential rise at the injection point for different mesh sizes

4.5.5 Effect of current injection point

The location of the injection point can improve the grounding performance under lightning current, because it can create more paths for the current to flow from the grid to the soil. In this simulation, corner and centre injection points are considered for comparison, as depicted in Figure 4.32. The grid size is 40m x 40m with a 5m x 5m mesh size. Various impulse currents and front times with 1000Ω.m soil resistivity are considered in the simulation.

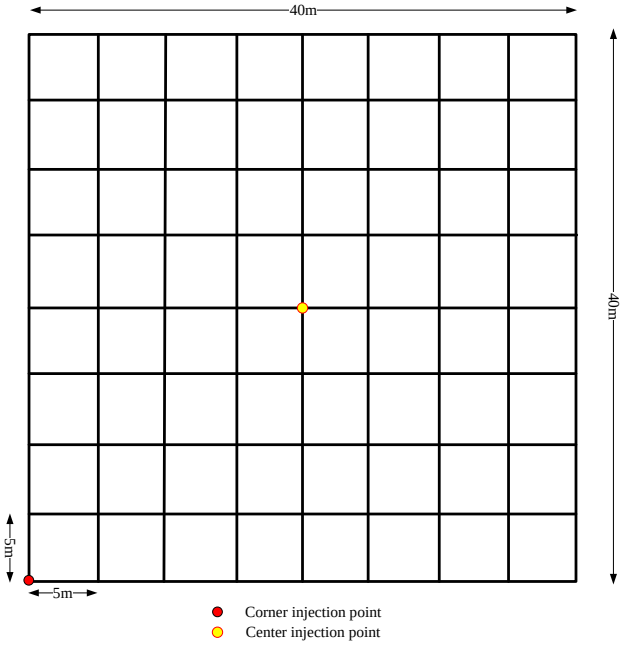

Figure 4.32: Location of injection point

Figure 4.33 shows the ground potential rise at the injection point of 1.2μs, 2.6μs, and 10μs front times. Centre injection will generate lower potential rise compared to corner injection. The maximum potential difference between the centre and corner injection point scenarios is almost 50% at a 1.2μs front time, while the difference for the slower rise time decreases to 20-30%. Therefore, it can be observed that the location of the injection point is more important for faster rise time impulses.

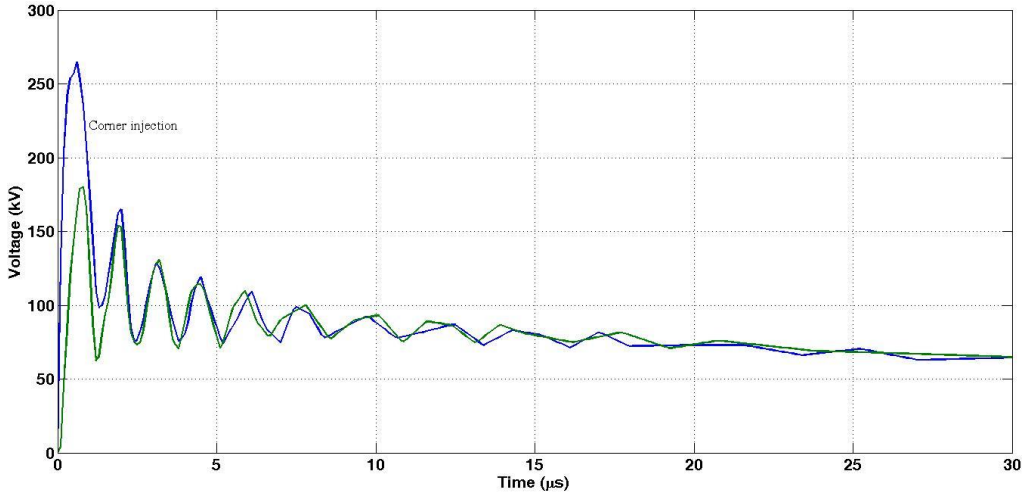

(a) Front time: 1.2μs

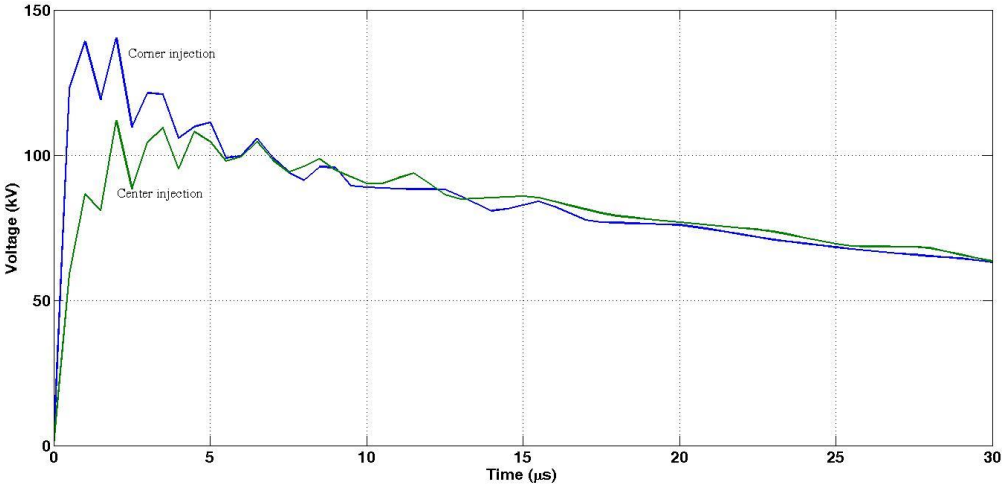

(b) Front time: 2.6μs

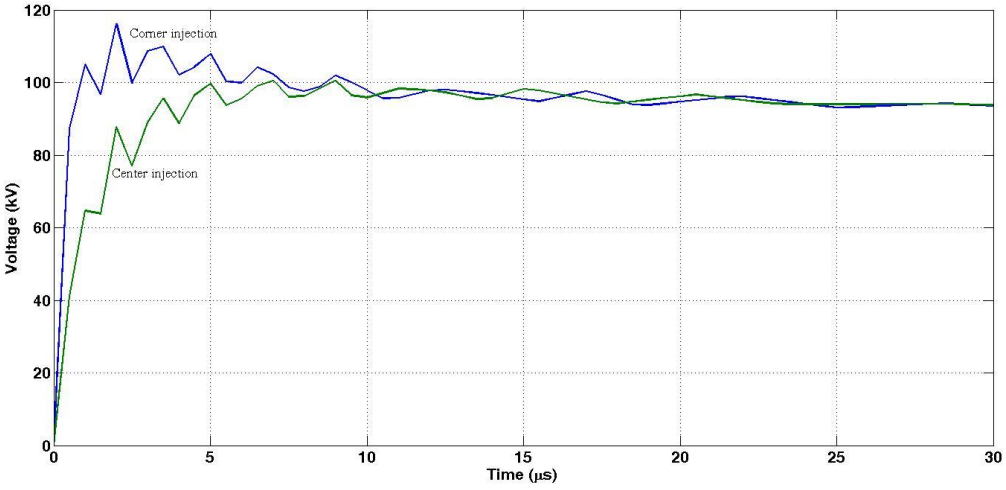

(c) Front time: 10μs

Figure 4.33: Injection of ground potential rise for soil resistivity of 1000Ω.m

4.6 Conclusion

This chapter presents a simulation procedure for a grounding system, which was based on the solution of Maxwell's equation. The modelling was carried out by applying the Finite Element Method, which required a finite boundary to simulate, and hence introduced significant challenges when the modelling process included some practical situations with un-defined boundaries. The best way to address the boundary issue is to increase the size of the boundary. However, higher computational time will be incurred. Therefore, it was very important to determine the minimum boundary size to achieve less computational time with a trade-off of insignificant impact on the simulation results. Therefore, this chapter demonstrated the effect of different sizes of boundary for the evaluation of current density, at varying distances between grounding grid and boundary. It was proven that the proposed method was an optimum approach to determine the minimum boundary size required during the modelling stage with un-bounded scenario, and where a perfect match layer (PML) function was not available in the software. It was evident in the results that a 100m distance between the grounding grid and the boundary was sufficient to achieve accurate results. The results were a specific outcome of the performance of the grounding grids under lightning conditions, with soil resistivity of less than 1000Ω.m, and current rise time of not less than 0.4μs. The simulations were validated by comparing with the published simulation results that applied the MOM technique and as well as from experiments. The effects pertaining to different parameters were also simulated, which revealed similar behaviours to the existing description given in the literature. Hence, sufficient validating procedures were carried out to conform the precision of the proposed model.

Chapter 5

Effective Area Evaluation and Proposal of New Formulation

5.1 Introduction

The electromagnetic approach and finite element method (FEM) can be used to model a grounding system under lightning conditions, as discussed in the previous chapter. Therefore, in this chapter, the ground potential rise will be investigated across different sizes of grid, with taking into consideration the power frequency and the impulse injection currents. Comparisons are made to demonstrate the different behaviours of grounding grids on the effective area under the conditions of lightning and power frequencies. Grid configuration is the best approach to improve the grounding design, compared to controlling the soil resistivity and lightning front time. Furthermore, increasing the mesh density near the injection point can provide additional paths for current to dissipate into the soil, which will reduce the potential rise at the injection point. However, this method is limited to the effective area of the grounding grid. In this chapter, the effects of the down conductor and grid depth are studied for different front times and soil resistivities, and compared with direct injection method to the grid. The inductance of conductor change when the depth of buried grid change as longer down conductor will be used. A significant impact can be observed on the effective area if the down conductor is considered in the simulation. Therefore, a new empirical formulation for effective area is proposed, where the down-conductor is taken into consideration at a 0.5m depth with square grounding grid. A

new formulation is important to guide the engineers in designing a better grounding system under the condition of lightning current.

5.2 Comparison between power frequency current and impulse current on the effective area

Grounding grid resistance is a key parameter that engineers apply to evaluate the effectiveness of the grounding design for power frequencies. Effective grounding design offers the lowest grounding resistance and concurrently provides the best path for unwanted current. The grounding resistance value can be reduced by decreasing the soil resistivity value and increasing the size of the grid. As suggested by IEEE 80-2000, the formula in Equation (5-1) is used to estimate the minimum grounding resistance (*R*) [2]. The equation assumes the resistance to be in a uniform soil. Potential rise at the injection point can be calculated by multiplying the grounding resistance with fault current magnitude.

$$\mathrm{R} = \frac{\rho}{4}\sqrt{\frac{\pi}{A}} \tag{5-1}$$

where ρ is the soil resistivity (Ω.m) and *A* is the area occupied by grounding grid.

Figure 5.1 depicts the peak potential rise at injection point for different front times of lightning current, which is compared against the power frequency at different square grounding grid sizes. In this simulation, the soil resistivity is 100Ω.m with 1.2μs, 2.6μs and 10μs front times. The magnitude of the impulse and fault currents are 10kA in this simulation. The result revealed that the ground potential rise at the injection point is higher under the condition of lightning current compared to the power frequency. Furthermore, faster front time will generate higher potential. However, under all circumstances, the potential gradient grows smaller when the size of the grid increases.

The gradient will reduce up to the stage where almost none or very small reduction in the impact towards the potential due to the increasing grid size. The condition can be explained by the effective area concept. Besides, the effective area of impulse current is smaller compared to that of the power frequency. In Figure 5.2, the peak potential rise can be observed at the injection point under power frequency and impulse current. The peak arises due to the increasing grid size from 5m x 5m to 40m x 40m at 100 Ω.m, 300 Ω.m, and 1000Ω.m of soil resistivity. Similar case can be observed at 100Ω.m soil resistivity at both potential rise and effective area. However, for high resistivity soil, the potential difference is small for the grid below 10m x 10m between power frequency and impulse injected current.

From the overall observation, the effective area becomes smaller under impulse current. However, the effective area expands for long rise time and higher soil resistivity. In the case of grounding grid design, the size of the grounding grid is an important requirement for power frequency design to cover the entire area of substation equipment installed. Therefore, the effective area under lightning current is more useful in enhancing the grid conductor for improved protection from transient ground potential rise.

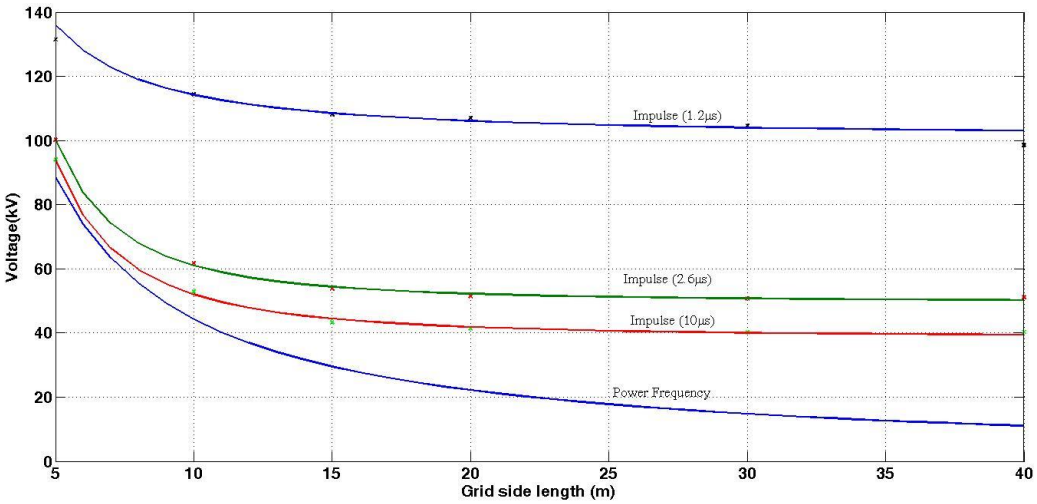

Figure 5.1: Peak voltages for different sizes and impulse current front times (ρ = 100Ω.m)

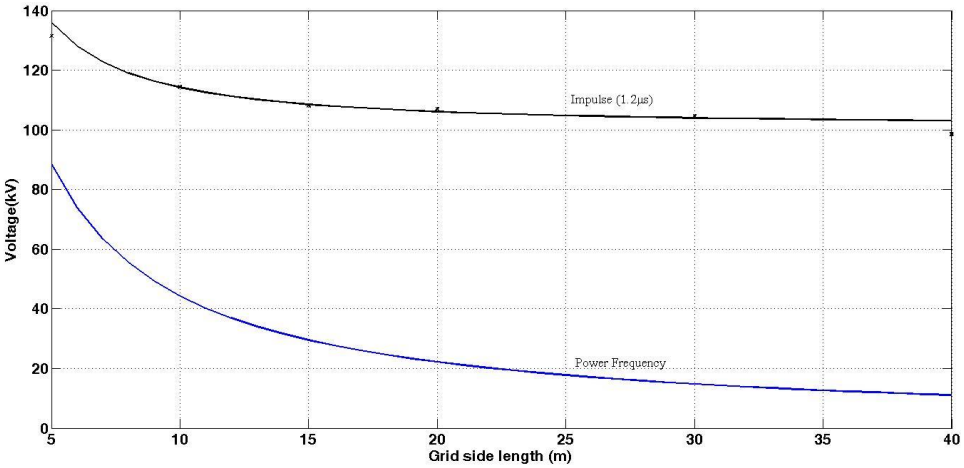

(a)

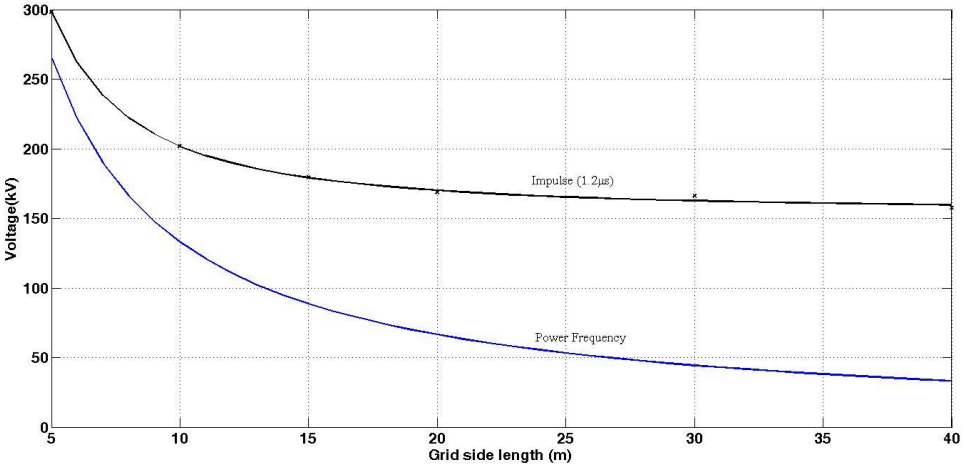

(b)

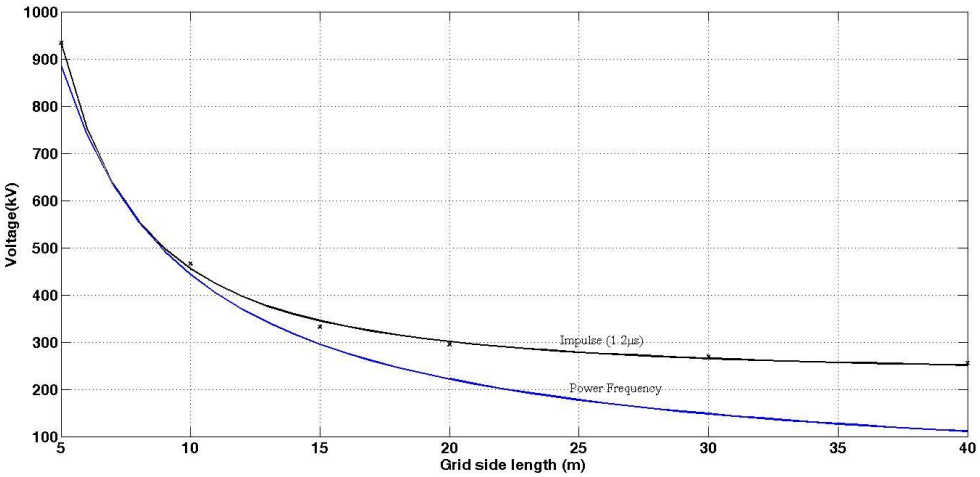

(c)

Figure 5.2: Peak voltage at the injection point for different grid sizes, where the ft=1.2μs and soil resistivity are (a) 100Ω.m, (b) 300 Ω.m, and (c) 1000 Ω.m

5.3 Effective area evaluation

The effective area is defined as the optimum size of the grid that can improve the grounding impedance at the injection point. It is widely known that the current will flow through the conductor via the lowest impedance path. The effective area that is used in this study is illustrated in Figure 2.18. The evaluation of the transient potential rise throughout the conductor will be discussed in the next chapter.

Figure 5.3 shows the injection current and voltage at injection point for grid with size 5mx5m and 40mx40m. The voltage rise time is more faster compare to current rise time for larger grid. It shown the inductive effect is more significant for larger grid as more conductor involve to disperse current to the soil. The grounding impedance calculated by divide the maximum voltage with maximum current at injection point. While, the effective area is calculated in this study based on the flow chart shown in figure 5.4. Different sizes of grid are used in the simulation, namely 5m x 5m to 60m x 60m and 5m x 5m grid mesh. Grounding impedance is calculated for every size with different parameters to simulate the soil resistivity and lightning front time. The computed grounding impedance is plotted relative to different sizes of the grid. The effective area is achieved when an improvement in the grounding grid becomes less than 1% relative to an increase of 1m in the grid size.

For example, Figure 5.4 exhibits the grounding impedance for different sizes of the grid at 1000Ω.m soil resistivity and 2.6μs front time. At 39m side length, the impedance value is 15.29Ω, while at 40m the impedance is 15.14Ω. Therefore, the effective area is achieved at 39m because the improvement at 40m is less than 1%.

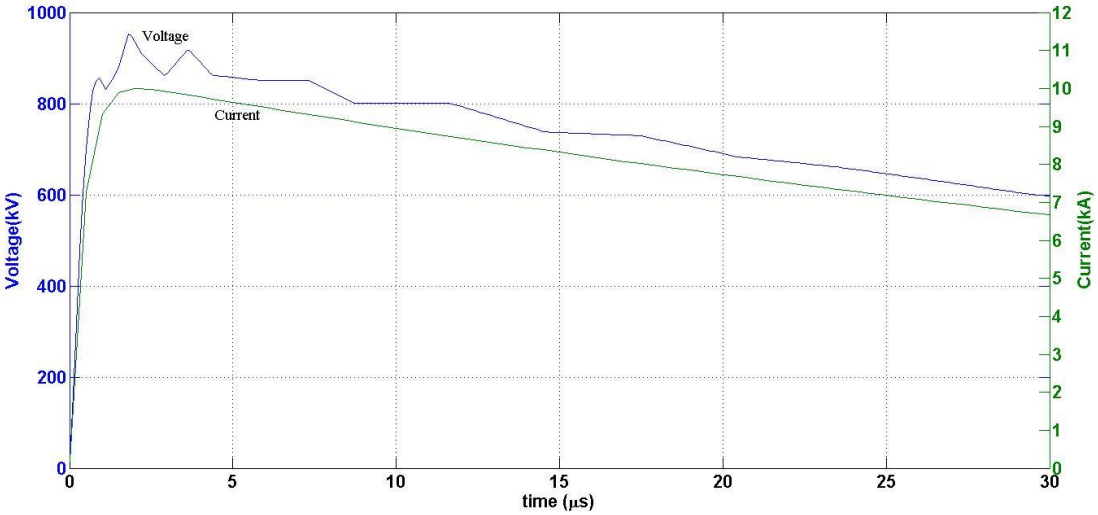

(a) 5mx5m

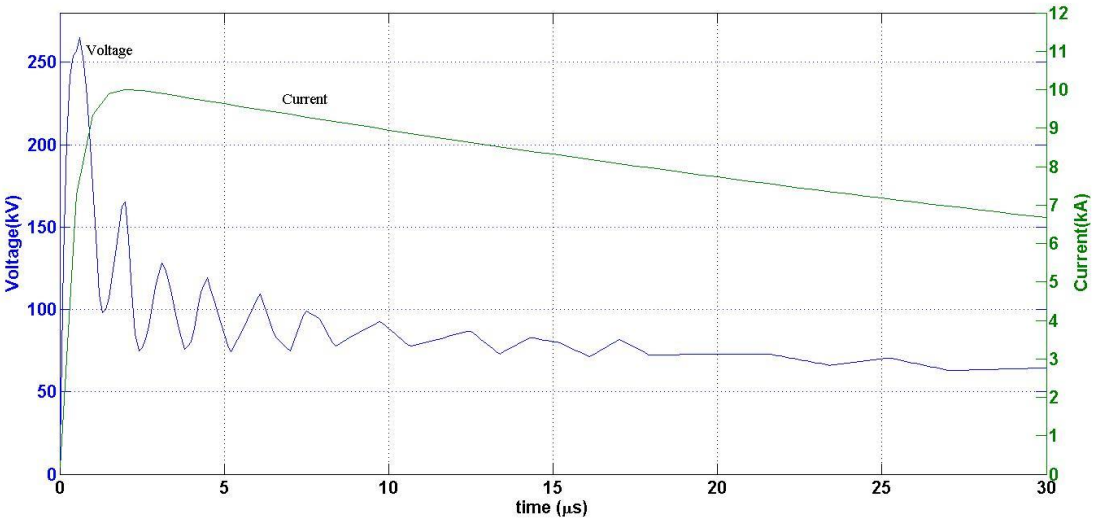

(b) 40mx40m

Figure 5.3: Voltage at injection point when 1.2/50μs impulse current injected at corner of different size, (a) 5mx5m and (b) 40mx40m

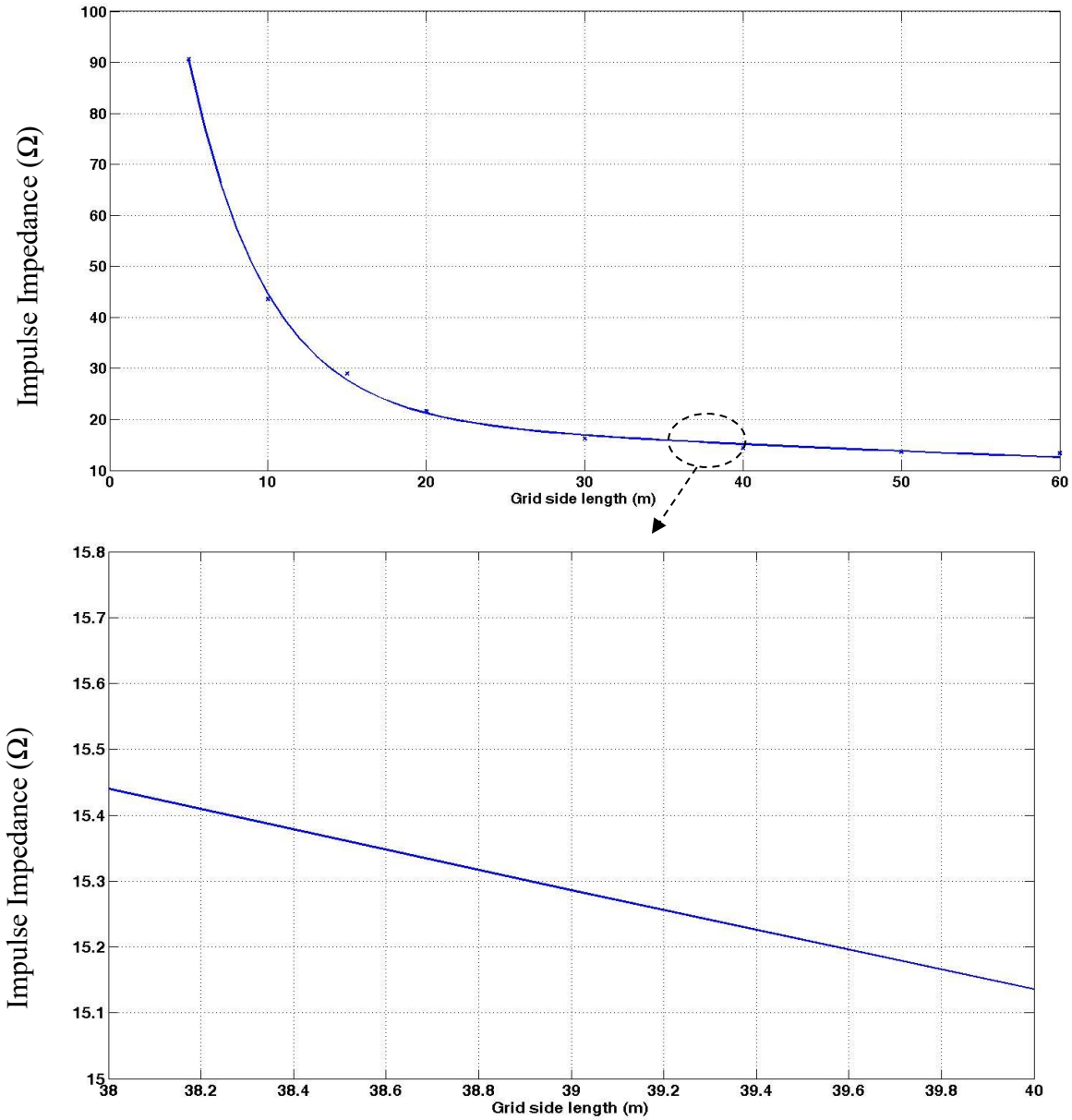

Figure 5.4: Grounding impedance at different grid sizes

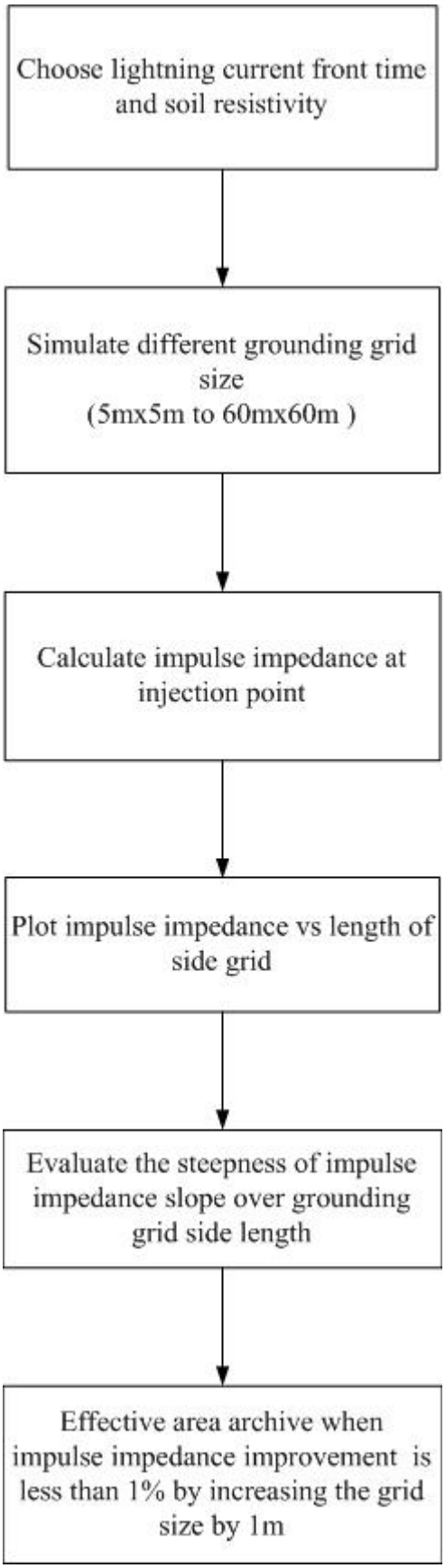

Figure 5.5: Effective Area calculation process

5.4 Influence of down-conductor on effective area

In this section, the effects of the down-conductor towards the impulse impedance and effective area are evaluated. Figure 5.6 illustrates the direct injection and injection at the top of soil through the down- conductor. The injection at the top of soil is assumed to have no significant loss in the air. Simulations are carried out with different soil resistivity values and front times for both conditions.

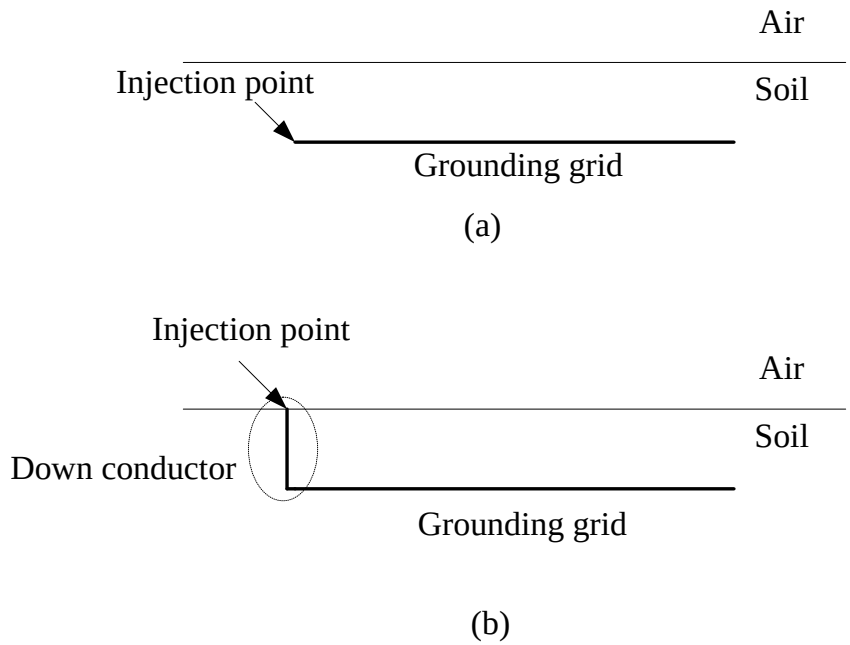

Figure 5.6: Illustration of models (a) injecting directly to the grid and (b) injecting through down-conductor

The effects of down-conductor are investigated when the grid conductor is buried 0.5m below the ground. A comparative analysis is conducted between direct injections to the grid and injection through the down-conductor from the top of the soil. Figure 5.7 shows the grounding impedance over the grid side length for soil resistivity values of 100 Ω.m, 300 Ω.m, and 1000 Ω.m, with a 1.2μs front time. It can be observed that the impedance is higher when the injected current is at the top of soil for 100 Ω.m soil,

across all sizes of the grid. In the case of 300 Ω.m and 1000 Ω.m soil, the impedance for the top soil injection is lower for smaller grid size.

Figure 5.8 shows the grounding impedance for different front time injection currents. The grounding impedance value is dependent on the soil resistivity, but the saturation point achieved rapidly when the down-conductor in the model is considered for a longer rise time. Although grounding impedance values differ by approximately 5% to 10%, a faster saturation point is achieved by considering the down-conductor in the modelling. Table 5.1 presents an effective area comparison between direct injection to the grid, and injection through the down-conductor for a 0.5m depth. It is clear that no impact can be observed for the effective area with 1.2μs front time across all the values of soil resistivity. However, the effective areas are smaller when the down-conductor is considered in the simulation at the rate of 2.6μs and 10μs rise times. A longer rise time produced a significant impact on the effective area calculation for grounding grids under the impulse current. Therefore, the assumption used by the previous effective area equations is less accurate for longer rise times, while in practice, the down-conductor should be connected to the grounding grid. In addition, the lightning current front time ranges from 0.2μs to 20μs or 30μs, which is measured at the attachment point of the lightning receptor [130-132]. The lightning current can be longer at the grounding grid, either through a down-conductor or surge arrestor. Therefore, the down-conductor should be considered to achieve a more accurate formulation to estimate the effective area in grounding grid simulation.

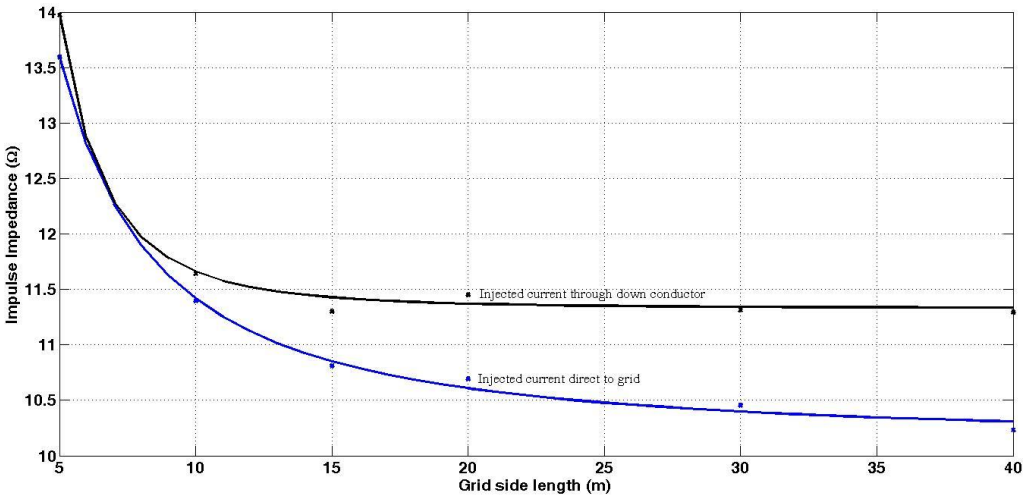

(a) 1.2µs

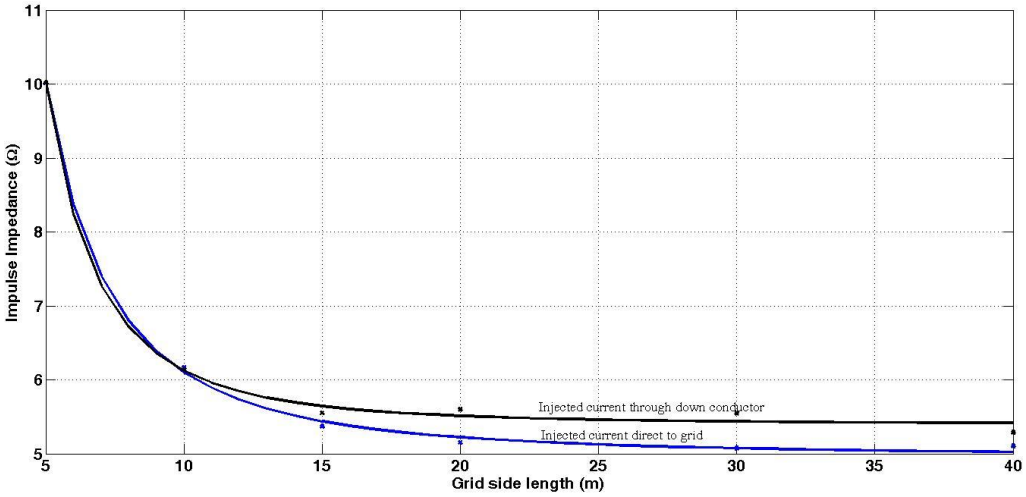

(b) 2.6µs

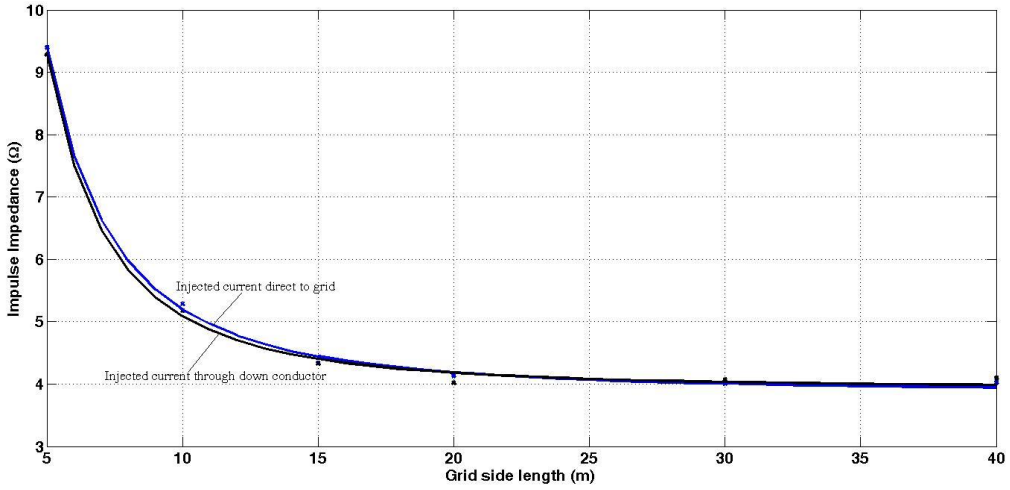

(c) 10µs

Figure 5.7: Impulse impedance for 100Ω.m soil resistivity with different front times at (a) 1.2 µs, (b) 2.6 µs, and (c) 10 µs

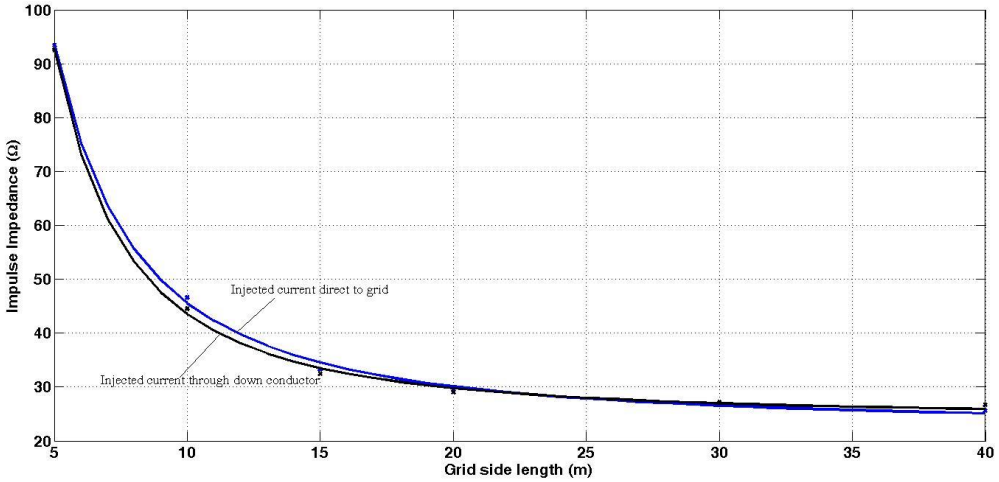

(a) 1.2μs

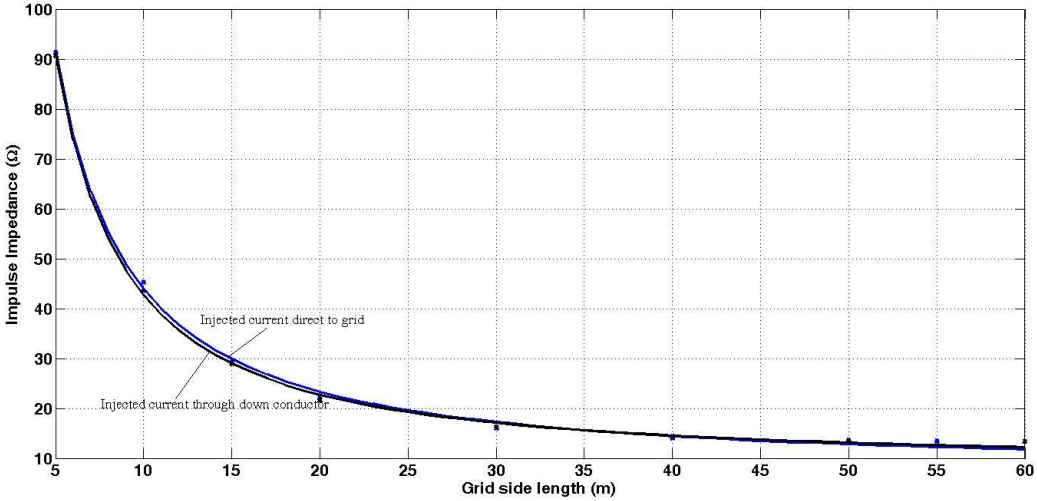

(b) 2.6 μs

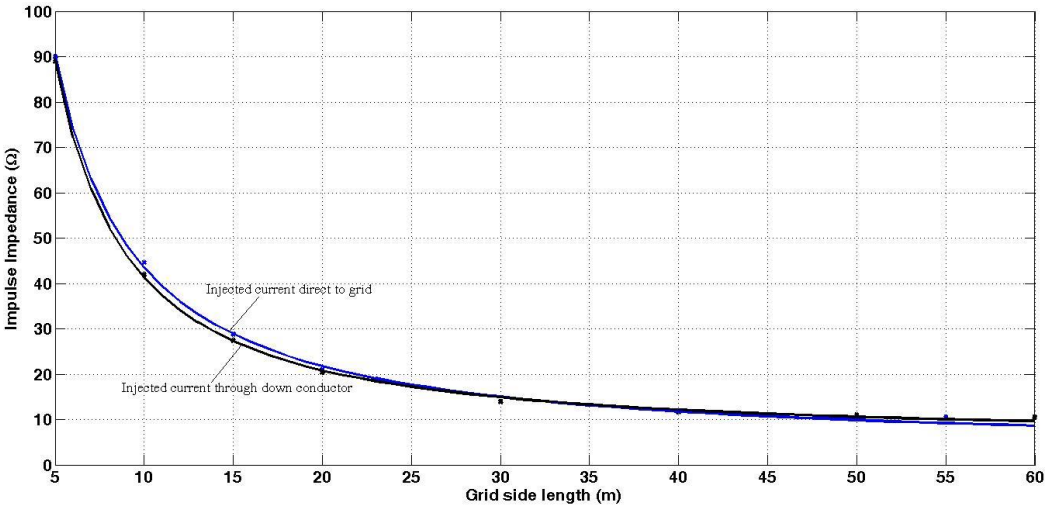

(c) 10 μs

Figure 5.8: Impulse impedance for 1000Ω.m soil resistivity and different front times at (a) 1.2 μs, (b) 2.6 μs, and (c) 10 μs

Table 5.1: Effective area side length comparison for different considerations of the location of injection

Current front time (μs)	Soil resistivity (Ω.m)	Effective area side length (m)	
		Injection directly to the grid (0.5m depth)	Inject through down-conductor (0.5m depth)
1.2	100	11	11
	1000	25	22
2.6	100	17	15
	1000	43	39
10	100	18	17
	1000	54	49

5.5 New empirical equation for grounding grid design

Consideration of the down-conductor in the simulation is an utmost important step for the calculation of the effective area in grounding grid design. Therefore, in this study, the effective area formulation for a grid with 0.5m depth is proposed for engineers to apply during the grounding grid design. Table 5.2 presents the effective area across all soil resistivity and front time values when current injected at corner of grounding grid. The effective area is increased proportionally with soil resistivity for all front times, as shown in Figure 5.9. Figure 5.10 depicts the effective area against front time for different soil resistivity values. It is clear that the effective area increased rapidly for high soil resistivity. The empirical equation of the effective area is proposed

based on the obtained simulation data for square grounding grid, as illustrated in Figure 5.11. A regression technique is used to fit the data with a 93.16% R^2 value and 92.54% adjusted R^2 value. It can be observed that the proposed equation fits well with the simulation data, where the proposed equation is

$$a_{effective} = 1.696(\rho T)^{0.3271} \quad (5\text{-}2)$$

Table 5.2: Effective side length at different conditions

Front time (μs)	Soil Resistivity (Ω.m)	Effective area side length (m)
1.2	50	11
	100	11
	300	15
	1000	22
2.6	50	12
	100	14
	300	23
	1000	39
10	50	14
	100	17
	300	29
	500	38
	1000	54

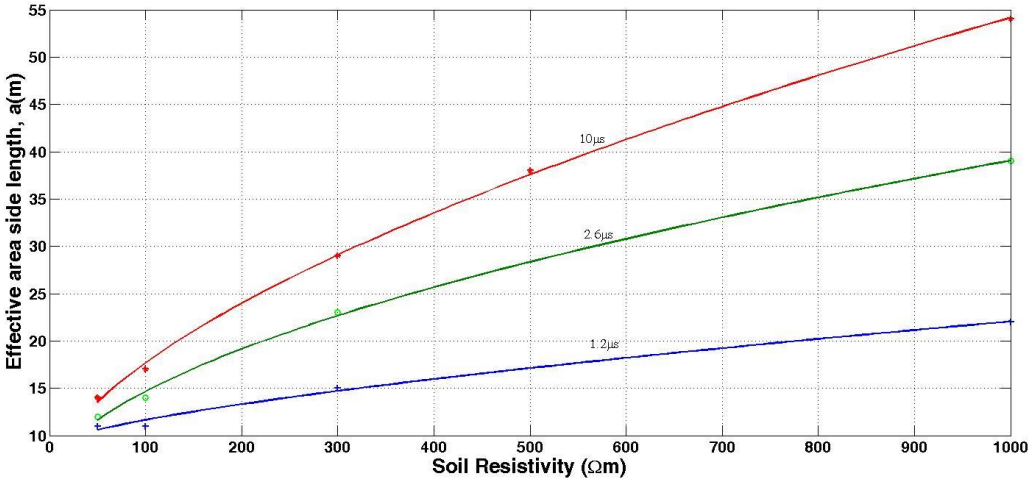

Figure 5.9: Effective Area vs soil resistivity at different front times

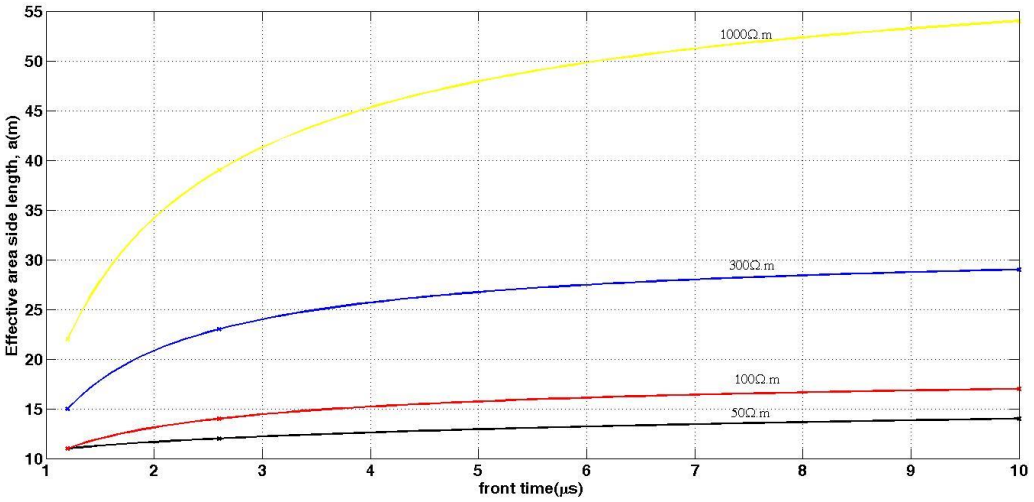

Figure 5.10: Effective area vs front time at different soil resistivity

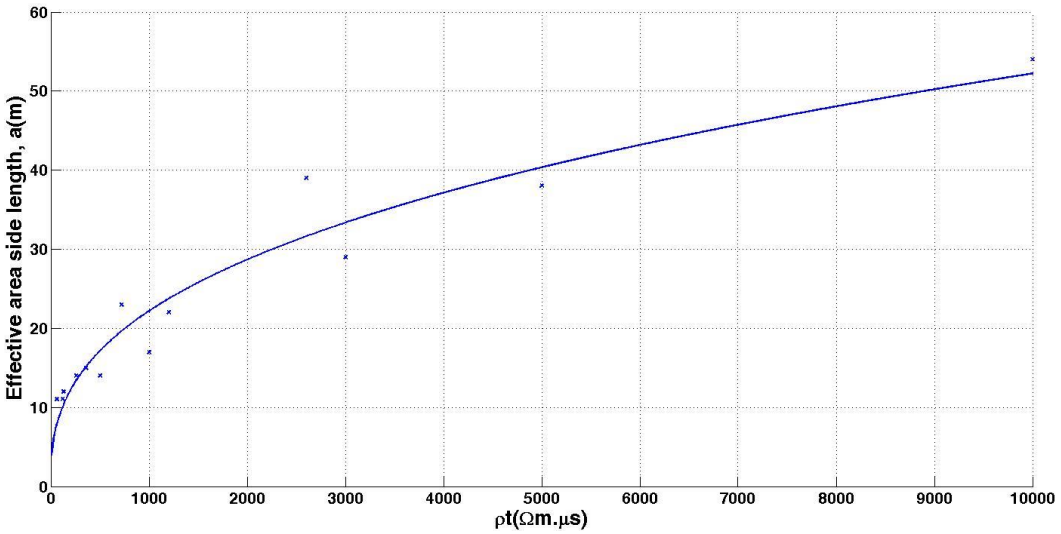

Figure 5.11: Regression plot of the effective area side length

Equation (5-2) is formulated based on the corner injection simulation. In the effective area formulation, the relationship between the centre and the corner injection varies from the previous researches. Gcev [69] reported that the effective area at the centre injection point was doubled for corner injection, while Zeng et al. [74] and Gupta[40] reported that centre injection had 60% more effective area compared to corner injection. The relationship between the locations of the injection is based on the potential rise, as discussed in Section 4.5.5.

In order to understand the relationship, the simulations are performed to compare both locations of the injection at different soil resistivity and front times. Figure 5.12 illustrates the grounding impedance for various grid sizes, which includes both the centre and the corner injection points. From the graph, the effective area of both injection points are calculated, as presented in Table 5.3. It can be observed that the centre injection offers double the effective area compared to the corner injection. The proposed effective area formulation for square grounding grid is presented in equation (5-3).

$$a_{effective} = K.[1.696(\rho T)^{0.3271}] \quad (5\text{-}3)$$

Where $K = 2$, for centre injection

$K = 1$, for corner injection

ρ = soil resistivity (Ω.m)

T = impulse front time (μs)

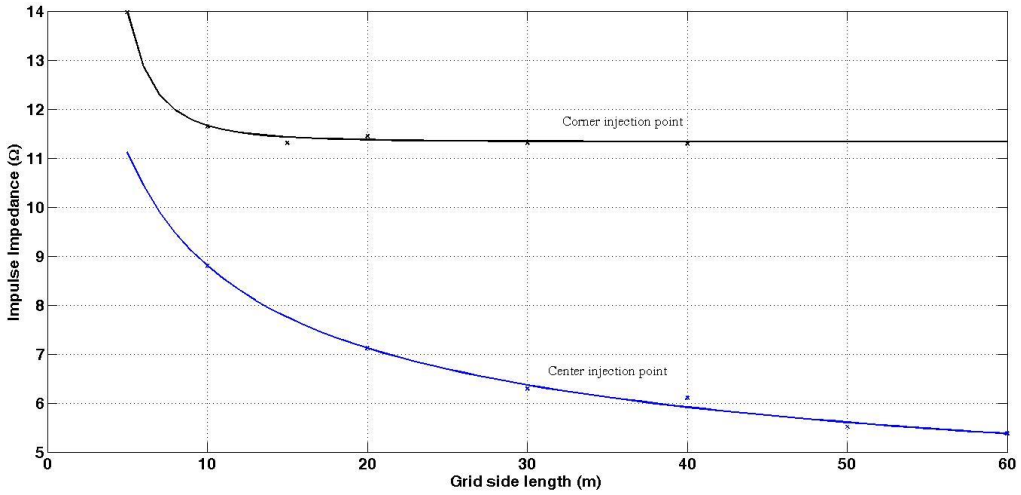

(a) Front time = 1.2 μs, ρ = 100Ω.m

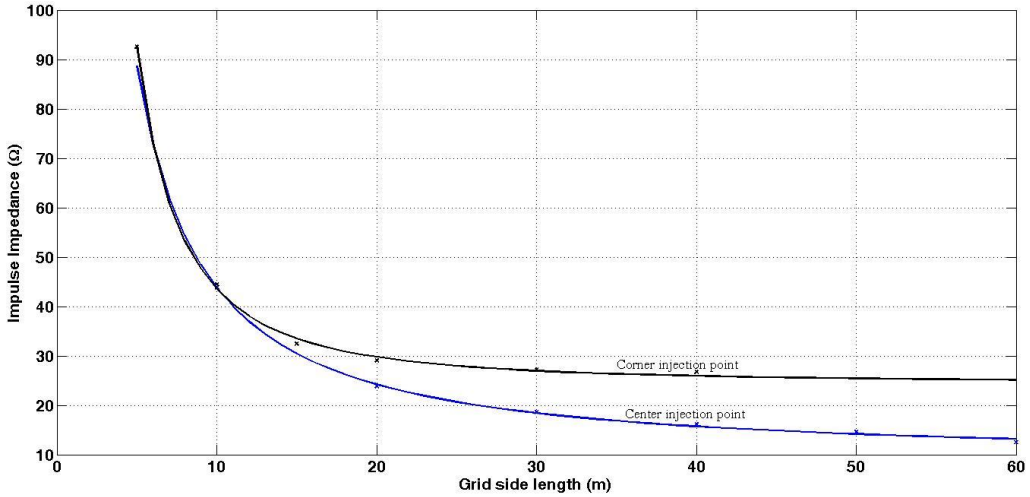

(b) Front time =1.2 μs, ρ = 1000Ω.m

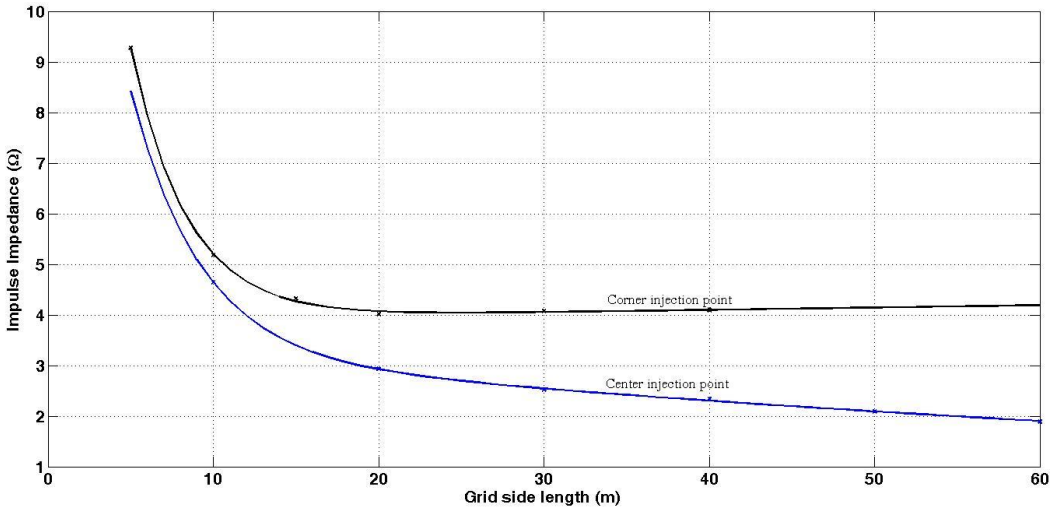

(c) Front time =10 μs, ρ = 100Ω.m

Figure 5.12: Comparison of centre and corner injections at different grid sizes

Table 5.3: Effective area side length for both centre and corner injections

Front time ,T (μs)	Soil Resistivity, ρ (Ω.m)	Effective area side length	
		Corner injection (m)	Center injection(m)
1.2	100	11	22
1.2	1000	22	44
10	100	17	35

5.6 Empirical equation comparison with previous works

Formulae for effective area were proposed by Grcev [57], Gupta et al. [40] and Zeng et al. [75], as discussed in section 2.5.2. In order to compare the proposed formulas, equations (2-11) and (2-12) are considered as the definitions of the effective area, which will be used in this research framework, as shown in Equations (5-4) and (5-5).

$$a_{effective} = (1.45 - 0.05s).\sqrt{\pi\rho T} \quad (5\text{-}4)$$

$$a_{effective} = 0.34\sqrt{\pi}\rho^{0.42}T^{0.34} \quad (5\text{-}5)$$

Figure 5.13 illustrates a comparison of the various effective area equations specifically for the corner injection. The comparison includes previously-published work, and the proposed empirical Equation (6-3) of this framework, which considered the effect of the down-conductor. A comparison with the Grcev formula suggests that the differences could be due to the limited simulation data. Grcev equation was derived from a 0.8μs front time at different soil resistivity values, as shown in Table 2.7 [69].

In addition, the effective area of Grcev's formulation is based on the impulse impedance being equal to the ground resistance, which is not applicable for all cases, as shown in Section 5.2.

In the case of Zeng et al. [75], the equation demonstrated a similar trend as the proposed equation herein. However, it is only applicable for smaller effective area. The limitation is due to Zeng et al.'s simulation that assumed soil ionization to occur in every case, which led to the observed difference. The proposed equation in this thesis considered the down-conductor effect, which effectively provided a smaller estimation effective size than those simulations conducted by Gupta and Thapar equations. In addition, the underlying simulation method may introduce the differences. Moreover, the validity of curve-fitting for the equation was not discussed in the previous publications.

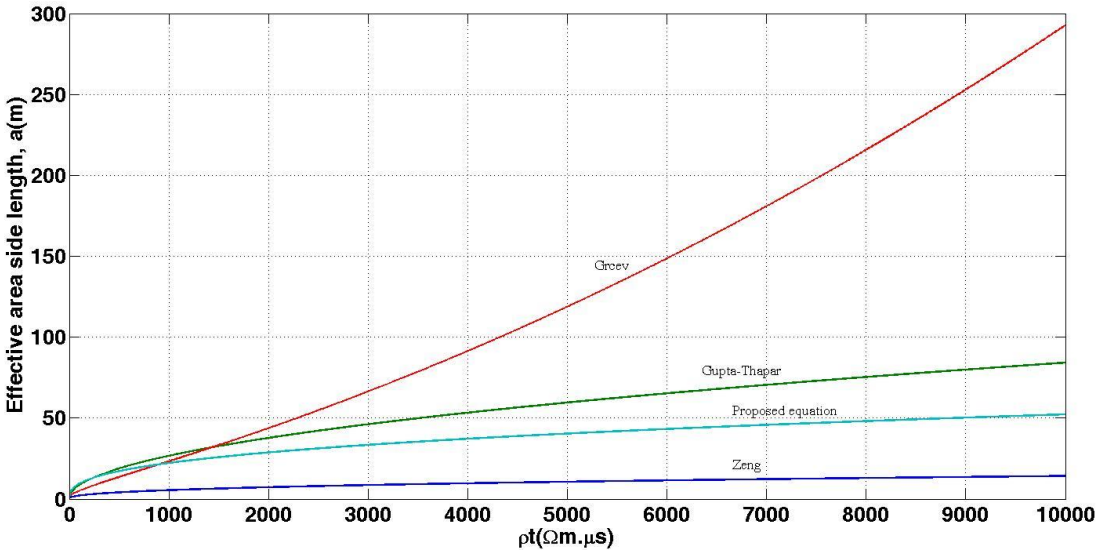

Figure 5.13: Comparisons of previous equations with the proposed equation

5.7 Conclusion

The grounding performance is measured by using the impulse impedance at the injection point. The extension of the grid size provided some degree of improvement, but it is limited to the effective area. When the down-conductor is considered in the simulation, the short rise time (1.2μs) currents did not impact the effective area. However, during the longer rise times (2.6μs and 10μs), the effective area became smaller. In order to amplify the advantage of down-conductor, a new empirical effective area formulation is proposed, where the down-conductor effect is taken into account during the simulation. Apart from down-conductor, the formulation also considered both corner and centre injection points. The proposed formulation operates at different front times, ranged from 1.2μs to 10μs, while the soil resistivity values ranged from 10Ω.m to 1000Ω.m. The square grid sizes varied from 5m x 5m to 60m x 60m, which also includes a 5m x 5m mesh size, and the down- conductor is considered from the top of the soil to the grounding grid that is buried 0.5m underground. A comparative analysis is carried out by comparing the proposed formulation with the previously published formulae. As effective area for impulse is smaller than effective area for power frequency, grid size need to fulfill power frequency requirement. Refine the mesh around possible lightning current injected point can improve protection level but it limit to effective area.The relationship between the effective area and the transient ground potential rise will be discussed in the next chapter.

Chapter 6

Transient Ground Potential Rise (TGPR)

6.1 Introduction

As discussed in the previous chapter, the effective grounding grid area is achieved when there is no significant change in the impulse impedance relative to the increasing grid size. However, the graphical illustration shown in Figure 2.17 and Figure 2.18 demonstrated the differences among the ideas of various researchers. In this chapter, the potential rise is presented for a location that is further from the injection point. The relationship between the potential rise and the effective area is also discussed. In addition, the step voltages are evaluated inside and outside of the grid, so that the location of the maximum step voltage occurrence for a typical grounding grid design can be explored. The step voltages are evaluated across different locations, and the locations are chosen based on the distance from the injection point.

6.2 Transient Ground potential rise

The potential rise during the transient period is a very important parameter during the evaluation of the effectiveness of the grounding grid. Ground potential rising throughout the grid can be dangerous to equipment and humans. In this simulation, an impulse current of 10kA, with a 1.2/50μs front time, is injected at the corner of the grid. The soil resistivity is fixed at 1000Ω.m, while the transient ground potential rises (TGPR) at the surface of the conductor throughout the grid are also calculated.

Figure 6.1 depicts the TGPR at different locations, which is was obtained from computer simulation. It can be observed that a large potential rise during the transient period actually occurs at the injection point for a couple of microseconds. This phenomena takes place when the lightning current flows to the ground. Thereafter, the potential is reduced over time until it reaches a steady state value throughout the whole grid. For example, the potential sharply increased at the injection point for the first 2μs, and the transient time lasted up to 10μs. Figure 6.2 depicts the peak transient ground potential rise throughout a 40m x 40m grid when the lightning current is injected at one corner. This is followed by a reduction throughout the grid as a function of moving farther from the injection point. This finding agreed with the illustration that demonstrated the effective area a square area with $a_{\text{effective}}$ side length, as reported by Grcev. Similarly, the illustration agreed with the proposed effective area formulation in the previous chapter.

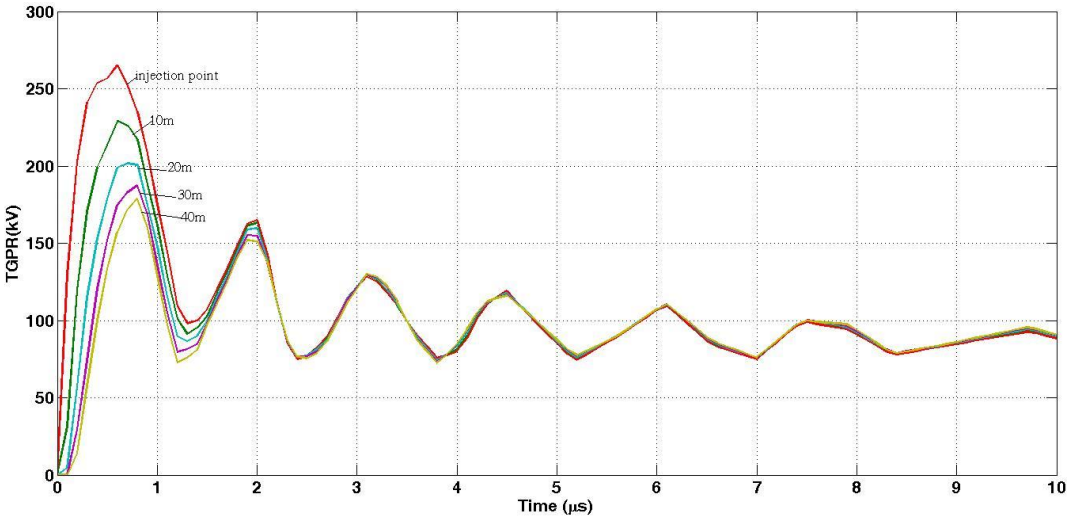

Figure 6.1: TGPR at different points away from the injection point

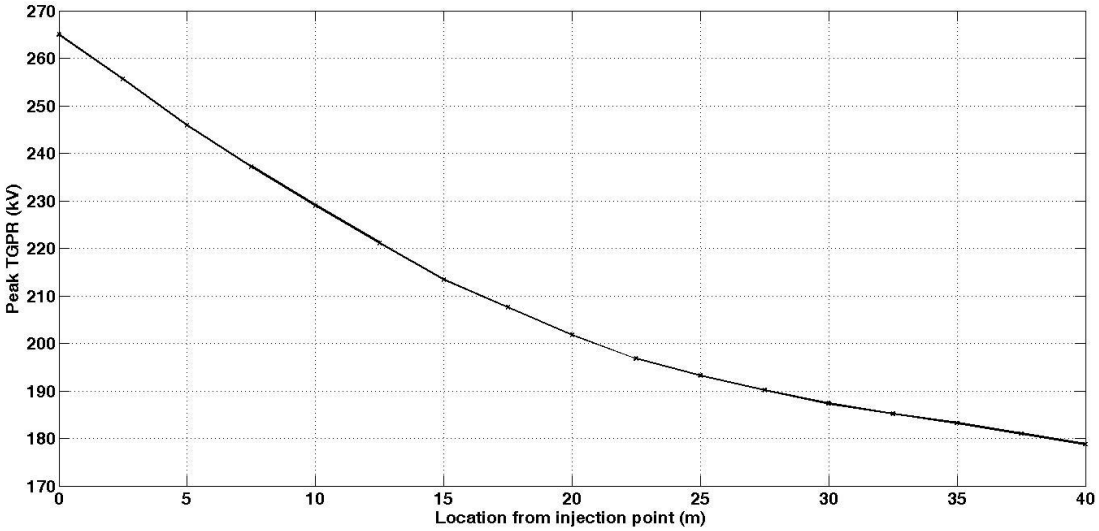

Figure 6.2: Peak transient ground potential rise at the grounding grid with 1.2μs front time and ρ=1000Ω.m

6.3 Relationship between TGPR and effective area

As suggested in [69], the effective area is not directly-proportional to the area of the conductor that effectively discharges the impulse current. It is instead related to the control mechanism of the grounding impedance by increasing the size of the grid. Therefore, in this section, the author attempts to understand the relationship between potential rise through the conductors of the grid, and within the effective area. Five different grounding grid configurations, as shown in Figure 4.26, are adopted for simulation. The size of the grids are varied from 5m × 5m to 40m × 40m, which includes a 5m × 5m inner mesh size. The grids are then buried 0.5m below the earth surface, and a 10kA impulse current is injected at a corner of the structure through the down-conductor. Based on the peak TGPR shown in Figure 6.2, the peak TGPR alongside the conductors are evaluated at every 1m distance for both 5m x 5m and 10m x 10m grids, while evaluation for other grid sizes is performed at every 2.5m. The results are then compared with the effective area from the previous chapter, as

presented in Figure 6.1. Simulations are performed for different soil resistivity, grid sizes, and front times of an impulse current.

Figure 6.3 illustrates the relationship of peak TGPR that is alongside the grid conductor for both different soil resistivity and grounding grid sizes. It is found that the peak TGPR will start to reduce along the grid when it moves further from the injection point. Figure 6.3(a) exhibits results from a grid that is buried in 100Ω.m soil, where the effective area is 11m x 11m, as presented in Table 6.1. The result revealed that increasing the grid size larger than the effective area actually did not improve the potential rise at the injection point, and as well as along the grid. Similar trend can be observed for high resistivity soil, as depicted in Figure 6.3(b). The trend unveiled a reduction of the gradient of the peak TGPR value over the distance is actually influenced by soil resistivity. It can be seen that the gradient of the reduction is higher for low-resistivity soil. Figure 6.3(c) shows the peak TGPR against the grid size for 100Ω.m soil resistivity, with 10μs front time of the injected impulse current and effective area of 17m x 17m. The graph revealed that the peak TGPR did not offer any improvement when the effective area is achieved. Furthermore, the peak TGPR is also influenced by the rise time, where a fast rise time will generate a larger ground potential, and therefore reaches the effective area quicker.

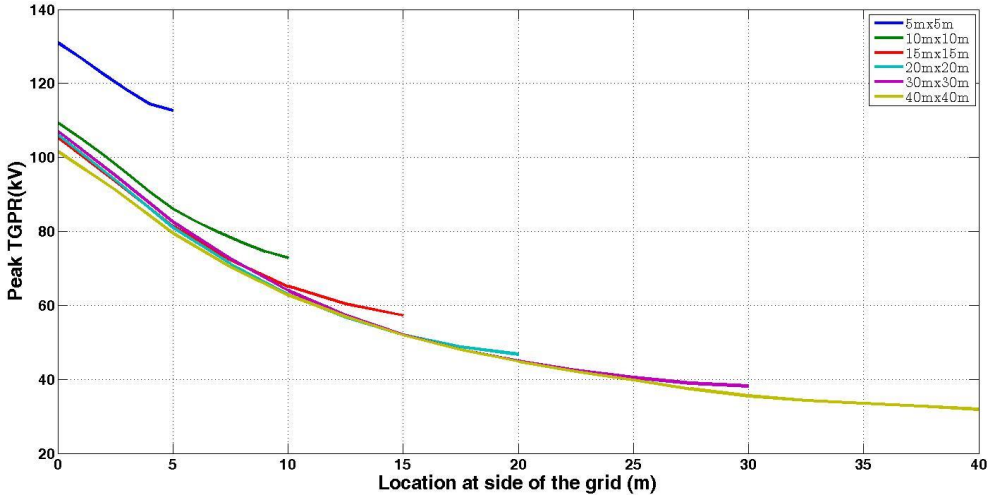

(a) Front time = 1.2μs and soil resistivity = 100Ω.m

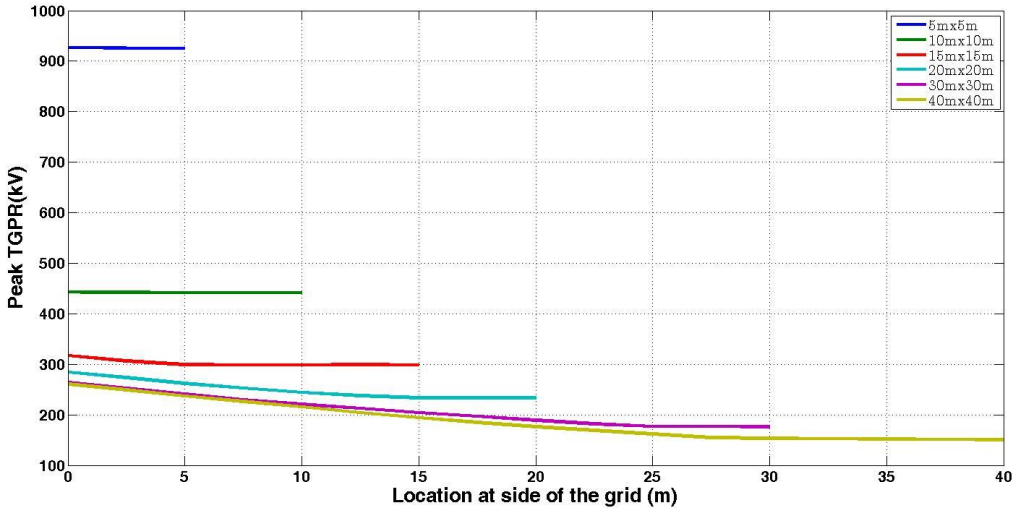

(b) Front time = 1.2μs and soil resistivity = 1000Ω.m

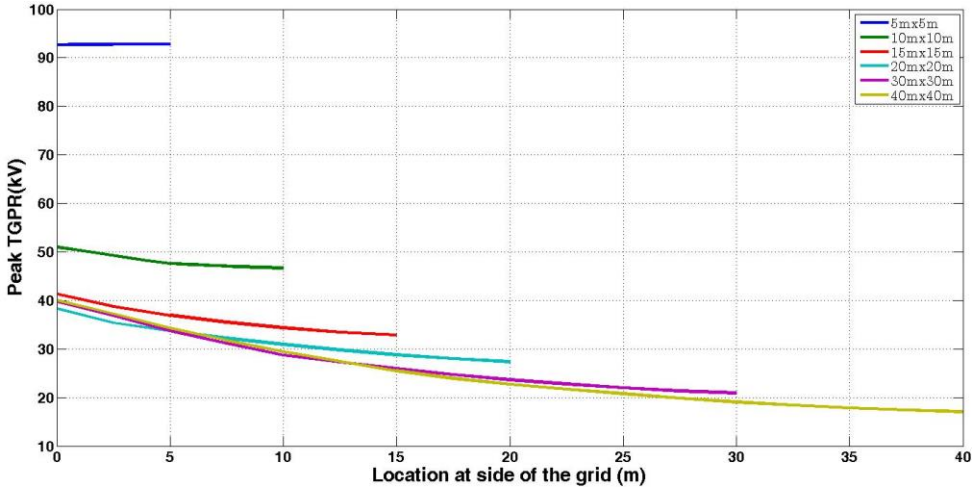

(c) Front time = 10μs and soil resistivity = 100Ω.m

Figure 6.3: Peak TGPR for 40m x 40m grounding grid with injection at corner, investigating across varying front time and soil resistivity

Table 6.1: The effective Area for corner injection

Front Time (μs)	Soil Resistivity (Ω.m)	Effective Side length (m)
1.2	100	11
1.2	1000	22
10	100	17

6.4 Step Voltage Evaluation

The step voltage is the Thevenin voltage at the top of the soil, with a 1m separation between the elements. The voltage represents the potential difference between two feet that can induce current flow through human body. Under transient conditions, TGPR can produce a step voltage beyond the safety limit. Therefore, an attempt is made to evaluate the location and the size that influences the step voltage.

As a result, maximum step voltages at different locations above the grid are calculated. Figure 6.4 depicts a 20m x 20m grid with 5m x 5m mesh, which is buried 0.5m deep under 1000Ω-m soil. An impulse current with 10kA peak and 1.2/50μs wave shape is injected through the corner of the grid.

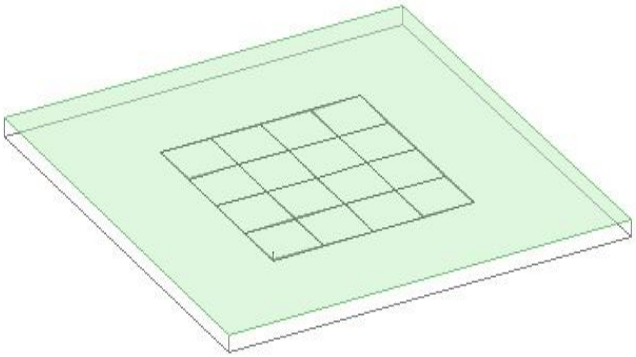

Figure 6.4 Grounding model

6.4.1 Maximum step voltage

Six different locations near the injection point are chosen to evaluate the maximum step voltage, as shown in Figure 6.5. The locations of a, b, and c are chosen to represent actual situations of a human standing with both feet inside the grid, while locations d, e, and f represent the situations when one of the feet is located outside of the grid. The locations that are chosen should cover step voltages as a possible scenario, while the injection point becomes a reference.

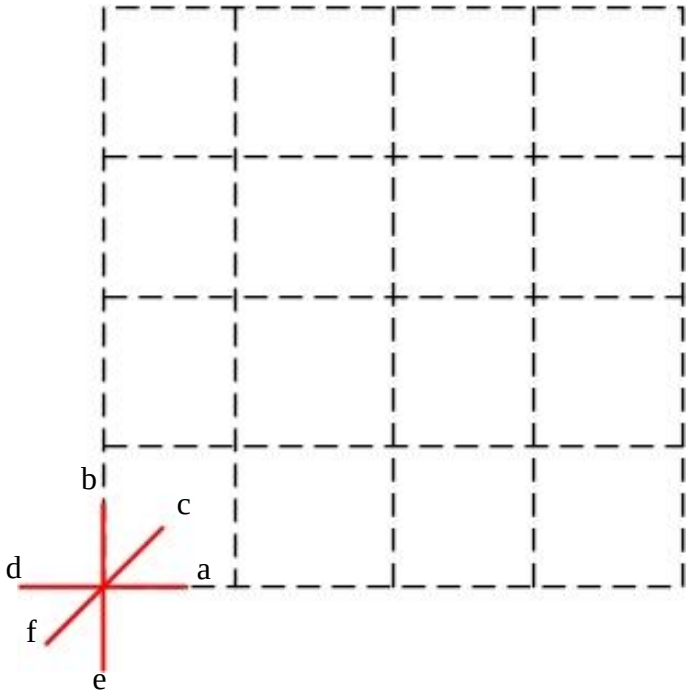

Figure 6.5: Locations near the injection point

Figure 6.6 demonstrated that the step voltages inside the grid are approximately 50% - 60% lower compared to the cases where one of the feet is located outside the grid perimeter. Step voltages are calculated inside or outside the grid, and are not influenced by the positions of the human that is standing above the grid.

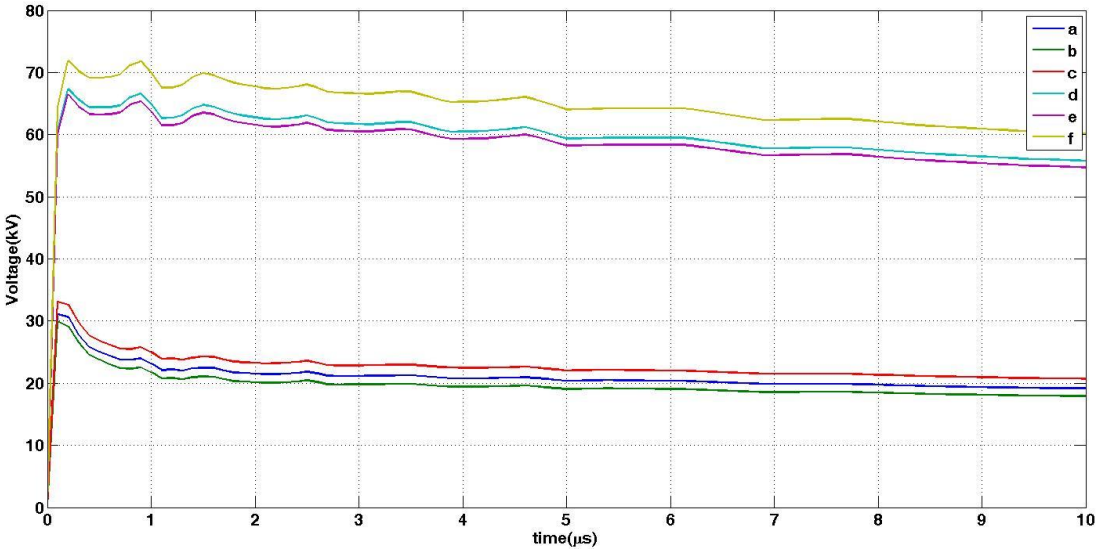

Figure 6.6: Step voltages at different point of locations near the injection point

In order to enhance the knowledge of step voltages during the flow of lightning current through the grounding-grid, the step voltages occurred further away from the injection point are calculated, as depicted in Figure 6.7. Four directions are chosen, both inside and outside the grid, where step voltages are calculated for every 2.5m movement from the injection point.

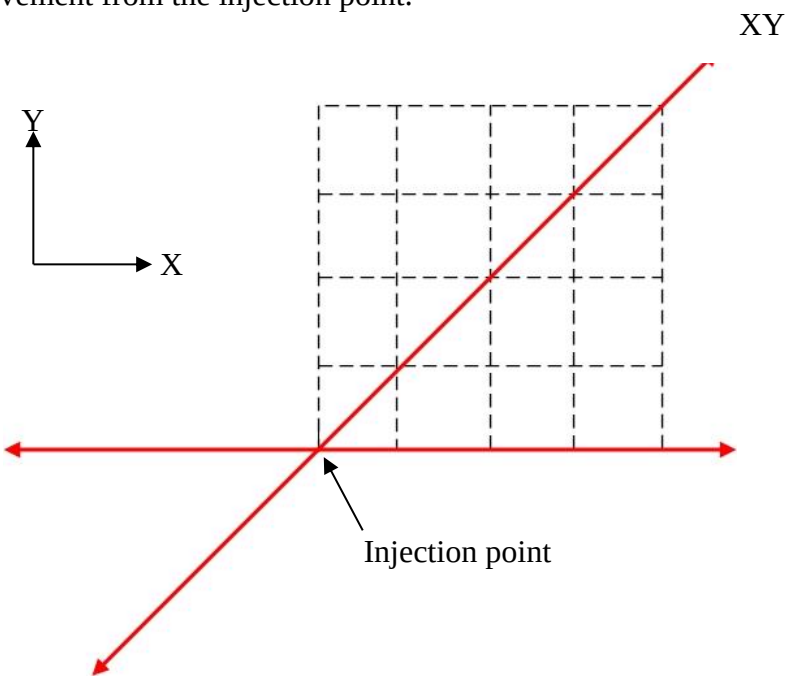

Figure 6.7: The locations where step voltages move further away from the injection point

In Figure 6.10, the peak values of the step voltages can be observed for both the X direction and the XY direction. The XY direction is diagonal to the grid from the injection point. The step voltage decreases with distance moving farther from the injection point. However, it still remains inside the grid. The step voltage inside the grid did not vary much when the location is away from the injection point. However, high step voltage values are observed when one of the human legs is on the edge of the grid, and the other leg is outside of the grid.

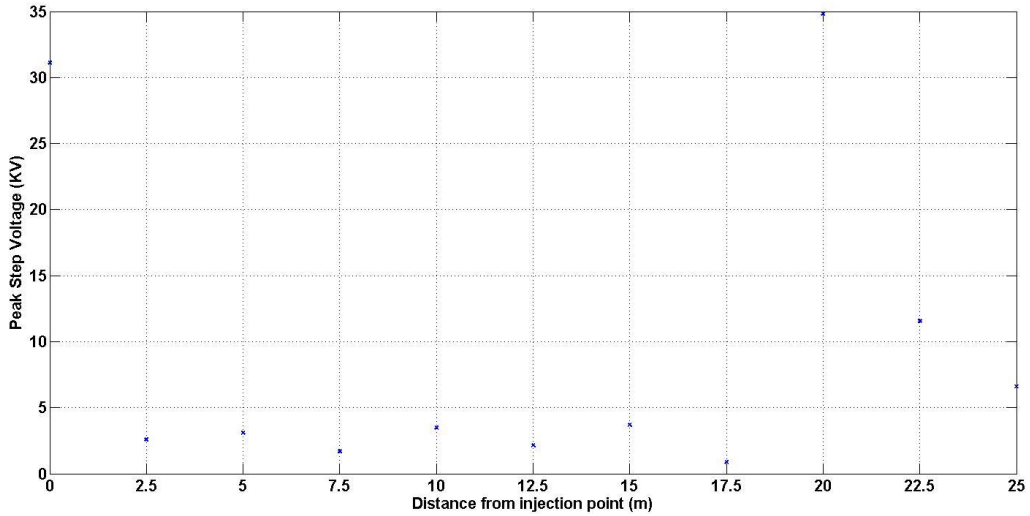

(a) X direction

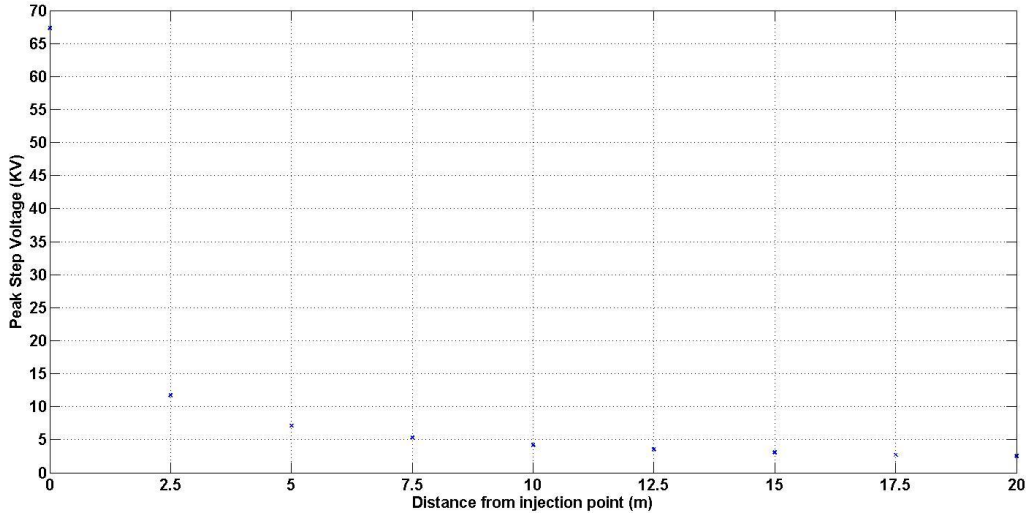

(b) XY direction

Figure 6.8: Peak step voltage measured while being away from the injection point, but remains inside the grid

Figure 6.9 illustrates the step voltages that are being computed while from the injection point and outside of the grid. It can be observed that the step voltage decreases non-linearly as a function of the distance from the injection point. The step voltage reduces to almost 20% of the maximum value when a human being is placed 2.5m from the grid. However, the step voltage is almost constant and exhibits low value when a certain distance from the injection point is reached.

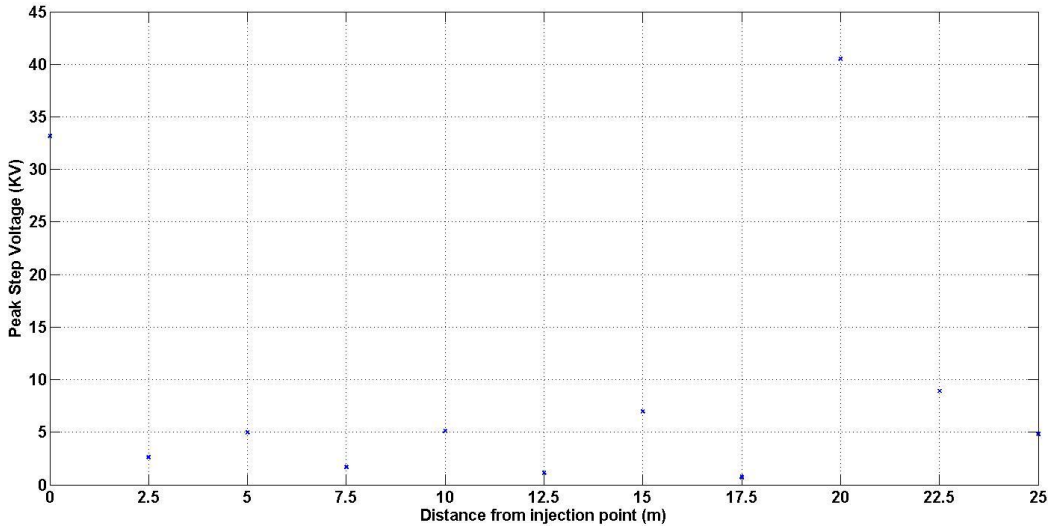

(a) -X direction

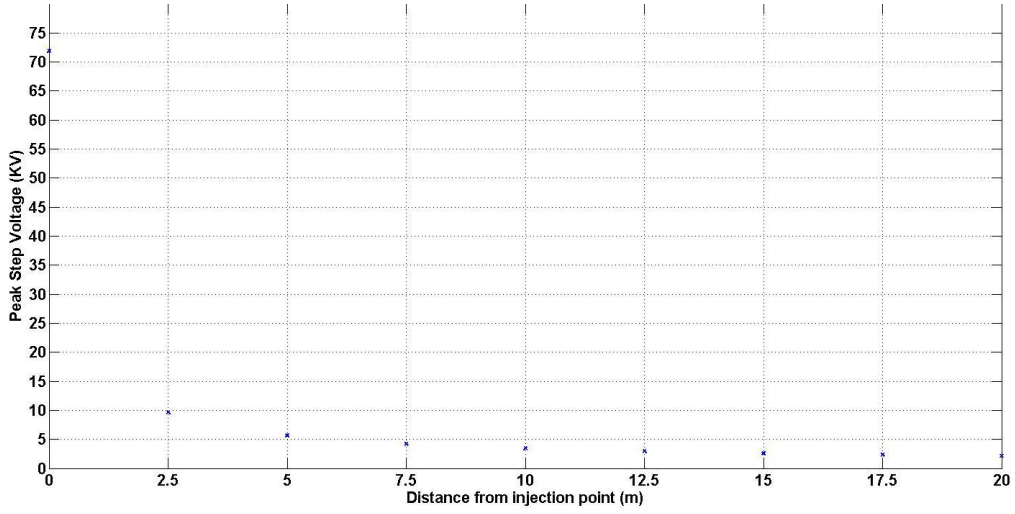

(b) -XY direction

Figure 6.9: Peak step voltage away from injection point and outside of the grid

6.4.2 Influence of size

Five grounding grid configurations, as shown in Figure 4.26, are adopted for the simulation. The size of the grid is varied from 5m × 5m to 40m × 40m, while the inner mesh size remained as 5m × 5m. The grids are buried 0.5m below the earth surface, and a 10kA impulse current with a 1.2/50μs front time is injected at a corner of the structure. Three soil resistivity values, namely 100Ω.m, 300Ω.m, and 1000Ω.m, are used for the comparative analysis to observe the effect of different soil resistivity.

Peak step voltages are evaluated for situations where one of the human legs is positioned outside of the grid. Figure 6.10 shows the peak step voltages for different soil resistivity and grids sizes, where the result revealed that higher soil resistivity proportionally increased the value of the step voltage. It is also evident that, by increasing the size of the grid, the step voltage can be reduced up until the grid reaches the effective size. The actual effective size is achieved when the change in the ground potential rise (GPR) is not significant relative to the increasing grid size.

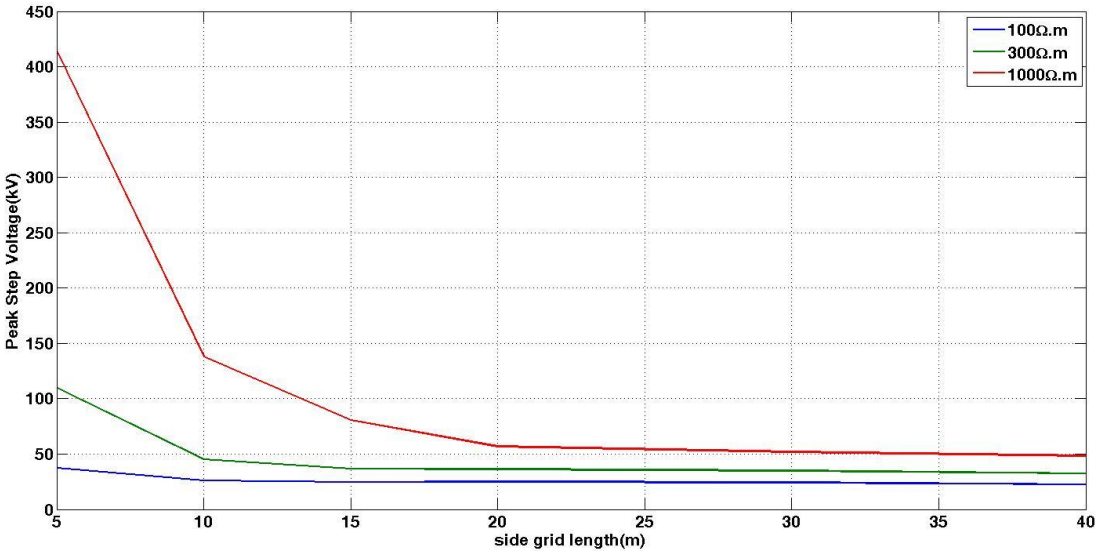

Figure 6.10: Peak Step Voltage at different sizes and soil resistivity

6.5Conclusion

The simulations described in this chapter indicated that the TGPR occurred at high peak potential values near to the injection point, which lasts for a few microseconds. This finding agreed with the reported findings from the literature. The relationship between numerical formulation and TGPR under the umbrella of the grid conductor is evaluated. The reduction in TGPR is quite significant when both the optimum and excessive size of the grid is achieved. The impulse impedance evaluation can be used to represent the effectiveness of the grid to dissipate lightning current to the soil. Maximum step voltages can be observed when a human is standing with one of their legs outside of the grid. Conversely, the step voltage is reduced when the location of the step moved away from the grid. Increasing the size of the grid reduced the peak step voltage value. However, the reduction is insignificant once the grid size exceeds the dimensions given by the effective area.

Chapter 7

Conclusion and Recommendation for Future Work

7.1 Conclusion

The main objectives of this research were to gain a better understanding and further improve the grounding grid design under lightning conditions. An extensive set of literature reviews on the grounding grid design under lightning condition were conducted for both experiment and simulation based research work. The topic of interest also covered both step and touch voltages' safety limits that were suggested by various standards. The limits were dependent on the allowable current flow through human body, contact resistance, body resistance and accidental circuit. The literature reviews highlighted the behaviour of grounding under impulse current was to be different compared to power frequency. However, most grounding design had to satisfy the power frequency requirement. The previous researchers suggested certain improvements to the grounding performance under impulse current condition, namely by reducing the soil resistivity, introducing parallel insulated conductor above grounding grid conductor or increasing the conductor near injection point with a limitation relative to the effective area of the grounding grid.

Many mathematical models were developed to improve the grounding grid design, including both laboratory based and field based tests and developments. The mathematical model development techniques included circuit, transmission line and

electromagnetic approaches. The circuit approach used basic electrical components, such as resistance, capacitance and inductance to emulate the effect of impulse current to the grounding system. In the case of electromagnetic approach, Maxwell's equation was solved by using FEM, FDTD or MOM methods. The electromagnetic approach was known for providing the most accurate result, however additional computational time and memory were required. The comparison between basic circuit approach and electromagnetic approach by using FEM was carried out in this thesis at different sizes of grounding grid and soil resistivity. It was found that the basic circuit approach underestimated the potential rise at the injection point. The technical reason for this scenario was that the circuit approach ignored both the propagation effect of the wave and the magnetic coupling between the elements.

The electromagnetic approach based on Ampere's equation was used to model the grounding system under lightning current condition. A partial differential equation was solved by using the FEM, where simulation and modelling tasks were performed in 3D mode via radio frequency (RF) module in COMSOL Multiphysics software package. The boundary conditions were determined by applying current density analysis at different sizes of the boundary. Such approach was picked because the absorption layer cannot be implemented in a time-domain study. A distance of 100m from the edge of the grid was found to effectively prevent reflection from a boundary of a perfect conductor. The finding was valid for soil resistivity of less than 1000Ω.m and front time of not less than 0.4μs. The simulation approach and solution were validated through comparative analysis with the existing results, which were solved by both using the MOM and experiment. In this study, the impulse impedance was used to measure the ratio peak voltage to peak current at the injection point. The simulation demonstrated that impulse impedance value was proportional to the soil

resistivity, while the impulse impedance value got lower for current injection at the centre of the grid compared to injection at the corner. Besides that, the impulse impedance decreased when the grounding grid size increased. However, the gradient of the reduction grown from little improvement to no improve at all for the impulse impedance after hitting certain size of the grid. The inefficient improvement was due to the effective area of the grid.

The increased mesh density near to the injection point provided better impulse impedance, which revealed the performance of the grid that produced low ground potential rise. The mesh density improvement was limited to the effective area. Therefore, it was important to estimate the effective area of the grounding grid. In the case of power frequency, its effective area was bigger compared to impulse current injection. As a result, the size of the grounding grid design needed to fulfil the requirement of power frequency. This had to take place before the enhancement of the mesh density near the injection point within the effective area to achieve better performance under impulse current. In this study, the down-conductor generated 5% - 10% of grounding impedance differences at a 0.5m of grid depth, which depended on the soil resistivity value and grid size. However, the longer rise time reduced the effective area when the down-conductor was considered. The consideration of including the down-conductor actually provided a better estimation of effective area which is not considered in previous equations. Therefore, for a more concrete contribution, an effective area empirical formula was proposed for the square grounding grid, where down- conductor from the top of the soil to the grounding grid was considered at a depth of 0.5m. Lightning current was injected at top of the down conductor. The proposed equation considered different injection locations, soil resistivity, and lightning current front times. The comparison of the proposed equation

relative to the previously-developed equations unveiled an improvement to the effective area formulation.

Apart from formulation, the transient ground potential rise analysis was also performed, which was important to gain better understanding on the potential distribution during the lightning transient. The analysis provided better understanding of the impulse impedance value at the injection point that was used for performance evaluation. The impulse impedance evaluation revealed the effectiveness of the current dissipation throughout the grid and soil. The high step voltages occurred near the injection point, and as well as during human leg being off the grounding grid.

7.2 Future Work

Based on the experience acquired from this research framework and the related literature in grounding grid behaviour under lightning current conditions, the following areas are proposed for future investigation:

- Understanding the frequency-dependence of the soil parameters, especially for soil conductivity, which can lead to more accurate modelling. Therefore, the consideration of frequency-dependent conductivity in the time domain simulation can provide better improvement. The simulation may be carried out by finding the relationship between the frequency components of the lightning current and the steepness of the injection current in the time domain.
- In this work, the grounding grids reacted differently in lightning conditions. In the future, standards should consider the effect of lightning current in grounding grid design. However, further studies are required to combine and integrate the power frequency and lightning protection requirements.

- Laboratory and field tests for different sizes of grid are imperative, so that the modelling of investigating the effective area estimation can be viable through simulation. The modelling can also improve the understanding of the ground potential rise during lightning condition.

Appendices

Appendix A

Reference levels for occupational exposure to time-varying electric and magnetic fields (unperturbed rms values) [35]

Frequency range	E-field strength (V/m)	H-field strength (A/m)	B-field (μT)	Equivalent plane wave power density (W/m^2)
up to 1Hz	-	$1.63x10^5$	$2x10^5$	-
1-8 Hz	20 000	$1.63x10^5/f^2$	$2x10^5/f^2$	-
8-25Hz	20 000	$2x10^4/f$	$2.5x10^4/f$	-
0.025–0.82 kHz	500/f	20/f	25/f	-
0.82–65 kHz	610	24.4	30.7	-
0.065–1 MHz	610	1.6/f	2/f	-
1–10 MHz	610/f	1.6/f	2/f	-
10–400 MHz	61	0.16	0.2	10
400–2,000 MHz	$3f^{1/2}$	$0.008f^{1/2}$	$0.01f^{1/2}$	f/40
2–300 GHz	137	0.36	0.45	50

Reference levels for general public exposure to time-varying electric and magnetic fields (unperturbed rms values) [35]

Frequency range	E-field strength (V/m)	H-field strength (A/m)	B-field (μT)	Equivalent plane wave power density (W/m^2)
up to 1Hz	-	$3.2x10^4$	$4x10^4$	-
1-8 Hz	10 000	$3.2x10^4/f^2$	$4x10^4/f^2$	-
8-25Hz	10 000	4000/f	5000/f	-
0.025–0.8 kHz	250/f	4/f	5/f	-
0.8–3 kHz	250/f	5	6.25	-
3-150kHz	87	5	6.25	
0.065–1 MHz	87	0.73/f	0.92/f	-
1–10 MHz	$87/f^{1/2}$	0.73/f	0.92/f	-
10–400 MHz	28	0.073	0.092	2
400–2,000 MHz	$1.375f^{1/2}$	$0.0037f^{1/2}$	$0.0046\ f^{1/2}$	f/200
2–300 GHz	61	0.16	0.20	10

Appendix B: flow chart of method of moment (MOM)

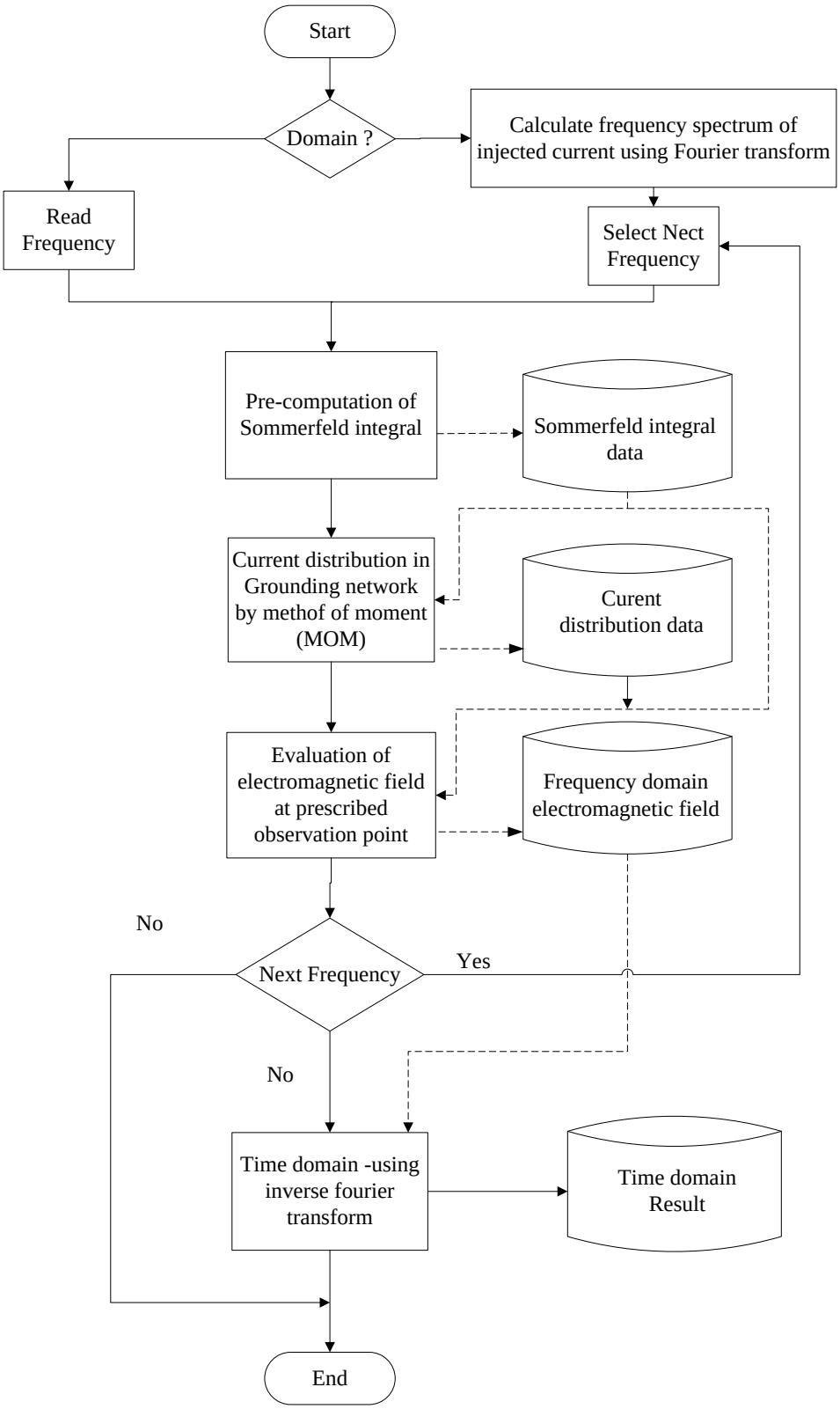

Appendix C: Equation used by previous researcher (FEM)

Governing equation used by Trlep et al.

$$\nabla([\sigma]\nabla V) = 0 \tag{C-1}$$

$$V = 0 \quad (\text{at infinity}), \frac{\partial V}{\partial n} = 0 \ (\text{at soil surface}) \tag{C-2}$$

$$J_{\text{displacement}} = \varepsilon\left(\frac{\partial^2 A}{\partial t^2} + \nabla\frac{\partial V}{\partial t}\right) \tag{C-3}$$

$$\nabla \times \frac{1}{\mu}\nabla \times A - \nabla\frac{1}{\mu}\nabla A + \sigma\left(\frac{\partial A}{\partial t} + \nabla V\right) + \varepsilon\left(\frac{\partial^2 A}{\partial t^2} + \nabla\frac{\partial V}{\partial t}\right) = 0 \tag{C-4}$$

$$\nabla.\left[\sigma\left(\frac{\partial A}{\partial t} + \nabla V\right) + \varepsilon\left(\frac{\partial^2 A}{\partial t^2} + \nabla\frac{\partial V}{\partial t}\right)\right] = 0 \tag{C-5}$$

Governing equation used by Nekhoul et al.

$$\nabla \times \frac{1}{\mu}\nabla \times A - \nabla\frac{1}{\mu}\nabla A + \sigma\left(\frac{\partial A}{\partial t} + \nabla V\right) = 0 \tag{C-6}$$

$$\nabla.\left[\sigma\left(\frac{\partial A}{\partial t} + \nabla V\right)\right] = 0 \tag{C-7}$$

$$\nabla \times \frac{1}{\mu}\nabla \times A - \nabla\frac{1}{\mu}\nabla.A = 0 \tag{C-8}$$

References

[1] BS7430, "Code of practice for protective earthing of electrical installations," ed: British Standard 2011.

[2] "IEEE Guide for Safety in AC Substation Grounding," in *IEEE Std 80-2000*, ed, 2000, pp. i-192.

[3] B. E. 50522:2010, "Earthing of power installations exceeding 1 kV a.c.," ed, 2010.

[4] BS7354, "Design of high-voltage open-terminal stations," ed: British Standard 1990.

[5] V. Cooray, C. Cooray, and C. J. Andrews, "Lightning caused injuries in humans," *Journal of Electrostatics*, vol. 65, pp. 386-394, 2007.

[6] R. H. Golde and W. R. Lee, "Death by lightning," *Proceedings of the Institution of Electrical Engineers*, vol. 123, pp. 1163-1180, 1976.

[7] IEC60479-1, "Effects of current on human beings and livestock - Part 1: General aspect," ed, 2005.

[8] H. Griffiths, A. Haddad, and N. Harid, "Characterisation of earthing systems under high frequency and transient conditions," in *39th International Universities Power Engineering Conference*, Bristol, UK, 2004, pp. 188-192 Vol. 1.

[9] UK Power Network, "Earthing Design Criteria ", ed, 2015.

[10] H. Zhao, H. Griffiths, A. Haddad, and A. Ainsley, "Safety-limit curves for earthing system designs: appraisal of standard recommendations," *IEE Proceedings-Generation, Transmission and Distribution*, vol. 152, pp. 871-879, 2005.

[11] A. Dimopoulos, H. Griffiths, A. Haddad, A. Ainsley, F. Ainslie, and D. Frame, "Parametric Analysis of Safety Limit-Curves in Earthing Systems and Comparison of International Standard Recommendations," in *Proceedings of the 41st International Universities Power Engineering Conference, UPEC '06.* , Newcastle Upon Tyne , UK 2006, pp. 272-276.

[12] R. L. Holle, "Some aspects of global lightning impacts," in *International Conference on Lightning Protection (ICLP)*, Shanghai, China, 2014, pp. 1390-1395.

[13] M. A. Cooper, "Whether the medical aspects of lightning injury are different in developing countries," in *International Conference on Lightning Protection (ICLP)*, Vienna, Austria, 2012, pp. 1-6.

[14] M. Xu, Z. Wang, R. Fan, J. Zhou, Q. Zeng, and B. Zhou, "The distribution analysis of lightning density and lightning current amplitude in Jiangsu province," in *2nd International Conference on Mechanical and Electronics Engineering (ICMEE)*, Kyoto,Japan, 2010, pp. V1-213-V1-216.

[15] E. R. Williams, "Lightning and climate: A review," *Atmospheric Research*, vol. 76, pp. 272-287, 2005.

[16] L. P. Ferris, B. G. King, P. W. Spence, and H. B. Williams, "Effect of Electric Shock on the Heart," *Transactions of the American Institute of Electrical Engineers*, vol. 55, pp. 498-515, 1936.

[17] W. B. Kouwenhoven and O. R. Langworthy, "Effect of Electric Shock," *Transactions of the American Institute of Electrical Engineers*, vol. 49, pp. 381-394, 1930.

[18] W. B. Kouwenhoven and O. R. Langworthy, "Effects of Electric Shock-II," *Transactions of the American Institute of Electrical Engineers*, vol. 50, pp. 1165-1170, 1931.

[19] W. B. Kouwenhoven, D. R. Hooker, and E. L. Lotz, "Electric Shock Effects of Frequency," *Transactions of the American Institute of Electrical Engineers*, vol. 55, pp. 384-386, 1936.

[20] W. B. Kouwenhoven, "Effect of Capacitor Discharges on the Heart," *Power Apparatus and Systems, Part III. Transactions of the American Institute of Electrical Engineers*, vol. 75, pp. 12-15, 1956.

[21] C. F. Dalziel and W. R. Lee, "Reevaluation of Lethal Electric Currents," *IEEE Transactions on Industry and General Applications*, vol. IGA-4, pp. 467-476, 1968.

[22] C. F. Dalziel, "Threshold 60-Cycle Fibrillating Currents," *Power Apparatus and Systems, Part III. Transactions of the American Institute of Electrical Engineers*, vol. 79, pp. 667-673, 1960.

[23] C. F. Dalziel and W. R. Lee, "Lethal electric currents," *IEEE Spectrum,* vol. 6, pp. 44-50, 1969.

[24] C. F. Dalziel, "Electric shock hazard," *IEEE Spectrum,* vol. 9, pp. 41-50, 1972.

[25] C. F. Dalziel, "Dangerous Electric Currents," *Transactions of the American Institute of Electrical Engineers,* vol. 65, pp. 579-585, 1946.

[26] C. F. Dalziel, "Effect of Wave Form on Let-Go Currents," *Transactions of the American Institute of Electrical Engineers,* vol. 62, pp. 739-744, 1943.

[27] C. F. Dalziel, E. Ogden, and C. E. Abbott, "Effect of Frequency on Let-Go Currents," *Transactions of the American Institute of Electrical Engineers,* vol. 62, pp. 745-750, 1943.

[28] C. F. Dalziel, "The Threshold of Perception Currents," *Power Apparatus and Systems, Part III. Transactions of the American Institute of Electrical Engineers,* vol. 73, pp. 990-996, 1954.

[29] C. F. Dalziel, "A Study of the Hazards of Impulse Currents," *Power Apparatus and Systems, Part III. Transactions of the American Institute of Electrical Engineers,* vol. 72, pp. 1032-1043, 1953.

[30] T. Ishikawa, T. Miyazawa, M. Ohashi, T. Muto, N. Kitagawa, K. Takagi, K. Kinoshita, and S. Tsurumi, "Experimental studies on the effect of artificial respiration after lightning accidents," *Research in Experimental Medicine,* vol. 179, pp. 59-68, 1981/02/01 1981.

[31] T. Ishikawa, M. Ohashi, N. Kitagawa, Y. Nagai, and T. Miyazawa, "Experimental study on the lethal threshold value of multiple successive voltage impulses to rabbits simulating multi-stroke lightning flash," *International Journal of Biometeorology,* vol. 29, pp. 157-168, 1985.

[32] C. Portela, "Frequency and transient behavior of grounding systems. I. Physical and methodological aspects," in *International Symposium on Electromagnetic Compatibility,* Austin, Texas, USA 1997, pp. 379-384.

[33] IEC60479-2, "Effects of current on human beings and livestock - Part 2: Special aspects relating to human beings," 2007.

[34] B. T., "Effects of electricity and lightning on man and animals," *J Forensic Sci,* vol. 18, 1973.

[35] ICNIRP, "Guidelines for Limiting Exposure to Time-Varying Electric, Magnetic, and Electromagnetic Fields (up to 300 GHz) ", ed, 1998.

[36] E. D. Sunde, "Surge Characteristics of a Buried Bare Wire," *Transactions of the American Institute of Electrical Engineers,* vol. 59, pp. 987-991, 1940.

[37] P. L. Bellaschi, "Impulse and 60-Cycle Characteristics of Driven Grounds," *Transactions of the American Institute of Electrical Engineers,* vol. 60, pp. 123-128, 1941.

[38] P. L. Bellaschi, R. E. Armington, and A. E. Snowden, "Impulse and 60-Cycle Characteristics of Driven Grounds - II," *Transactions of the American Institute of Electrical Engineers,* vol. 61, pp. 349-363, 1942.

[39] P. L. Bellaschi and R. E. Armington, "Impulse and 60-Cycle Characteristics of Driven Grounds--III Effect of Lead in Ground Installation," *Transactions of the American Institute of Electrical Engineers,* vol. 62, pp. 334-345, 1943.

[40] B. R. Gupta and B. Thapar, "Impulse Impedance of Grounding Grids," *IEEE Transactions on Power Apparatus and Systems,* vol. PAS-99, pp. 2357-2362, 1980.

[41] A. C. Liew and M. Darveniza, "Dynamic model of impulse characteristics of concentrated earths," *Proceedings of the Institution of Electrical Engineers,* vol. 121, pp. 123-135, 1974.

[42] R. Velazquez and D. Mukhedkar, "Analytical Modelling of Grounding Electrodes Transient Behavior," *Power Apparatus and Systems, IEEE Transactions on,* vol. PAS-103, pp. 1314-1322, 1984.

[43] N. Harid, H. Griffiths, S. Mousa, D. Clark, S. Robson, and A. Haddad, "On the Analysis of Impulse Test Results on Grounding Systems," *IEEE Transactions on Industry Applications,* vol. 51, pp. 5324-5334, 2015.

[44] S. Visacro and G. Rosado, "Response of Grounding Electrodes to Impulsive Currents: An Experimental Evaluation," *IEEE Transactions on Electromagnetic Compatibility,* vol. 51, pp. 161-164, 2009.

[45] A. Haddad, H. Griffiths, M. Ahmeda, and N. Harid, "Experimental investigation of the impulse characteristics of practical ground electrode systems," in *International Conference on High Voltage Engineering and Application (ICHVE), 2010*, New Orleans, LA, USA, 2010, pp. 469-472.

[46] S. Mousa, N. Harid, H. Griffiths, and A. Haddad, "Experimental investigation of high frequency and transient performance of earth rod systems," *Electric Power Systems Research,* vol. 113, pp. 196-203, 2014.

[47] R. Kosztaluk, M. Loboda, and D. Mukhedkar, "Experimental Study of Transient Ground Impedances," *IEEE Transactions on Power Apparatus and Systems,* vol. PAS-100, pp. 4653-4660, 1981.

[48] N. M. Nor, A. Haddad, and H. Griffiths, "Characterization of ionization phenomena in soils under fast impulses," *IEEE Transactions on Power Delivery,* vol. 21, pp. 353-361, 2006.

[49] A. M. Mousa, "The soil ionization gradient associated with discharge of high currents into concentrated electrodes," *IEEE Transactions on Power Delivery,* vol. 9, pp. 1669-1677, 1994.

[50] CIGRE, "Guide to Procedures for Estimating the Lightning Performance of Transmission Lines," Int. Council Large Electr. Syst. (CIGRE), Paris, France1991.

[51] N. M. Nor, A. Haddad, and H. Griffiths, "Determination of threshold electric field E_c of soil under high impulse currents," *IEEE Transactions on Power Delivery,* vol. 20, pp. 2108-2113, 2005.

[52] N. M. Nor, A. Haddad, and H. Griffiths, "Performance of earthing systems of low resistivity soils," *IEEE Transactions on Power Delivery,* vol. 21, pp. 2039-2047, 2006.

[53] N. Nor and A. Ramli, "Soil characteristics of wet sand under different impulse polarity and earth electrode's dimensions," *IEEE Transactions on Dielectrics and Electrical Insulation,* vol. 15, pp. 910-914, 2008.

[54] S. Visacro, R. Alipio, M. H. Murta Vale, and C. Pereira, "The Response of Grounding Electrodes to Lightning Currents: The Effect of Frequency-Dependent Soil Resistivity and Permittivity," *IEEE Transactions on Electromagnetic Compatibility,* vol. 53, pp. 401-406, 2011.

[55] H. Jinliang, G. Yanqing, Z. Rong, Z. Jun, L. Xidong, Z. Bo, L. Jaebok, and S. Chang, "Effective length of counterpoise wire under lightning current," *IEEE Transactions on Power Delivery,* vol. 20, pp. 1585-1591, 2005.

[56] L. Grcev, "Impulse Efficiency of Ground Electrodes," *IEEE Transactions on Power Delivery,* vol. 24, pp. 441-451, 2009.

[57] N. Mohamad Nor, S. Abdullah, R. Rajab, and Z. Othman, "Comparison between utility sub-station and imitative earthing systems when subjected

under lightning response," *International Journal of Electrical Power & Energy Systems,* vol. 43, pp. 156-161, 2012.

[58] N. Mohamad Nor, S. Abdullah, R. Rajab, and K. Ramar, "Field tests: Performances of practical earthing systems under lightning impulses," *International Journal of Electrical Power & Energy Systems,* vol. 45, pp. 223-228, 2013.

[59] N. Mohamad Nor, M. Trlep, S. Abdullah, and R. Rajab, "Investigations of earthing systems under steady-state and transients with FEM and experimental work," *International Journal of Electrical Power & Energy Systems,* vol. 44, pp. 758-763, 2013.

[60] N. M. Nor, M. Trlep, S. Abdullah, R. Rajab, and R. Ramar, "Determination of Threshold Electric Field of Practical Earthing Systems by FEM and Experimental Work," *IEEE Transactions on Power Delivery,* vol. 28, pp. 2180-2184, 2013.

[61] M. Ramamoorty, M. M. B. Narayanan, S. Parameswaran, and D. Mukhedkar, "Transient performance of grounding grids," *IEEE Transactions on Power Delivery,* vol. 4, pp. 2053-2059, 1989.

[62] Z. Stojkovic, M. S. Savic, J. M. Nahman, D. Salamon, and B. Bukorovic, "Sensitivity analysis of experimentally determined grounding grid impulse characteristics," *IEEE Transactions on Power Delivery*, vol. 13, pp. 1136-1142, 1998.

[63] S. Visacro, N. M. B. Guimaraes, R. A. Araujo, and L. S. de Araujo, "Experimental impulse response of grounding grids," in *7th Asia-Pacific International Conference on Lightning (APL)*, Chengdu, China, 2011, pp. 637-641.

[64] M. N. Guimaraes, L. Araujo, R. V. Castro, L. F. D. Santos, M. H. M. Vale, and S. Visacro, "Impulse response of grounding grids: Experimental versus simulated results," in *International Conference on Lightning Protection (ICLP)*, Vienna, Austria, 2012, pp. 1-4.

[65] S. Visacro, M. B. Guimarães, and L. S. Araujo, "Experimental impulse response of grounding grids," *Electric Power Systems Research,* vol. 94, pp. 92-98, 2013.

[66] D. Guo, D. Lathi, N. Harid, H. Griffiths, A. Haddad, and A. Ainsley, "Experimental investigation into the performance of large-scale earthing electrodes," in *International Conference on High Voltage Engineering and Application (ICHVE)*, New Orleans, LA, USA, 2010, pp. 465-468.

[67] D. Clark, D. Guo, D. Lathi, N. Harid, H. Griffiths, A. Ainsley, and A. Haddad, "Controlled Large-Scale Tests of Practical Grounding Electrodes -Part II: Comparison of Analytical and Numerical Predictions With Experimental Results," *IEEE Transactions on Power Delivery*, vol. 29, pp. 1240-1248, 2014.

[68] D. Guo, D. Clark, D. Lathi, N. Harid, H. Griffiths, A. Ainsley, and A. Haddad, "Controlled Large-Scale Tests of Practical Grounding Electrodes-Part I: Test Facility and Measurement of Site Parameters," *IEEE Transactions on Power Delivery*, vol. 29, pp. 1231-1239, 2014.

[69] L. Grcev, "Lightning Surge Efficiency of Grounding Grids," *IEEE Transactions on Power Delivery*, vol. 26, pp. 1692-1699, 2011.

[70] A. El Mghairbi, "Assessment of earthing systems and enhancement of their performance," PhD Thesis, Cardiff University, 2012.

[71] B. Zedan, "Characterisation of substation earth grid under high frequency and transient conditions," PhD Thesis, Cardiff University, 2005.

[72] L. Yaqing, M. Zitnik, and R. Thottappillil, "An improved transmission-line model of grounding system," *IEEE Transactions on Electromagnetic Compatibility*, vol. 43, pp. 348-355, 2001.

[73] L. D. Grcev and M. Heimbach, "Frequency dependent and transient characteristics of substation grounding systems," *IEEE Transactions on Power Delivery*, vol. 12, pp. 172-178, 1997.

[74] Z. Rong, G. Xuehai, H. Jinliang, Z. Bo, and G. Yanqing, "Lightning Impulse Performances of Grounding Grids for Substations Considering Soil Ionization," *IEEE Transactions on Power Delivery*, vol. 23, pp. 667-675, 2008.

[75] M. A. Cooper, Holle, R. L., Andrews, A, "Distribution of Lightning Injury Mechanisms," presented at the 20th International Lightning Detection Conference, Arizona, USA, 2008.

[76] P. I. T. 60479-4:2011, "Effects of current on human beings and livestock," in *Part 4: Effects of lightning strokes*, ed, 2011.

[77] W. Xiong and F. P. Dawalibi, "Transient performance of substation grounding systems subjected to lightning and similar surge currents," *IEEE Transactions on Power Delivery*, vol. 9, pp. 1412-1420, 1994.

[78] F. P. Dawalibi, X. Wei, and M. Jinxi, "Transient performance of substation structures and associated grounding systems," *IEEE Transactions on Industry Applications*, vol. 31, pp. 520-527, 1995.

[79] L. D. Grcev, "Computer analysis of transient voltages in large grounding systems," *IEEE Transactions on Power Delivery*, vol. 11, pp. 815-823, 1996.

[80] W. Ruan, S. Fortin, F. P. Dawalibi, F. Grange, and S. Journet, "Transient Ground Potential Rises at a nuclear fusion experimental power plant hit directly by a lightning strike," in *7th Asia-Pacific International Conference on Lightning (APL)*, Chengdu, China, 2011, pp. 192-197.

[81] T. Chenghuan, Z. Yi, C. Li, W. Jianguo, H. Songbo, and W. Yan, "Lightning transient characteristics of a 500-kV substation grounding grid," in *7th Asia-Pacific International Conference on Lightning (APL)*, Chengdu, China, 2011, pp. 711-715.

[82] S. Suchanek, V. Hinrichsen, R. Brocke, and K. Muller, "Investigations of earth termination systems with respect to optimised step voltages," in *International Conference on Lightning Protection (ICLP)*, Vienna, Austria, 2012, pp. 1-7.

[83] R. Brocke, V. Hinrichsen, S. Suchanek, and G. Jing, "Step-voltage-optimized Lightning Protection earth-termination systems analysis and simulation," in *International Symposium on Lightning Protection (XI SIPDA)*, Fortaleza, Brazil, 2011, pp. 272-277.

[84] D. S. Gazzana, A. S. Bretas, G. A. D. Dias, M. Telló, D. W. P. Thomas, and C. Christopoulos, "A study of human safety against lightning considering the grounding system and the evaluation of the associated parameters," *Electric Power Systems Research*, vol. 113, pp. 88-94, 2014.

[85] CIGRE, "Guide on EMC in power plants and substations," *CIGRE Brochure 124*, 1997.

[86] B. E. 62305-1:2011, "Protection against lightning , Part 1: General principles," ed, 2011.

[87] L. Grcev, "Improved earthing system design practices for reduction of transient voltages," *CIGRE 36*, vol. 302, 1998.

[88] A. P. Meliopoulos and M. G. Moharam, "Transient Analysis of Grounding Systems," *IEEE Transactions on Power Apparatus and Systems*, vol. PAS-102, pp. 389-399, 1983.

[89] A. D. Papalexopoulos and A. P. Meliopoulos, "Frequency Dependent Characteristics of Grounding Systems," *Power Delivery, IEEE Transactions on*, vol. 2, pp. 1073-1081, 1987.

[90] A. Geri, "Behaviour of grounding systems excited by high impulse currents: the model and its validation," *IEEE Transactions on Power Delivery*, vol. 14, pp. 1008-1017, 1999.

[91] A. F. Otero, Cidra, x, J. s, and J. L. del Alamo, "Frequency-dependent grounding system calculation by means of a conventional nodal analysis technique," *IEEE Transactions on Power Delivery*, vol. 14, pp. 873-878, 1999.

[92] J. Cidras, A. F. Otero, and C. Garrido, "Nodal frequency analysis of grounding systems considering the soil ionization effect," *IEEE Transactions on Power Delivery*, vol. 15, pp. 103-107, 2000.

[93] F. Dawalibi, "Electromagnetic Fields Generated by Overhead and Buried Short Conductors Part 1 - Single Conductor," *IEEE Transactions on Power Delivery*, vol. 1, pp. 105-111, 1986.

[94] F. Dawalibi, "Electromagnetic Fields Generated by Overhead and Buried Short Conductors Part 2 - Ground Networks," *IEEE Transactions on Power Delivery*, vol. 1, pp. 112-119, 1986.

[95] "IEEE Recommended Practice for Grounding of Industrial and Commercial Power Systems (IEEE Green Book)," *ANSI/IEEE Std 142-1982*, pp. 1-135, 1982.

[96] S. Visacro and A. Soares, Jr., "HEM: a model for simulation of lightning-related engineering problems," *IEEE Transactions on Power Delivery*, vol. 20, pp. 1206-1208, 2005.

[97] S. Visacro and F. H. Silveira, "Evaluation of current distribution along the lightning discharge channel by a hybrid electromagnetic model," *Journal of Electrostatics*, vol. 60, pp. 111-120, 2004.

[98] M. A. F. Mattos, "Grounding grids transient simulation," *IEEE Transactions on Power Delivery*, vol. 20, pp. 1370-1378, 2005.

[99] C. Christopoulos, *The transmission-line modeling method: TLM*: Institute of Electrical and Electronics Engineers, 1995.

[100] Z. Bo, W. Jinpeng, H. Jinliang, and Z. Rong, "Analysis of Transient Performance of Grounding System Considering Soil Ionization by Time Domain Method," *IEEE Transactions on Magnetics,* vol. 49, pp. 1837-1840, 2013.

[101] P. Yutthagowith, A. Ametani, N. Nagaoka, and Y. Baba, "Application of the Partial Element Equivalent Circuit Method to Analysis of Transient Potential Rises in Grounding Systems," *IEEE Transactions on Electromagnetic Compatibility,* vol. 53, pp. 726-736, 2011.

[102] A. E. Ruehli, "Equivalent Circuit Models for Three-Dimensional Multiconductor Systems," *IEEE Transactions on Microwave Theory and Techniques,* vol. 22, pp. 216-221, 1974.

[103] C. Mazzetti and G. M. Veca, "Impulse Behavior Of Ground Electrodes," *IEEE Transactions on Power Apparatus and Systems,* vol. PAS-102, pp. 3148-3156, 1983.

[104] R. Verma and D. Mukhedkar, "Impulse Impedance of Buried Ground Wire," *IEEE Transactions on Power Apparatus and Systems,* vol. PAS-99, pp. 2003-2007, 1980.

[105] G. Ala and M. L. Di Silvestre, "A simulation model for electromagnetic transients in lightning protection systems," *IEEE Transactions on Electromagnetic Compatibility,* vol. 44, pp. 539-554, 2002.

[106] L. Yaqing, N. Theethayi, and R. Thottappillil, "An engineering model for transient analysis of grounding system under lightning strikes: nonuniform transmission-line approach," *IEEE Transactions on Power Delivery,* vol. 20, pp. 722-730, 2005.

[107] F. T. Ulaby, *Electromagnetics for engineers*: Pearson/Prentice Hall, 2005.

[108] K. Tanabe and A. Asakawa, "Computer analysis of transient performance of grounding grid element based on the finite-difference time-domain method," in *IEEE International Symposium on Electromagnetic Compatibility*, Istanbul, Turkey, 2003, pp. 209-212 Vol.1.

[109] K. Tanabe, "Novel method for analyzing the transient behavior of grounding systems based on the finite-difference time-domain method," in *IEEE Power*

Engineering Society Winter Meeting, Columbus, OH, USA, 2001, pp. 1128-1132 vol.3.

[110] M. Tsumura, Y. Baba, N. Nagaoka, and A. Ametani, "FDTD Simulation of a Horizontal Grounding Electrode and Modeling of its Equivalent Circuit," *IEEE Transactions on Electromagnetic Compatibility*, vol. 48, pp. 817-825, 2006.

[111] S. Yamaguchi, M. Inoue, S. Sekioka, T. Sonoda, Y. Kato, N. Nagaoka, and A. Ametani, "A frequency-dependent counterpoise model for a transient analysis," in *ICEE*, Rio de Jeneiro, Brazil 1998, pp. 753-756.

[112] L. Grcev and F. Dawalibi, "An electromagnetic model for transients in grounding systems," *IEEE Transactions on Power Delivery*, vol. 5, pp. 1773-1781, 1990.

[113] L. Grcev and D. Hristov, "More accurate modelling of earthing systems transient behaviour," in *15th International Telecommunications Energy Conference*, Paris, France, 1993, pp. 167-173 vol.2.

[114] M. Heimbach and L. D. Grcev, "Grounding system analysis in transients programs applying electromagnetic field approach," *IEEE Transactions on Power Delivery*, vol. 12, pp. 186-193, 1997.

[115] M. Trlep, A. Hamler, and B. Hribernik, "The analysis of complex grounding systems by FEM," *IEEE Transactions on Magnetics*, vol. 34, pp. 2521-2524, 1998.

[116] A. Habjanic, M. Jesenik, and M. Trlep, "Application of the finite element method for the analysis of the grounding grid implying the finite line elements," in *IET 8th International Conference on Computation in Electromagnetics*, Wroclaw,Poland, 2011, pp. 1-2.

[117] Q. Lei, C. Xiang, Z. Zhibin, and L. Huiqi, "Grounding Performance Analysis of the Substation Grounding Grids by Finite Element Method in Frequency Domain," *IEEE Transactions on Magnetics*, vol. 43, pp. 1181-1184, 2007.

[118] M. Trlep, M. Jesenik, and A. Hamler, "Transient Calculation of Electromagnetic Field for Grounding System Based on Consideration of Displacement Current," *IEEE Transactions on Magnetics*, vol. 48, pp. 207-210, 2012.

[119] B. Nekhoul, C. Guerin, P. Labie, G. Meunier, R. Feuillet, and X. Brunotte, "A finite element method for calculating the electromagnetic fields generated by

substation grounding systems," *IEEE Transactions on Magnetics,* vol. 31, pp. 2150-2153, 1995.

[120] O. Biro, K. Preis, and K. R. Richter, "On the use of the magnetic vector potential in the nodal and edge finite element analysis of 3D magnetostatic problems," *IEEE Transactions on Magnetics,* vol. 32, pp. 651-654, 1996.

[121] O. Biro and K. Preis, "On the use of the magnetic vector potential in the finite-element analysis of three-dimensional eddy currents," *IEEE Transactions on Magnetics,* vol. 25, pp. 3145-3159, 1989.

[122] L. Grcev and M. Popov, "On high-frequency circuit equivalents of a vertical ground rod," *Power Delivery, IEEE Transactions on,* vol. 20, pp. 1598-1603, 2005.

[123] R. Courant, "Variational methods for a solution of problems of equilibriumand vibrations," *Bull. Amer. Math. Soc,* pp. pp. 1–23, 1943.

[124] H. D. Bruns, C. Schuster, and H. Singer, "Numerical Electromagnetic Field Analysis for EMC Problems," *IEEE Transactions on Electromagnetic Compatibility,* vol. 49, pp. 253-262, 2007.

[125] M. N. O. Sadiku, "A simple introduction to finite element analysis of electromagnetic problems," *IEEE Transactions on Education,* vol. 32, pp. 85-93, 1989.

[126] J. Jin, *The finite element method in electromagnetics*: John Wiley & Sons, 2014.

[127] A. Stohchniol, "A general transformation for open boundary finite element method for electromagnetic problems," *IEEE Transactions on Magnetics,* vol. 28, pp. 1679-1681, 1992.

[128] A. COMSOL, "Comsol Multiphysics Reference Manual," ed: Version, 2007.

[129] C. Multiphysics, "RF Module User's guide," ed: COMSOL, 2008.

[130] T. CIGRE, "549, Lightning Parameters for Engineering Applications, WG C4. 407, VA Rakov, Convenor (US), A," *Borghetti, Secretary (IT), C. Bouquegneau (BE), WA Chisholm (CA), V. Cooray (SE), K. Cummins (US), G. Diendorfer (AT), F. Heidler (DE), A. Hussein (CA), M. Ishii (JP), CA Nucci (IT), A. Piantini (BR), O. Pinto, Jr.(BR), X. Qie (CN), F. Rachidi (CH), MMF Saba (BR), T. Shindo (JP), W. Schulz (AT), R. Thottappillil (SE), S. Visacro (BR), W. Zischank (DE),* 2013.

[131] V. A. Rakov, "Lightning parameters for engineering applications (keynote speech)," in *Asia-Pacific Symposium on Electromagnetic Compatibility (APEMC)*, Beijing, China, 2010, pp. 1120-1123.

[132] W. R. Gamerota, J. O. Elisme, M. A. Uman, and V. A. Rakov, "Current Waveforms for Lightning Simulation," *IEEE Transactions on Electromagnetic Compatibility*, vol. 54, pp. 880-888, 2012.